# 論文 / 著書情報
# Article / Book Information

| | |
|---|---|
| 題目(和文) | |
| Title(English) | Composition Dependence of Nanocluster Characteristics in Natural- and Pre-aged Al-Mg-Si alloys Responsible for Two-step Aging Behavior |
| 著者(和文) | 金聖寧 |
| Author(English) | Seong Nyeong Kim |
| 出典(和文) | 学位:博士（工学）,<br>学位授与機関:東京工業大学,<br>報告番号:甲第10305号,<br>授与年月日:2016年9月20日,<br>学位の種別:課程博士,<br>審査員:小林 郁夫,中村 吉男,熊井 真次,曽根 正人,村石 信二 |
| Citation(English) | Degree:,<br>Conferring organization: Tokyo Institute of Technology,<br>Report number:甲第10305号,<br>Conferred date:2016/9/20,<br>Degree Type:Course doctor,<br>Examiner:,,,, |
| 学位種別(和文) | 博士論文 |
| Type(English) | Doctoral Thesis |

# Composition Dependence of Nanocluster Characteristics in Natural- and Pre-aged Al-Mg-Si alloys Responsible for Two-step Aging Behavior

by

SeongNyeong KIM

Doctoral Thesis

Department of Metallurgy and Ceramics Science

Tokyo Institute of Technology

2016

*"The Lord is my shepherd, I shall not be in want."*

*(Psalms 23:1)*

# Acknowledgements

Completion of this thesis was possible with the support of several people.

My sincere appreciation first goes to my major professor, Dr. Tatsuo Sato for encouraging me to pursue my dream. Without his guidance and persistent help this thesis would not have been possible. I consider it as a great opportunity to do my master and doctoral program under his guidance and to learn from his research expertise and philosophy.

I would like to thank associate professor, Dr. Equo Kobayashi who has given great opportunities such as teaching assistant, other many activities and experiences to be helpful my master and doctoral program. Also, I would like to express thank Mr. Hiroyasu Tezuka for his sincere concern and invaluable advice on my life in Japan. Thank you for your consistent encouragement and comments on my thesis.

Besides my advisors, I would like to thank the rest of my thesis committee: Prof. Yoshio Nakamura, Prof. Shinji Kumai, Prof. Shinji Muraishi and Prof. Masato Sone, for their insightful comments and encouragement, but also for the hard question which incented me to widen my research from various perspectives.

My sincere thanks also goes to Dr. Yasuhiro Aruga, Dr. Masaya Kozuka and Dr. Yasuo Takaki, who provided me an opportunity to use the atom probe tomography and who gave access to the laboratory and research facilities. Without they precious support and comment it would not be possible to conduct this research.

I deeply thank to Dr. JaeHwang Kim, for her invaluable advice and comments on understanding age-hardening behavior in Al-Mg-Si alloys. I also thank to Prof. Shoichi Hirosawa, Prof. Tomo Ogura and Prof. Ai Serizawa, for their concern and encouragement.

I thank my fellow labmates in Kobayashi laboratory, for the stimulating discussions and for their care and precious friendship during my stay in Tokyo Tech. I am also indebted to my friends, SunKyung Choi and Ram Song, who squeeze time from their busy schedule to help me finish my thesis. They are willing to give their helping hands as soon as I am in need.

Finally, I take this opportunity to express the profound gratitude from my deep heart to my beloved parents, and brother for his love and continuous support. This thesis would not have come to a completion, without their pray and concern.

Above all, I owe it all to Almighty God for granting me the wisdom, health and strength to undertake this research task and enabling me to its completion

# Abstract

The Al-Mg-Si alloys have been widely used for automobile body panels due to the attractive advantages such as excellent formability, high corrosion resistance. Especially, they can be strengthened by age-hardening during paint baking at 443K for 1.2 ks in practical processes. However, unavoidable natural aging at an ambient temperature due to shipping and storage deteriorates the age-hardening response. It is called as negative effect of two-step aging. In order to avoid this phenomenon, the nanoclusters formed by aging should be clarified because some of them act as a precursor of β" which is strengthening phase. In the present thesis, the nature of nanoclusters and its dependence on alloy composition and aging conditions are examined by three-dimensional atom probe (3DAP), differential scanning calorimetry (DSC) and hardness measurements. The correlation between nanocluster characteristics investigated by the 3DAP analysis and two-step aging behavior is also discussed. Finally, the more detailed model for two-step aging behavior and optimum nanocluster control conditions are proposed.

DSC is greatly useful technique to identify nanocluster formation. Therefore, the formation behavior of nanoclusters in the Al-Mg-Si alloys with different Mg and Si compositions is investigated using DSC analysis. Two overlapped exothermic peaks indicating Cluster (1) and Cluster (2) formation are clearly detected using DSC analysis in all examined alloys and separated using a Gaussian function method. The peak area was obtained by each separated exothermic peaks and it corresponds to volume fraction of the formed nanoclusters. As a results, the most favorable Mg/Si ratio of the alloys was 1.0 in terms of the Cluster (1) and Cluster (2) formation, which is lower than that of equilibrium β-($Mg_2Si$).

3DAP is powerful technique to directly observe and characterize the nanoclusters. Therefore, the nature of nanoclusters and its dependence on alloy composition, aging temperature and time can be investigated using 3DAP analysis. It was found that the internal composition of nanoclusters is closely dependent on alloy compositions. Namely, the high Mg containing alloy produces more Mg-rich clusters. As a new finding, Cluster (1) and Cluster (2) were composed of the Mg-rich clusters, Mg-Si clusters and Si-rich clusters regardless of the alloy compositions. In addition, the fraction of three types of nanoclusters was different depending on the aging temperature and time.

In the previous approach, Cluster (1) is formed by natural aging at room temperature and leads to retarding of age-hardening response during artificial aging at 44K, while Cluster (2) formed by pre-aging at around 373K increase hardness promptly. However, new approach applying for the new categorization obtained by the 3DAP analysis is needed. Based on the results of two-step aging behavior, the Mg/Si ratio of the alloys greatly affects to the two-step aging, especially, the negative effect caused by natural aging becomes larger in high Si

containing alloys. It was also found that the two-step aging behavior is determined by the fraction of the Mg-Si clusters and Si-rich clusters regardless of aging temperature.

The quenched-in excess vacancies are also significant factor to help the nanocluster formation in initial stage of aging. The Al-Zn-Mg alloy was considered as a comparison target of Al-Mg-Si alloy because they have a different quench sensitivity and two-step aging behavior. In the Al-Mg-Si alloy, it is likely to form the Si-vacancy complex after step-quenching (SQ). However, in the Al-Zn-Mg alloy, it is likely to form the dislocation loops and/or vacancy aggregation by absence of Si atoms. This dislocation loop acts as the annihilation point of vacancies as well as the source of vacancy supply into the matrix.

In practical field, the bake-hardening (BH) treatment was generally performed at 433K for 1.2 ks. The natural aging before the BH treatment leads to the insufficient the BH response. Also, as prolonged natural aging time, the BH response was greatly reduced by reversion of pre-formed clusters. It was found that the reversion phenomenon is only observed after long-term natural aging in high Si containing alloy, which has a lot of unstable Mg-Si clusters.

In conclusion, this is the first challenge in the field of the Al-Mg-Si alloy that the cluster categorization based on the 3DAP results. It allows us for better understanding a correlation between the cluster fraction and two-step aging behavior. In addition, the dependence of alloy compositions and aging conditions on the nanocluster formation was clarified. Based on these results, the more detailed model for the two-step aging behavior and optimum nanocluster control conditions were proposed. These research achievements contribute to the practical fields by the precise nanocluster and two-step aging control.

# Table of Content

# Chapter 1.
# General Introduction

## 1.1 Background

Global society faces important challenge to shift human economic activity and lifestyles to a sustainable path, including meeting threats from climate change. Global warming, aside from environmental pollution is one of scientist's biggest concerns and this is a huge problem that we must solve. As the automobile consumption and production rates increase, the world is currently facing an energy crisis, such as running out of fossil fuels. However, this problem can be resolved by improving the fuel efficiency of automobiles. One of the possible alternatives in achieving the high fuel efficiency is to decrease the weight of the automobile without sacrificing safety and performance. The light-weighting of automobile parts is most effective method to reduce exhaust gas such as $CO_2$ and NOx and directly connected to an environmental improvement and prevention of global warming. Aluminum alloys have been in the spotlight as materials leading automotive and transportation innovation due to their excellent characteristics as follows:

- Reduced Weight (fuel-efficient, perform better, easy to handle)
- Excellent Formability (extremely workable, wide range of shapes)
- High Strength (support vehicle structure, safety for passengers)
- Resistance to Corrosion (naturally formed impermeable aluminum oxide coating)
- Recyclability (ecologic advantages and environmentally sustainable)

## 1.2 Aluminum Alloys and 6xxx Series Alloys in the Automobile Industry

In the past, the usage of aluminum alloys for vehicle applications has limited to powertrain (i.e. heat exchanges, engine blocks and transmissions) [1]. However, recently, aluminum alloys have greatly expanded to structural components (i.e. bumpers, frames) and body panels (i.e. engine hoods, trunk lid and door) [2,3]. Wrought aluminum alloy can be classified into non-heat treatable alloys and heat treatable alloys according to adding elements as below:

- Non-heat treatable alloys
  - 1xxx Aluminum (99.000%, minimum)
  - 3xxx Al-Mn alloys
  - 4xxx Al-Si alloys
  - 5xxx Al-Mg alloys
- Heat treatable alloys
  - 2xxx Al-Cu alloys
  - 6xxx Al-Mg-Si alloys
  - 7xxx Al-Zn-Mg alloys

The heat treatable alloys are composed of Al-Cu (2xxx), Al-Mg-Si (6xxx), Al-Zn-Mg (7xxx) alloys, and can be strengthened by age-hardening.

Al-Mg-Si alloys (6xxx series aluminum alloys) have been extensively used for body panels of automobiles due to the attractive properties, such as good formability which is required for press-forming process and high corrosion resistance. The representative commercial 6xxx alloys are described in Fig. 1.1. The magnesium and silicon contents of 6xxx alloys vary depending on their material properties such as extrusion ability, mechanical property and quenching sensitivity. These Al-Mg-Si alloys have a unique advantage such as paint bake response, which is increment of yield strength (or hardness)

caused by paint baking. In general, conventional paint baking is performed at around 170 °C for 1.2 ks after press-forming in the automobile manufacturing process, resulting in improving the mechanical strength due to their significant precipitation hardening.

## 1.3 Age-hardening Characteristic in 6xxx Series Alloys

### 1.3.1 Precipitation Sequence

Figure 1.2 shows the equilibrium phase diagram of the Al-Mg-Si ternary system [4]. There exists quasi-binary line of chemical compound, which is refer to $Mg_2Si$. The phase diagram of quasi-binary Al-$Mg_2Si$ alloys is described in Fig. 1.3 [5]. Therefore, the Al-Mg-Si ternary commercial alloy can be considered as quasi-binary Al-$Mg_2Si$ alloys. The maximum solubility of $Mg_2Si$ in the Al matrix at 595 °C is approximately 1.85 wt.% (1.14%Mg, 0.66%Si) [6]. However, this solubility of Mg and Si is rapidly reduced as decreased temperature. The age-hardening in Al-Mg-Si alloys occurs in accordance with the variation of solubility. The precipitation sequence generally accepted in Al-Mg-Si alloys is as follows [7-10]:

- Balanced alloy

  SSSS → nanoclusters → β'' → β' → β-($Mg_2Si$) (1.1)

- Excess Si alloy

  SSSS → nanoclusters → β'' → β', U1, U2, B' → β-($Mg_2Si$) / Si (1.2)

where SSSS is the super saturated solid solution and the U1, U2 and B' phases refer to type A, B and C, respectively. All phases, except for the β-($Mg_2Si$) and Si, are metastable. The nanoclusters refer to aggregation of Mg and Si solute atoms without specific structures. The formation and growth mechanisms of nanoclusters must be fully

understood, because they play an important role as a precursor of the β″ phase. The detailed feature of nanoclusters in the literatures will be discussed in the next section.

The β″ is strengthening phase in Al-Mg-Si alloys, resulting in attainment of peak-aged condition [11]. The β″ phase is needle-like coherent precipitate, which is monoclinic along the <100> direction of the Al planes with lattice parameters of a=1.516 nm, b=0.405 nm and c=0.674 nm and an angle between a and c of 105.3° [11-13]. Andersen et al. have proposed that the composition of the β″ phase is approximately $Mg_5Si_6$ using the high resolution electron microscopy (HREM) and electron diffraction (ED) [12]. However, from the atom probe tomography results, Serizawa et al. reported that the Mg/Si ratio inside β″ phase can be greater than 1.0 [14]. Hasting et al. [15] proposed that the all possible composition of the β″ phase using calculation of enthalpy, which is good agreement with the atom probe tomography (APT) experimental results. They concluded that the $Mg_5Al_2Si_4$-β″ phase is more favorable due to the replacement of $Si_3$ position with Al in the $Mg_5Si_6$ model. Recently, Ninive et al. [16] suggested that the most favorable composition of β″ is $Mg_4Al_3Si_4$ as a result of high-angle annular dark field scanning transmission electron microscopy (HADDF-STEM). Otherwise, the results of calculation based on density functional theory (DFT) indicated that $Mg_5Al_2Si_4$ is more stable than $Mg_4Al_3Si_4$.

The rod-shaped β' is similar to the morphology of β″ and grows along the <100> direction of Al planes. It has a hexagonal structure with lattice parameter of a=0.705 nm and c=0.405 nm [13, 17] and more stable than the β″ phase thermodynamically. From the TEM results, larger-sized β' can be observed with a length of ~500 nm [18].

### 1.3.2 Clustering

Pashley et al. [19] first proposed a model taking into account the solute atom clusters

and Dutta et al. [20] support this result based on Differential Scanning Calorimetry (DSC). Gupta et al. [21] reported that two overlapped peaks associated to clustering were found in temperature range between 20 °C and 100 °C. They have shown that the C1 and C2 peaks are regarded as Si-rich co-clusters and Mg-rich co-clusters. It can be explained that there is no observation of clustering peaks in binary Al-Si and Al-Mg alloys. Yamada et al. [22] also reported that the possible existence of two types of clusters (indicated as Peak (1) and Peak (2)) based on adiabatic calorimetry as shown in Fig. 1.4. They suggested that these clusters are competitively formed and refer to Si-rich clusters and Mg-Si clusters, respectively.

As appearance of developed instrument such as the three-dimensional atom probe (3DAP), the formation of nanoclusters in Al-Mg-Si alloys are directly observed [14, 23, 24]. Edwards et al. [23] found the presence of separated Si-clusters, Mg-clusters and Mg-Si co-clusters after aging at 70 °C. They also reported that the Mg/Si ratio of Mg-Si co-clusters are close to 1.0. However, clustering during natural aging at RT was not investigated in their research. Murayama et al. [24] revealed that the presence of Mg-Si co clusters as well as separated Si and Mg atom clusters after long-term natural aging. After that, Serizawa et al. [14] proposed the characterization of the two types of nanoclusters, which are designated as Cluster (1) and Cluster (2) as shown in Fig. 1.5. Cluster (1) and Cluster (2) are defined as the clusters formed at around room temperature and 100 °C, respectively. Figure 1.6 shows (a) average size and (b) Mg/Si ratio of Cluster (1) and Cluster (2) formed at RT and 373 K (100 °C) as a function of aging time. They proposed that the Cluster (1) and Cluster (2) have a different growth mechanism, composition as well as formation temperature. In Fig. 1.6 (a), Cluster (1) is hardly grow, whereas Cluster (2) remarkably increase in size. In addition, in Fig. 1.6 (b), the chemical composition of Cluster (1) represents the Si-rich clusters at the early stage of NA and incorporated by Mg at the longer NA time, whereas the Mg/Si ratio of Cluster (2) approaches a certain value of approximate 1.67, which would represent the similar value

of the $\beta$" phases.

### 1.3.3 Role of Quenched-in Excess Vacancies

The excess vacancies induced by solution heat treatment (SHT) help diffusion to form solute-clusters in the initial natural aging time [25]. Therefore, the quenched-in excess vacancies affect significantly the entire precipitation sequence and behavior. According to the previous literatures, it was believed that there are three essential mechanisms for excess vacancies supplied by rapid quenching from high temperature [26-28]. First, under the "vacancy pump model", the excess vacancies are simply annihilated by diffusion (concurrently help to diffuse solute atoms), finally arrive at the thermal equilibrium state [26]. Second, the "vacancy trapping model" means that once solute atom and vacancy encounter each other, it's hard to detach due to the attractive interaction energy between solutes and vacancies [27]. Third, the secondary defects such as dislocation loops and vacancy aggregation can be formed [28]. In recent years, there has been an increasing interest in studies about vacancies and solute clustering inside Al alloys by using the muon spin relaxation and positron annihilation spectroscopy [29,30]. Wenner et al. [29] found that the Mg-Si clusters trap and keep vacancies inside the material during aging. This trapping may be deeply associated with solute-clustering during NA. Liu et al. [30] reported that after quenching there are two types of positron traps such as vacancy-related defects and vacancy-free solute clusters. Namely, the vacancies are retained by binding into the solute-vacancy complexes and transport solute atoms to emerging clusters.

### 1.3.4 Two-Step Aging Behavior

The schematic illustration of the current manufacturing process for the automotive body panels is described in Fig. 1.7. The sheets of Al-Mg-Si alloys are solution treated at

aluminum company and normally transported to automobile company. During this shipping, these sheets are exposed at room temperature for a certain long time before the paint baking process. This phenomenon is deeply associated with "*Negative effect of two-step aging*" caused by the formation of clusters during natural aging (NA) and firstly proposed by Pashley et al. [18]. That is, the complicated changes of the nano- or micro-scale structures in the Al matrix such as nanoclusters or G.P. zones during NA can affect the two-step aging behavior. As shown in Fig. 1.8, Yamada et al. [22] and Serizawa et al. [14] conclude that "*negative effect of two-step aging"* can be explained by the different characteristics of Cluster (1) and Cluster (2). Cluster (1), i.e. Si-rich cluster, is not transformed into the β" phases due to its high thermal stability. Cluster (2), i.e. Mg-Si cluster, can easily transfer into the β" phase based on its compositional similarity with the β" phase. However, the two-step aging behavior has complexity depending on the alloy compositions and natural aging time. Figure 1.9 shows the influence of natural aging on tensile strength after artificial aging at high temperature with various Mg and Si contents [31]. It is noted that the "*Negative effect of two-step aging*" can be seen in higher Mg and Si contents extensively. However, the natural aging causes "*Positive effect of two-step aging*" in lower Mg and Si contents. This is also confirmed by Chang et al. [32]. In addition, the degree of "*Negative effect of two-step aging*" is greatly affected by the Mg and Si contents. It is not fully understood and investigated which factor is essential to determine these phenomena. There remains problem to overcome, i.e. natural aging time-dependence on two-step aging behavior. Kim et al. [33] recently reported that there are three stages of two-step aging with natural aging time as shown in Fig. 1.10. It can be explained that the different types of nanoclusters are formed during natural aging such as Cluster (1), i.e. Si-rich cluster, and Mg-Si co-cluster. Based on these results, it must suggest improved idea and model for two-step aging behavior considering alloy composition- and natural aging time-dependence.

## 1.4 Objectives of Present Thesis

The present thesis mainly discusses the alloy composition, aging temperature and time dependence on age-hardening response, especially nanocluster formation in the early stage of decomposition using hardness, electrical resistivity, DSC measurements and 3DAP analysis. In addition, it will be reveal that the correlation between the nanocluster formation and two-step aging behavior. The aims of the present thesis are as follows:

- To clarify the formation behavior of nanoclusters using DSC with different Mg and Si compositions, i.e. volume fraction, kinetics, alloy composition influence on the nanocluster formation.
- To investigate the nature of clusters (their composition and size) and alloy composition, aging temperature and time-dependence of clusters: proposal of new categorization of clusters based on 3DAP results.
- To investigate the two-step aging behavior in alloys with the different Mg/Si ratio and correlation between the cluster categorization and two-step aging behavior: proposal of more detailed model for two-step aging behavior.
- To investigate the influence of quenched-in excess vacancies on the nanocluster formation and two-step aging behavior in Al-Mg-Si alloys: influence of quenching conditions, examination of the role of Si contents in comparison with an Al-Zn-Mg alloy.
- To evaluate the bake-hardening response (443K, 1.2 ks) after long-term natural aging in the viewpoint of reversion and thermal stability of pre-formed nanoclusters: proposal of optimized conditions for the nanocluster control.

## 1.5 Outline of Present Thesis

The schematic outline and conceptual framework in the present thesis is shown in Fig. 1.11 and Fig. 1.12.

The importance and necessity of the study on nanocluster characteristics is introduced in **Chapter 1** ***"General Introduction"***. In addition, the objective of the present thesis is described based on the recent problem and situations in the material science and industry.

The formation behavior of nanoclusters using mainly DSC analysis with different Mg and Si compositions of alloy is investigated in **Chapter 2** ***"Formation Behavior of Nanoclusters with Various Mg and Si Compositions"***. The evaluation of volume fraction, kinetics of clustering at lower temperature as well as alloy composition dependence on the nanocluster formation are discussed.

The nature of nanoclusters and its dependence on alloy composition, aging temperature and time are investigated in **Chapter 3** ***"Three-dimensional Atom Probe Analysis of Solute Clusters Formed in Natural- and Pre-Aged Alloys with Different Mg/Si Ratio"***. A new categorization of clusters is proposed in order to explain the two-step aging behavior based on 3DAP results.

The two-step aging behavior of the alloys with different Mg/Si ratios and the correlation between cluster categorization and two-step aging behavior are described in **Chapter 4** ***"Influence of Mg/Si Ratio and Natural- and Pre-Aging on Two-step Aging Behavior"***. A new model for the two-step aging is proposed by taking into consideration of the alloy composition, aging temperature and time.

The influence of quenching conditions on nanocluster formation and two-step aging behavior in Al-Mg-Si alloys are investigated in **Chapter 5** ***"Influence of Quenched-in Excess Vacancies on Nanocluster Formation and Two-step Aging"***. The role of

quenched-in excess vacancies and Si atoms is discussed in comparison with the Al-Zn-Mg alloy which does not contain Si.

The bake-hardening response after long-term natural aging and influence of the Mg/Si ratio are investigated in **Chapter 6** ***"Influence of Cluster Characteristics and Its Thermal Stability on Bake-hardening Response"***. The reversion and thermal stability of nanoclusters are discussed. In addition, the optimized conditions for the nanocluster control are proposed to apply to the industrial field.

Finally, the overall results and research achievements obtained from **Chapter 2** to **Chapter 6** are summarized in **Chapter 7** ***"General Conclusions"***.

## References


[1] *The Aluminum Association*. (n.d.). Retrieved May 24, 2013, from http://www.aluminum.org

[2] *Manufacturing in China: pa-international.com.au*. (n.d.). Retrieved from http://www.pa-international.com.au

[3] Study: Aluminum Best Material to Shed Vehicle Body Mass, Boost Fuel Economy [Audio podcast]. (2013, May 2). Retrieved from http://www.drivealuminum.org

[4] (社)軽金属学会: アルミニウムの組織と性質 (1991)

[5] (社)軽金属学会: アルミニウムの製品と製造技術 (2001)

[6] ASM Handbook: Vol.2, Properties and Selection: Nonferrous Alloys and Special-Purpose Materials, ed. J.R.Davis (1990), 32.

[7] G.A. Edwards, K. Stiller, G.L. Dunlop and M.J. Couper: Acta Mater. 46 (1998) 3893.

[8] K. Matsuda, Y. Sakaguchi, Y. Miyata, Y. Uetani, T. Sato, A. Kamio and S. Ikeno: J. Mater. Sci. 35 (2000) 179.

[9] S.J. Andersen, C.D. Marioara, A.G. Frøseth, R. Vissers and H.W. Zandbergen: Mater. Sci. Eng. A 390 (1-2) (2005) 127.

[10] C.D. Marionara, S.J. Andersen, H.W. Zandbergen and R. Holmestad: Metall. Mater. Trans. A, 36 (2005) 691.

[11] C.D. Marionara, S.J. Andersen, J. Jansen, H.W. Zandbergen: Acta Materialia, 51 (2003) pp. 789-796.

[12] S.J. Andersen, H.W. Zandbergen, J. Jansen, U. Tundal, O. Reiso: Acta Materialia, 46 (1998) pp. 3283-3298.

[13] J.P. Lynch, L.M. Brown, M.H. Jacobs: Acta Metallurgica, 30 (1982) pp. 1389-1395.

[14] A. Serizawa, S. Hirosawa, T. Sato: Metallurgical and Materials Transactions A, 39 (2008) pp. 243-251.

[15] H.S. Hasting, A.G. Froseth, S.J. Andersen, R. Vissers, J.C. Walmsley, C.D. Marioara, F. Danoix, W. Lefebvre, R. Holmestad: Journal of Applied Physics, 106, 123527 (2009).

[16] P.H. Ninive, A. Strandlie, S. Gulbrandsen-Dahl et al.:Acta Materialia, 69 (2014) pp. 126-134

[17] M.H. Jacobs: Philosophical Magazine, 26 (1972) pp. 1-3.

[18] C.D. Marioara, H. Nordmark, S.J. Andersen, R. Holmestad: Journal of Materials Science, 41 (2006) pp. 471-478.

[19] D.W. Pashley, J.W. Rhodes and A. Sendorek: J. Inst. Metals, 92 (1966) 41-49.

[20] I. Dutta and S.M. Allen: *J.Mater. Sci. Lett.*, 10 (1991) 323-326.

[21] A.K. Gupta, D.J. Lloyd: Metallurgical and Materials Transactions A, 13 (1999) pp. 879-884.

[22] K. Yamada, T. Sato, A. Kamio: Journal of Japan Institute of Light Metals, 51 (2001) pp. 215-221.

[23] G.A. Edwards, K. Stiller, G.L. Dunlop: Applied Surface Science 76/77 (1994) pp. 219-225.

[24] M. Murayama, K. Hono: Acta Mater. 47(5) (1999) pp. 1537

[25] J. Banhart, M.D.H. Lay, C.S.T. Chang, A.J. Hill, Physical Review B, 83 (2010), pp. 1-13.

[26] L.A. Girifalco and H. Herman, Acta Met. 13, 583 (1965)

[27] H. Kimura, R.R. Hasigute: Acta Metall. 16 (1975), pp. 361-368.

[28] 鈴木寿，菅野幹宏，伊藤吾朗　日本金属学会会報 24(1985)102.

[29] S. Wenner, K. Nishimura, K. Matsuda et al. Metallurgical and Materials Transactions A, 45A (2014) pp. 5777-5781.

[30] M. Liu et al.:Acta Materialia 91 (2015) pp. 335-364

[31] J. langerweger: Proc. Aluminium Technology (1986) Paper No. 49.

[32] C.S.T. Chang, I. Wieler, N. Wanderka and J. Banhart: Ultramicroscopy, 109 (2009) pp. 585.

[33] J. Kim, E. Kobayashi, T. Sato: Materials Transactions, Vol. 56, No. 11 (2015) pp. 1771-1

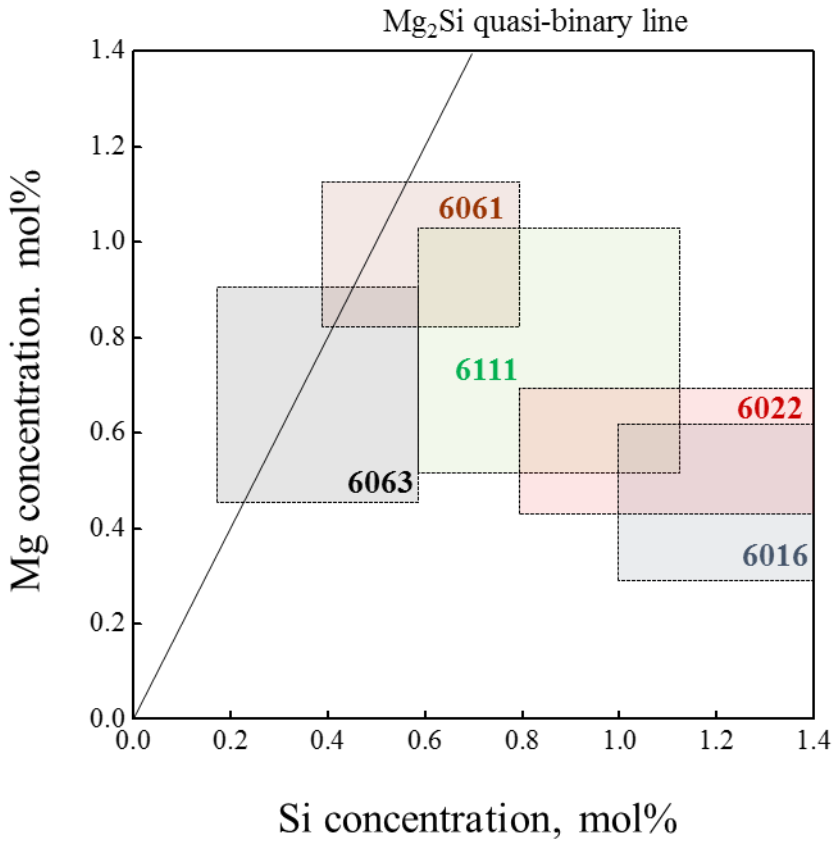


Figure 1.1 The limits of Mg and Si concentration (mol%) for the representative commercial 6xxx alloys.

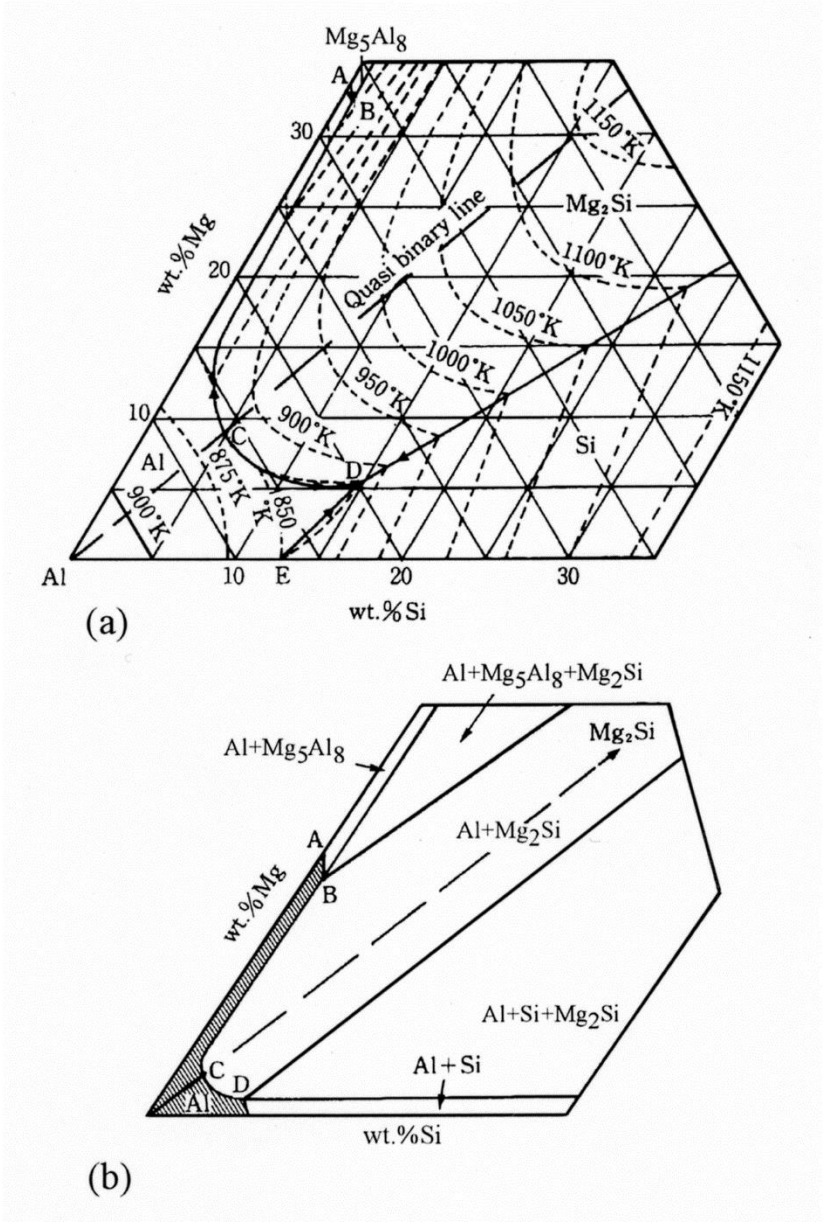


Figure 1.2 Equilibrium phase diagram of the Al-Mg-Si ternary system [4].

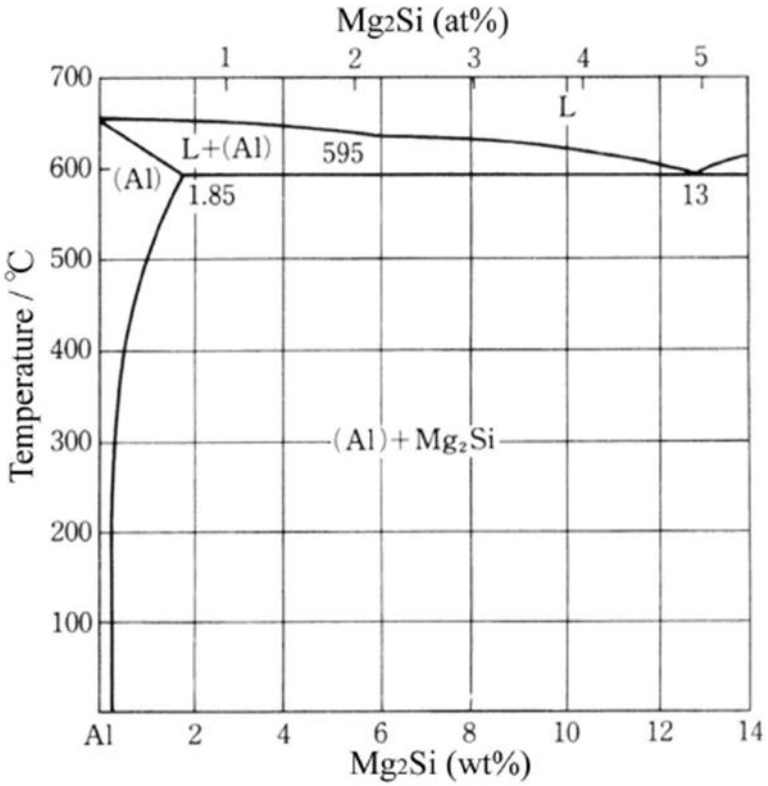


Figure 1.3 Al-$Mg_2Si$ quasi-binary phase diagram [5].

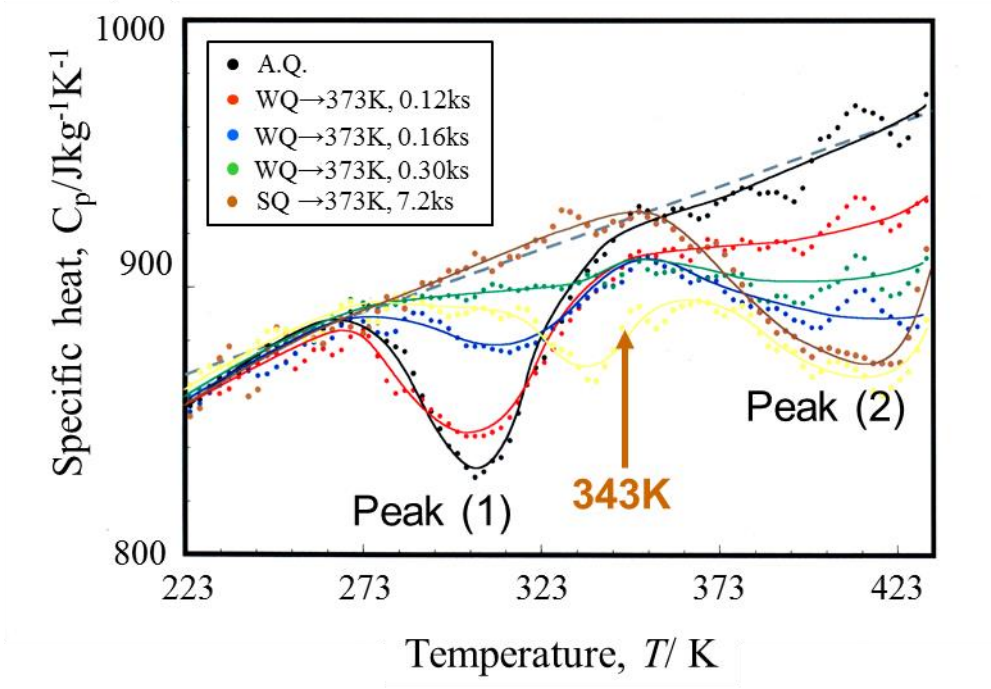


Figure 1.4 Two exothermal peaks obtained by adiabatic calorimetry measurements with different heat treatment pathway in Al-1.4%$Mg_2Si$-0.3Si (mass%) alloy [22].

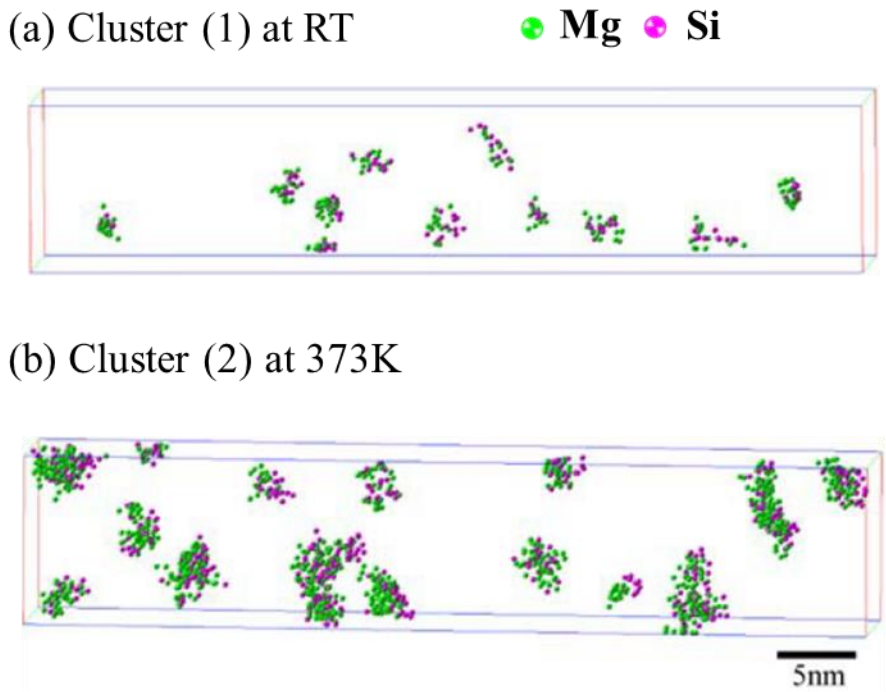


Figure 1.5 Three-dimensional atom probe map of two types of nanoclusters obtained by the maximum separation method in Al-0.95%Mg-0.81%Si (mass%) alloy [14].
(a) Cluster (1) in the naturally aged alloy at RT for 604.8 ks
(b) Cluster (2) in the aged alloy at 373 K for 604.8 ks

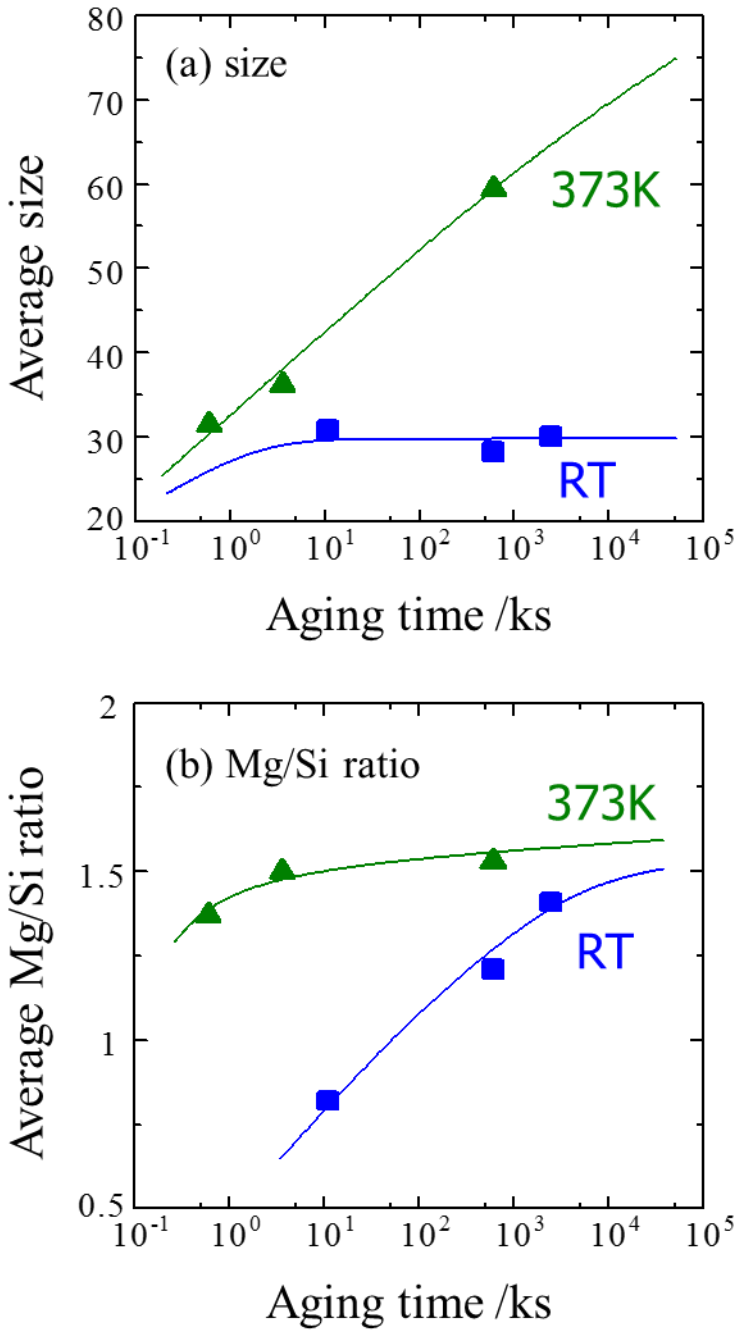


Figure 1.6 3DAP analysis results for (a) Average size and (b) Mg/Si ratio of Cluster (1) and Cluster (2) formed at RT and 373K in Al-0.95%Mg-0.81%Si (mass%) alloy as a function of the aging time [14].

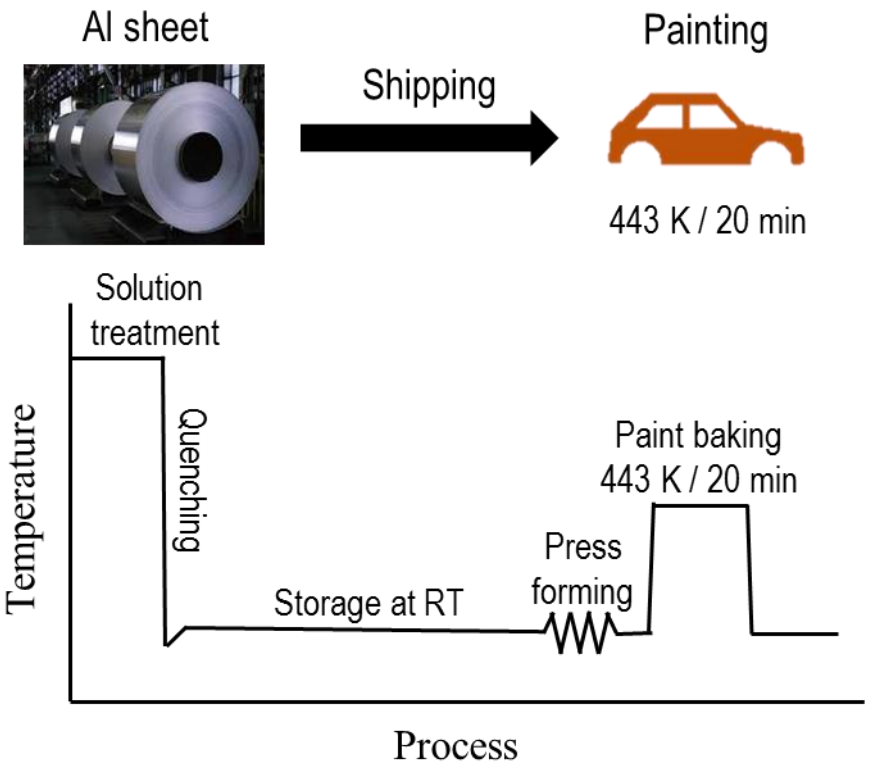


Figure 1.7 Schematic illustration and temperature profile during a manufacturing process from Al sheet to automotive body panels.

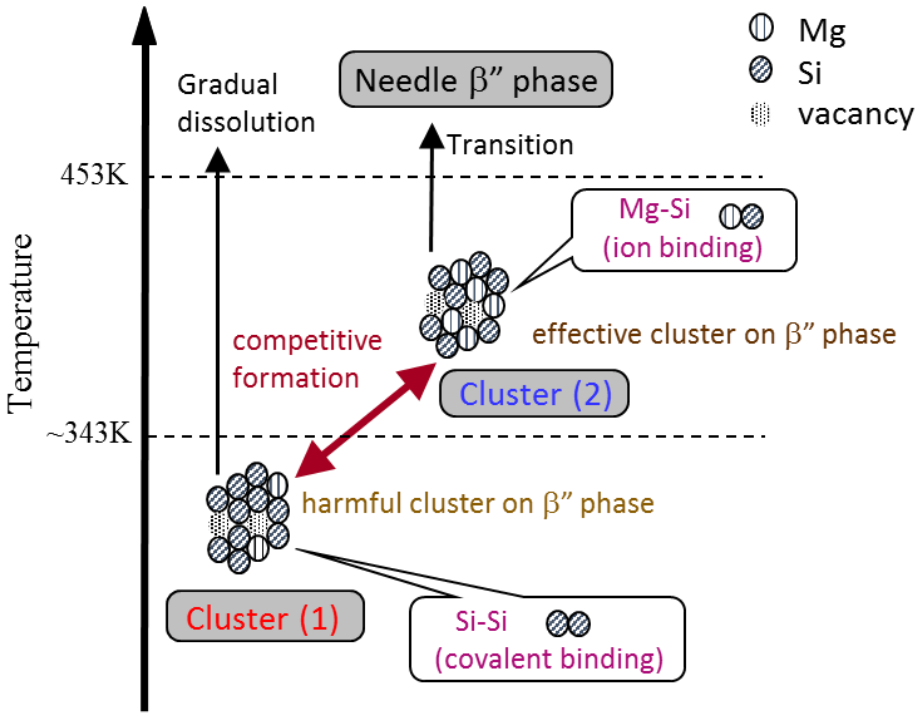


Figure 1.8 Previous proposed model for two-step aging behavior of Al-Mg-Si alloys, showing the characteristics of Cluster (1) and Cluster (2) and those transition behavior into needle β"-phase [22].

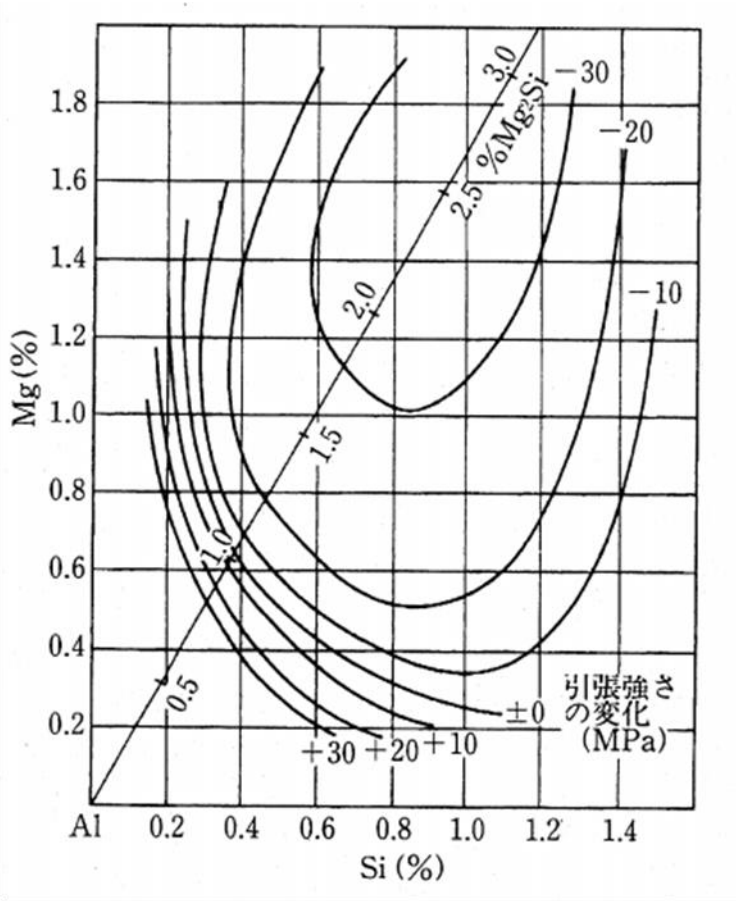


Figure 1.9 Influence of natural aging on tensile strength (MPa) after artificial aging at higher temperature in Al-Mg-Si alloys with various Mg and Si contents [31].

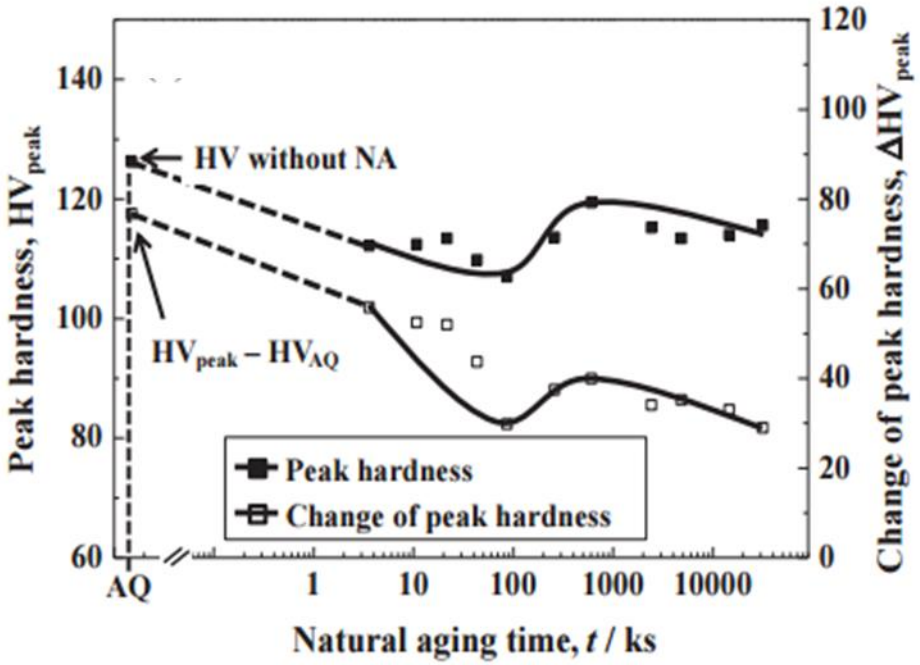


Figure 1.10 Peak hardness during two-step aging at 443K with natural aging time in Al-0.61Mg-0.98Si (mass%) alloy. $HV_{AQ}$ and $HV_{peak}$ refer to the hardness at the as-quenched condition and peak hardness [33].

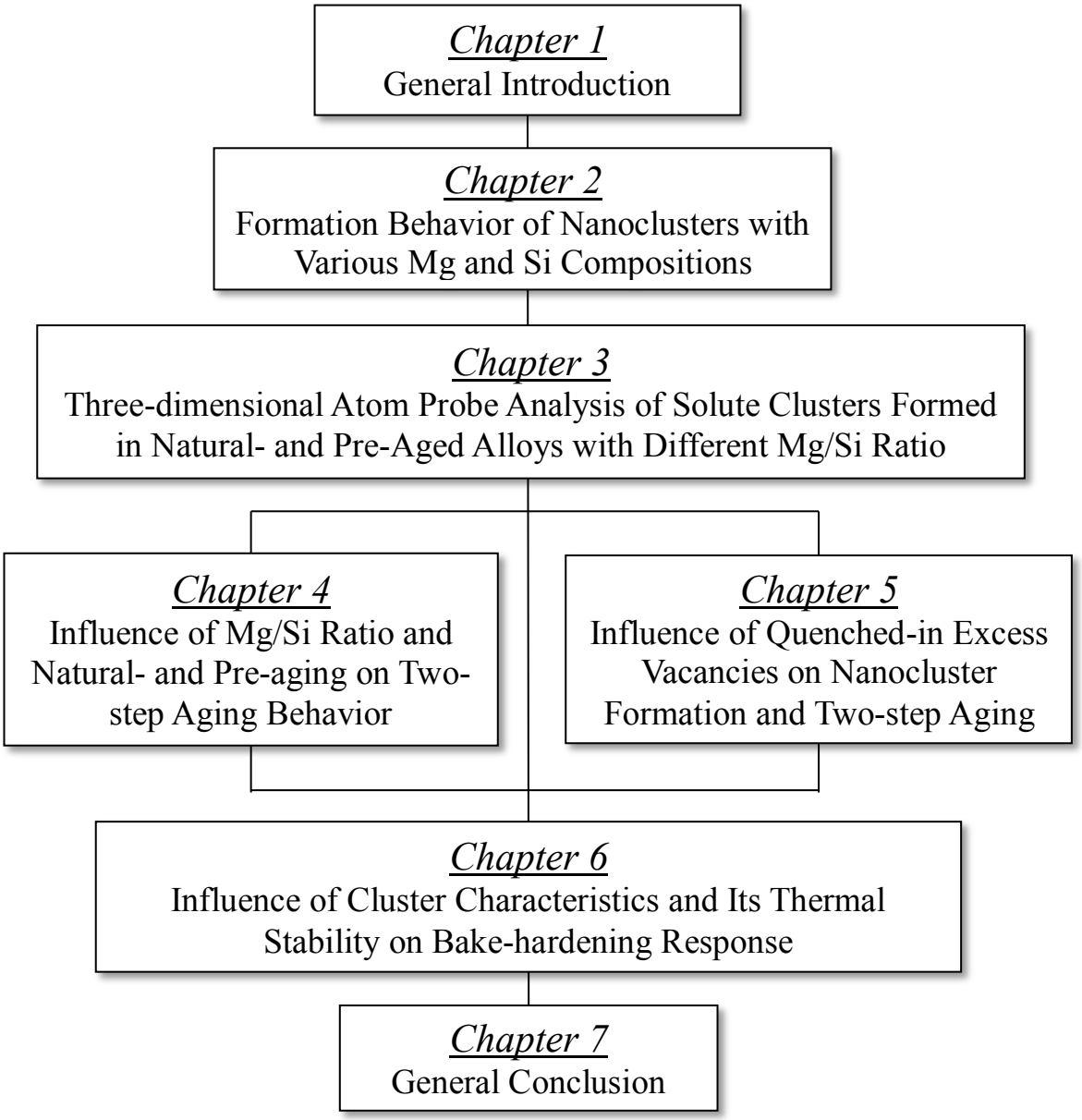


Figure 1.11 Schematic outline of the present thesis.

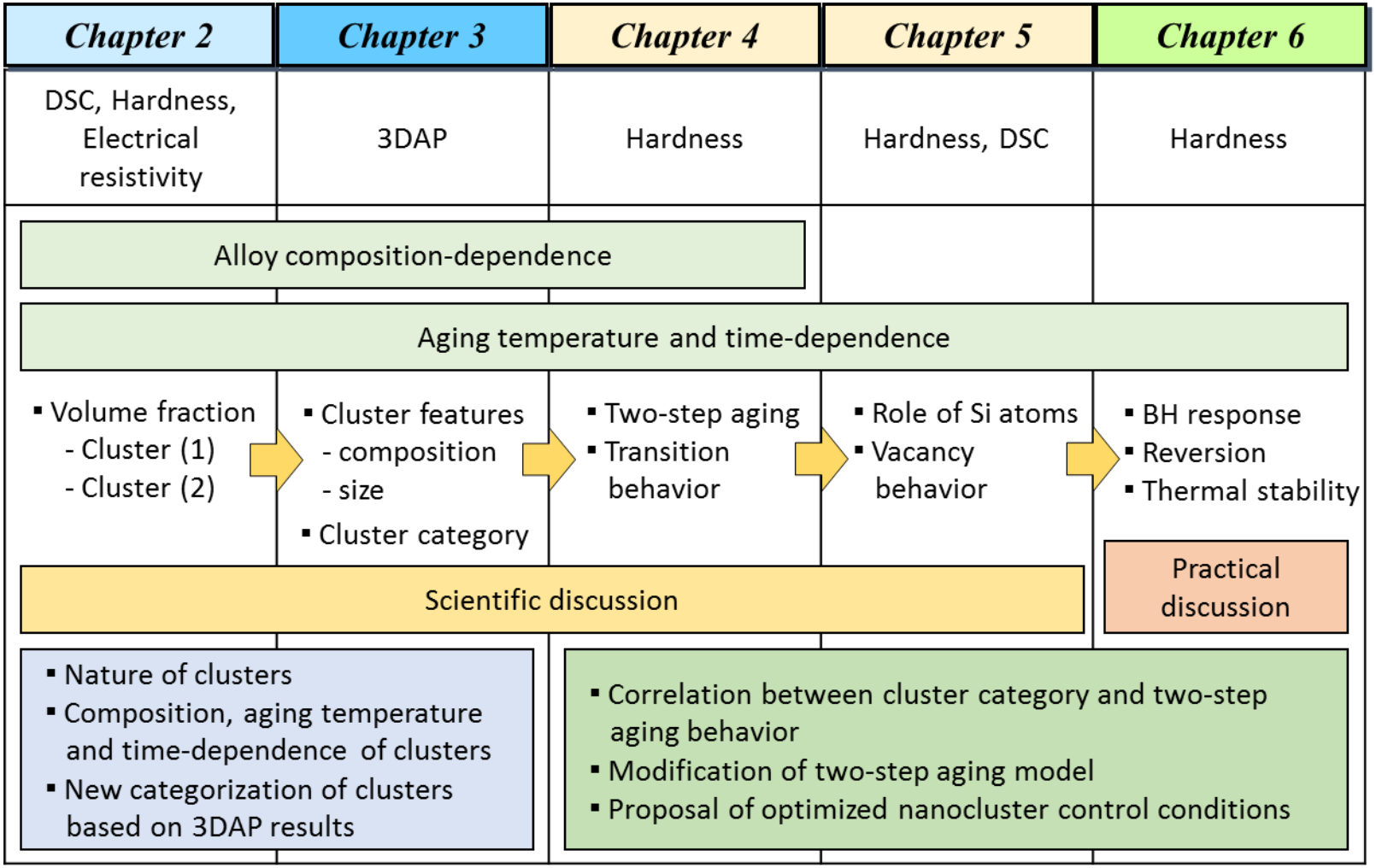


Figure 1.12 Conceptual framework for the whole experimental results in the present thesis.

# Chapter 2.
# Formation Behavior of Nanoclusters with Various Mg and Si Compositions

## 2.1 Introduction

As introduced in the previous **Chapter 1**, it is important to make clear the formation behavior of nanoclusters formed at the early stage of the phase decomposition in Al-Mg-Si alloys. There are several methods to investigate the nanocluster formation in Al-Mg-Si alloys [1-7]. One of the methods, DSC analysis are mainly focused in the present **Chapter 2**, which is well known as the useful instruments to detect the fine structure change such as clustering. The kinetics and thermodynamic information can be also obtained by the peak area and peak temperature from DSC curves. However, until now, the precipitation of the β" phase identified at a higher temperature range have been extensively investigated because the nanocluster peak is difficult to detect and showed the multiple overlapped peaks. In this chapter, DSC analysis were carried out by the optimized conditions to clearly detect the nanocluster peaks. The Gaussian function method will be applied to separate the multiply overlapped peaks, resulting in the possibility of quantitative analysis for the individual nanocluster formation. Therefore, the aims of the present chapter are to clarify the formation behavior of nanoclusters using DSC, hardness and electrical resistivity measurements in the alloys with different Mg and Si compositions and to evaluate the alloy composition dependence on nanoclusters in terms of volume fraction and activation energy. In addition, the optimum alloy composition for the formation of nanoclusters will be discussed based on the overall results.

## 2.2 Experimental Procedure

### 2.2.1 Alloy Compositions

The numerous Al-Mg-Si alloy samples with different Mg (0.31 to 0.93 mass%) and Si (0.18 to 1.17 mass%) contents were manufactured as shown in Fig. 2.1. Most of the alloys were located with the concentration close to those of commercial 6xxx alloys represented by shaded areas. The letters of M and S in the first column are abbreviation of Mg and Si. The number in front of M and S represents mass% of Mg and Si, respectively. These alloys were manufactured by the DC-cast, and cooled from an elevated temperature and naturally aged to a substantially stable condition. Then, these billets were extruded to plates with the 2 mm in thickness at 500 °C at Sumitomo Light Metal company (now, UACJ). The provided plates were cold-rolled to 1.3 mm in thickness at laboratory scale. Additionally, 9M6S, 8M7S, 7M8S, 6M9S, 5M10S and 3M12S alloys were manufactured as needed in Kobe Steel, Ltd. These alloys were made by the DC-cast, homogenized and hot and cold-rolled to 1.3 mm thick sheets.

Two types of systematic approaches were considered in order to investigate the influence of Mg and Si contents on the nanocluster formation. The chemical compositions (mol%) of the examined Al-Mg-Si alloys are listed in Table 2.1. The weight percent (mass%) is converted to mol% for precise evaluation of the atomic composition ratio. The location of Mg and Si concentration of the examined Al-Mg-Si alloys are described in Fig. 2.2. The blue and red shaded areas (see Fig. 2.2(a)) were selected to examine the effect of Mg and Si contents in alloy group within higher solute concentration. Furthermore, green, purple and orange shaded areas (see Fig. 2.2(b)) were selected to reveal the effect of atomic composition ratio on the nanocluster formation when the solute contents (Mg+Si) is 1.1, 1.3 and 1.5 mol%.

### 2.2.2 Heat Treatments

The cold-rolled Al-Mg-Si sheet alloys were solution treated for 1.8 ks in a salt bath furnace at 560 °C with the composition 50% $KNO_3$ and 50% $NaNO_3$, followed by quenching into ice-water at 0 °C for 60 s. This as-quenched state is abbreviated to A.Q. in the present study. These heat-treated alloys were naturally aged at room temperature and pre-aged at 100 °C up to 2419.2 ks (about 1 month) in an oil bath furnace, respectively.

### 2.2.3 Differential Scanning Calorimetry (DSC)

Differential Scanning Calorimetry (DSC) is an effective thermal technique to measure thermodynamics and kinetics of precipitation reactions in materials. Heat flow provides information for exothermic and endothermic reactions as a function of temperature or time. The DSC analysis was carried out using a Rigaku DSC8230 instrument (Rigaku Corporation) under a purified argon gas atmosphere after heat treatment with each different temperature and time path. In order to ensure accuracy of DSC measurements, all data was modified by calibration to remove errors of measurements itself. The reference material for a DSC analysis are made by pure Al with 99.99% purity disc shapes with 30 mg in weight. The Al-Mg-Si alloy specimens were made with the same weight as the reference material. After the specimen has been put into a furnace, the temperature program was designed such that the furnace temperature increases linearly from -50 to 500 °C with the different heating rates of 2, 5, 10, 15 and 20 °C/min. The starting temperature was decreased to -50 °C by a liquid nitrogen controller in order to detect nanoclusters formed at low temperature. In the present study, a heat evolution peak can be observed from an exothermic reaction corresponding to precipitation. DSC can provide not only the temperature at which the reaction occurs with the total heat involved, but also valuable information about the kinetics of the reaction.

### 2.2.4 Micro-Vickers Hardness Measurement

The specimens of 10 × 10 × 1.3 $mm^3$ for the hardness measurement are prepared in this study. Micro Vickers hardness measurements were performed for 15s with a load of 200 g or 300 g using Matsuzawa MMT-X6 with the specimens polished within 0.3 ks after each different aging temperature and time path. Its hardness can be measured from seven indentations, however maximum and minimum values were cut off to measure the average of the hardness.

### 2.2.5 Electrical Resistivity Measurement

All specimens for the electrical resistivity were prepared as a wire with the diameter of 1.0 mm and length of 30 mm. Electrical resistivity is measured at -196 °C using liquid nitrogen by a four-probe method with 120 mA direct current. Electrical resistivity is calculated using the following equation.

$$\rho = \frac{V_m}{I_{st}} \cdot \frac{A}{L} \quad [\Omega m] \qquad (2.1)$$

These symbols $\rho$, $I_{st}$, $A$, $V_m$ *and* $L$ represent resistivity, constant current (120 mA), area of a specimen (7.854 x $10^{-7}$ $m^2$), and gage length (0.3m).

## 2.3 Results

### 2.3.1 Nanocluster Formation Analysis by DSC

DSC results for as-quenched alloys

Figure 2.3 shows DSC results of the as-quenched (a) 9M10S and (b) 5M12S alloys in a heating rate of 10 °C/min as a function of temperature from 0 to 500 °C. The five exothermic peaks (designated by I, III, IV and V) and one endothermic peak II are

observed in both 9M10S and 5M12S alloys. Another exothermic peak designated by VI (nearby 350 °C) in Fig. 2.3 (b) is only observed at 5M12S alloy with excess Si. The exothermic peak I can be found at relatively low temperature range, and this represents the nanoclusters consisted of Mg, Si atoms. The endothermic peak II is formed by partial dissolution of pre-formed nanoclusters in the Al matrix due to its low thermal stability. Edwards et al. [1, 2] and Dutta et al. [3] also reported the existence of nanoclusters by means of DSC and atom probe field ion microscopy (APFIM). The exothermic reactions corresponding to peak III, IV and V refer to the precipitation of the metastable β", β' and the equilibrium β-($Mg_2Si$) phases. Miao et al. [8, 9] and Gupta et al. [10, 11] suggested the consistent results with the present study. The exothermic peak VI can only be observed by excess of Si, and considered as U1, U2 and B' (refer to type A, B and C) reported by Gupta et al. [11] and Matsuda et al [12]. They have also reported that U1, U2 and B' phases have significantly low influence on precipitation hardening. In the present study, the exothermic peak I corresponding to nanocluster formation is mainly treated and discussed, because the nanocluster formation has a significant effect on the precipitation of strengthening β"-phase.

Peak separation using Gaussian function method

The DSC curves for nanoclusters formed between 0 and 150 °C are shown in Fig. 2.4, which corresponds to enhancement of the peak I previously described in Fig. 2.3. Two overlapped exothermic peaks indicated by peak (1) and peak (2) are observed in the 9M10S alloy. However, the 5M12S alloy with excess Si shows slightly different curves, which exhibits three overlapped exothermic peaks including another peak (3). Yamada et al. [13] reported that the two peaks, i.e. peak (1) and peak (2) in this study, were obviously detected by adiabatic calorimetry at the lower temperature. After that, Serizawa et al. [14, 15] found that these peaks have a different characteristic to designate two types of nanoclusters, i.e. Cluster (1) and Cluster (2). There was almost no information about peak (3). However, it is inferred from the correlation with peak (3) and peak VI in Fig. 2.3 (b).

Two and three overlapped peaks were successfully separated by selecting number of peaks and the pinnacle of each peak. The Gaussian function method, utilized to analyze the nanocluster formation quantitatively, is given by the following equation,

$$y = y_0 + \frac{A}{w\sqrt{\pi/2}} e^{-2\frac{(x-x_C)^2}{w^2}} \quad (2.2)$$

where the parameters of $y_0$, $x_c$, w and A are bottom, center, width and area of a peak. Two nanocluster peaks in the 9M10S alloy are divided into the fitted peaks of Cluster (1) and Cluster (2). Three types of nanocluster peaks in the 5M12S alloy with excess Si can be fitted to Cluster (1), Cluster (2) and peaks (3). The R squared value reflects the accuracy of the fit, which is higher than 0.99, indicating the sufficiently good fitting. In the present study, the influence of alloy composition on nanocluster formation is investigated by the parameter of peak area corresponding to the volume fraction of the formed nanoclusters.

### 2.3.2 Effect of Mg and Si Compositions on Nanocluster Formation

DSC results for as-quenched alloys

Figure 2.5 shows DSC results indicating the formation of Cluster (1) and Cluster (2) with the different (a) Si and (b) Mg concentration. Two overlapped exothermic peaks, corresponding to Cluster (1) and Cluster (2), are observed in all examined alloys. It is found that the heat evolution, shape and position of each peak have a tendency to change with the Si and Mg concentration. In order to analyze the dependence of Mg and Si concentration on nanocluster formation, the Gaussian function method (as mentioned in section 2.3.1) was used to separate the exothermic peaks.

Quantitative analysis for nanocluster formation

The nanocluster formation is analyzed by using each parameter of peak area in Cluster (1) and Cluster (2) peaks. In the present study, the peak area is proportional to the volume

fraction of the formed nanoclusters, because it is caused by the heat effect of exothermic reaction.

Figure 2.6 shows the peak area changes for Cluster (1) and Cluster (2) as a function of (a) total concentration (Mg+Si) and (b) Mg/Si ratio of examined alloys. Peak areas gradually increase as the total concentration (Mg+Si) for both cases of Cluster (1) and Cluster (2) and saturate when the total concentration (Mg+Si) is more than 2.0. In addition, the unique characteristic is observed in Fig. 2.6(b), which represents the peak area as the function of Mg/Si ratio of alloys. The peak area is enhanced in the certain Mg/Si ratio of 1.0 in Cluster (1) and slightly distant Mg/Si ratio from 1.0 in Cluster (2). It is noted that the volume fraction of Cluster (1) and Cluster (2) are increased as Mg/Si ratio of alloys approaches to 1.0. In other words, the Mg/Si ratio of alloy composition is a significant factor to control the nanocluster formation.

Hardness and electrical resistivity changes

Figure 2.7 and Figure 2.8 shows the results of (a) hardness and (b) electrical resistivity changes during natural aging in the alloys with different Si and Mg concentration. The hardness and electrical resistivity changes are almost same at the initial stage and subsequently increases, then slow down at longer NA time. The hardness changes are correlated with the strong interaction between nanoclusters and dislocations [16]. The electrical resistivity is strongly affected by the number of solute atoms in the Al matrix and the nanocluster formation behavior [17]. In Fig. 2.7 and Fig. 2.8, the hardness and electrical resistivity increment is much faster and larger in the alloys with higher Si and Mg concentration. It is noted that the large amount of Cluster (1) is formed during NA in the alloys with higher Mg and Si concentration.

Figure 2.9 shows hardness and electrical changes at 1209 ks obtained from Fig. 2.7 and Fig. 2.8 as a function of the Mg/Si ratio of alloy. The hardness and electrical resistivity changes become largest when the Mg/Si ratio of alloy is close to 1.0. These results are in

good agreement with those of DSC as mentioned in Fig. 2.6 (b).

### 2.3.3 Effect of Mg/Si Ratio on Nanocluster Formation

The effect of Mg and Si contents on the nanocluster formation was discussed in the previous section. In this section, the effect of the Mg/Si ratio on the nanocluster formation is discussed when the total concentration (Mg+Si) is 1.1,1.3 and 1.5 mol%.

Quantitative analysis for nanocluster formation

Figure 2.10 shows DSC results corresponding to the formation of Cluster (1) and Cluster (2) in alloys with constant total concentration (Mg+Si) of (a) 1.5, (b) 1.3 and (c) 1.1 mol%. The variation of heat evolution seems to gradually change with the Mg/Si ratio of alloys even though constant total concentration of (Mg+Si). These overlapped peaks are successfully separated by the Gaussian function method as shown in Fig. 2.4.

Figure 2.11 shows peak area of Cluster (1) and Cluster (2) with the total concentration (Mg+Si) as a function of the Mg/Si ratio. These peak areas gradually increase with increasing total concentration of (Mg+Si). Especially, it is interesting that the peak area becomes maximum when the Mg/Si ratio is close to 1.0. It is noted that this tendency becomes more remarkable as higher total concentration of (Mg+Si). In other words, the formation behavior of Cluster (1) and Cluster (2) can be controlled by the Mg/Si ratio of alloys with higher total concentration of (Mg+Si).

In order to investigate the influence of heating rate of the DSC measurement on nanocluster formation, the heating rate was changed to be 2, 5, 10, 15 and 20 °C/min. Figure 2.12 shows that representative DSC result for 7M8S alloy with different heating rate. The rest of alloys with constant total concentration (Mg+Si) of 1.5 mol% was examined in the same method. The Cluster (1) and Cluster (2) peaks as indicated by arrows were shifted to higher temperature with increasing heating rate. Figure 2.13 shows peak area changes for (a) Cluster (1) and (b) Cluster (2) with different heating rate as a

function of the Mg/Si ratio of alloys. It is noted that the volume fractions of Cluster (1) and Cluster (2) are most enhanced when the Mg/Si ratio is close to 1.0, regardless of heating rate.

Reaction kinetics for nanocluster formation

Figure 2.14 shows peak temperature changes for (a) Cluster (1) and (b) Cluster (2) with different heating rate as a function of the Mg/Si ratio of alloys. The peak temperature has a tendency to shift to the lower temperature when the Mg/Si ratio of alloy increases and heating rate is slower. It is noted that the formation of Cluster (1) and Cluster (2) is kinetically controlled by the heating rate. The formation kinetics with the different Mg/Si ratio of alloys can be estimated by derivation of the activation energy, which is the energy barrier required for the formation of nanoclusters. There are several methods to determine the activation energy ($E_a$) for the precipitation process using peak temperature of DSC results, such as Ozawa, Takhor, Kissinger and Starink [18-20]. In the present study, Kissinger method, which has greater tendency to have high accuracy [19], is applied to evaluate the activation energy for the nanocluster formation. The Kissinger equation can be written as:

$$\ln\left(\frac{\gamma}{T_p^2}\right) = -\left(\frac{E_a}{R}\right)\left(\frac{1}{T_p}\right) + C \qquad (2.3)$$

where $\gamma$, $T_p$, $E_a$, $R$ and $C$ represent the heating rate, peak temperature, activation energy, gas constant and a constant, respectively. Figure 2.15 show the plot of $\ln(\gamma/T_p^2)$ as a function of $1000/T_p(K^{-1})$ obtained by Eq. (2.3) for (a) Cluster (1) and (b) Cluster (2). Based on the slope of the plots (given by the least square fitting), the $E_1$ and $E_2$ for Cluster (1) and Cluster (2) with the Mg/Si ratio of alloy were summarized in Table 2.2. The measured $E_1$ and $E_2$ are mostly about 72-90 kJ/mol. Much lower $E_1$ value is shown in the 7M8S alloy (72.83 kJ/mol), whereas $E_2$ value is lowest in the 9M6S alloy (77.02 kJ/mol). Starink [20] reported that the activation energy for the formation of clusters at low temperature are attributed to the migration energy of excess vacancies. In

other words, formation kinetics for nanoclusters is closely related to the interaction energy among Mg/Si/Vacancy.

## 2.4 Discussion

### 2.4.1 Applicability of Gaussian Function Method to Evaluate Nanocluster Formation

The precipitation behavior in the Al-Mg-Si alloys by means of the DSC measurement has been extensively reported in the previous literature [1-3, 10,11,14,15]. They mainly focused on the peak for precipitation observed at the higher temperature, because of difficulty to detect peaks at lower temperatures. In general, the heat flow is susceptible to the starting temperature for the DSC measurement and a heating rate. The starting temperature should be below the beginning of the first reaction in order to detect clear peaks. In this study, an attempt is made to find optimum starting temperature in order to keep the stable state for nanocluster reaction. As a result, the most optimum condition is from -50 °C using a liquid nitrogen controller.

From following study, the various Al-Mg-Si alloys with the different Mg and Si concentration were used to investigate the composition dependence of nanocluster formation using DSC measurements. In the DSC curves, two exothermic peaks were clearly detected, and indicates the formation of nanoclusters in all examined alloys. Two overlapping peaks were identified by a Gaussian function method. Although the assumption of its method for each exothermic peaks is not completely applicable due to the fitting symmetry, the comparison of the quantitative feature of the exothermic peaks is useful to understand the dependence of the nanocluster formation on the alloy composition. The R squared value reflecting the accuracy of the fit is higher as 0.99, which means a perfectly and successfully fit. In addition, the results obtained from the fitted two peaks well correlates the factor of the hardness and electrical resistivity

changes. From following evidences, the present author suggests that the Gaussian function method is more suitable to evaluate the nanocluster formation and useful to investigate the effect of alloy composition on the nanocluster formation.

### 2.4.2 Optimum Alloy Composition for Nanocluster Formation

The various Al-Mg-Si alloys with the different Mg/Si ratio were used in order to verify the influence of the alloy composition on the nanocluster formation. Based on the DSC results in Fig. 2.6 and Fig. 2.11, the formation of Cluster (1) and Cluster (2) is affected by the Mg + Si concentration as well as the Mg/Si ratio of the examined alloys. In addition, it was found that the peak area is enhanced in the certain Mg/Si ratio of 1.0 in Cluster (1) and Cluster (2). The volume fraction distribution for Cluster (1) and Cluster (2) of examined alloys is summarized in Fig. 2.16 based on DSC results. The normalized value by the maximum value represents the size of shaded circles. The arrows indicate the location of binary Al-1.0mol%Mg and Al-1.1mol%Si alloys. The previous research has suggested that the positron lifetime of the quenched-excess vacancies is rapidly decreasing in binary systems, compared to the slight decrease in the ternary system [21]. There is no any detection correlated to the clustering reactions in as-quenched binary systems by DSC [18,19]. It is sorted that the Mg-Mg and Si-Si binding is not favorable from atomistic calculations. However, once Si and Mg are added in Al-Mg and Al-Si alloys, nanocluster peaks are observed as shown in Fig. 2.5. It is most likely that Cluster (1) and Cluster (2) are relevant to high binding energy of Mg-vacancy, Si-vacancy and Mg-Si. In Fig. 2.16, volume fraction of Cluster (1) and Cluster (2) is mostly enhanced when the Mg/Si ratio is close to 1.0 as well as the higher total concentration of (Mg+Si). What is the reason why the most favorable Mg/Si ratio for the nanocluster formation is 1.0? One of possible mechanisms is that the thermodynamically metastable state for the nanocluster formation should be achieved when the matrix concentration approaches to 1.0 in Mg/Si ratio. It is deeply related that the Mg/Si ratio of the thermodynamically

equilibrium $\beta$-($Mg_2Si$) is 2.0. As the possible mechanism in the kinetics viewpoint, the activation energy needed for vacancy formation, migration and bonding among Mg/Si/Vacancy can be reasons. It is assumed that the vacancy formation energy is less important due to the existence of quenched-in excess vacancies. The diffusion kinetics might be favorable when the Mg/Si ratio is near 1.0 due to the interaction among solute atoms and vacancies. Pashley et al. [22] first proposed a model taking into account the solute atom clusters, and then, Dutta and Allen [3] reported that Si-clusters are formed during low temperature aging based on the DSC analysis. In order to examine the early stage of decomposition from the supersaturated solid solution, there have been many attempts to use a more direct technique using one-dimensional atom probe field ion microscopy (APFIM) and three-dimensional atom probe (3DAP) [1,14,15,23-25]. They revealed the direct evidence of the presence of Si-clusters, Mg-clusters and/or Mg-Si co-clusters. However, the correlations between the alloy composition and cluster composition are not clear. The alloy compositions were different in the previous research, and comparing those situations are difficult. In addition, it is also complicated because of the different heat treatment temperature and time as well as the parameters of measurements. According to these summarized results, Cluster (1) has initially various Mg/Si ratios in the alloy close to Mg/Si = 1.0, whereas much more Si-rich clusters exist than the Mg-rich clusters in the excess Si alloys. Mg atoms are incorporated into the Si-rich clusters with the NA time, and then Mg-Si co-clusters with the Mg/Si ratio close to 1.0 are formed. In the case of Cluster (2), the Mg/Si ratio becomes 1.0 in a short time at approximately 100 °C, different with Cluster (1) formation behavior. These results possibly explain the reason why the most favorable alloy composition is when the Mg/Si ratio is close to 1.0. In the next **Chapter 3**, the characteristics of solute clusters formed in natural and pre-aged alloys with the different Mg/Si ratio of alloy compositions using the 3DAP analysis.

## 2.5 Conclusions

The influence of Mg and Si contents on the nanocluster formation was discussed in the present chapter by means of DSC, hardness and electrical resistivity measurements. The obtained results are summarized as follows:

1. Two exothermic peaks were detected using DSC measurements in the all examined alloys with the different Mg and Si contents. It is clarified that the peak area and peak temperature of the two overlapped exothermic peaks depend on the alloy compositions. The overlapped peaks were successfully separated using the Gaussian function method.

2. The formation behavior of nanoclusters strongly depends on the Mg/Si ratio more than the total concentration of (Mg+Si). The most favorable Mg/Si ratio of alloy composition is close to 1.0 for the formation of Cluster (1) and Cluster (2), which is lower than that of the Mg/Si ratio of the equilibrium β-($Mg_2Si$).

## References


[1] G.A. Edwards, K. Stiller, G.L. Dunlop: App. Sur. Sci., 76/77 (1994) pp. 219-225.

[2] G.A. Edwards, K. Stiller, G.L. Dunlop, M.J. Couper: Acta Mater., 46 (1998) pp. 3893.

[3] I. Dutta, S.M. Allen: *J.Mater. Sci. Lett.*, 10 (1991) pp. 323-326.

[4] M.J. Starink, International Materials Reviews, Vol. 49, No. 3-4 (2004) pp. 191-226.

[5] M.W. Zandbergen, Q. Xu, A. Cerezo, G.D.W. Smith, Acta. Mater., 101 (2015) pp. 136-148.

[6] H. Seyedrezai, D. Grebennikov, P. Mascher, H.S. Zurob, Mater. Sci. Eng., A 525 (2009) pp. 186-191.

[7] J. Banhart, C.S.T. Chang, Z. Liang, N. Wanderka, M.D.H. Lay, A.J. Hill, Advanced Engineering Materials, Vol. 12, No. 7 (2010) pp. 559-571.

[8] W.F. Miao, D.E. Laughlin: Scrip. Mater., 40 (1999) pp. 873-878.

[9] W.F. Miao, D.E. Laughlin: Metall. Mater. Trans., A 31 (2000) pp. 361-371.

[10] A.K. Gupta, D.J. Lloyd, S.A. Court: Mater. Sci. Eng., A301 (2001) pp. 140-146.

[11] A.K. Gupta, D.J. Lloyd, S.A. Court: Mater. Sci. Eng., A316 (2001) pp. 11-17.

[12] K. Matsuda, Y. Sakaguchi, Y. Miyata, Y. Uetani, T. Sato, A. Kamio and S. Ikeno: J. Mater. Sci., 35 (2000) pp. 179.

[13] K. Yamada, T. Sato, A. Kamio: Mater. Sci. Forum, 331-337 (2000) pp. 669.

[14] A. Serizawa, S. Hirosawa, T. Sato: Mater. Sci. Forum, 519-521 (2006) pp. 245

[15] A. Serizawa, S. Hirosawa, T. Sato: Metall. Mater. Trans., 39A (2008) pp. 279.

[16] A. Serizawa, T. Sato, W.J. Poole: Philosophical Magazine Letters, Vol. 90, No. 4 (2010) pp. 279-287.

[17] K. Osamura, Y. Hiraoka, Y. Murakami: Philos. Mag., 28 (1973) pp. 809.

[18] H. Yinnon, D.R. Uhlmann: J. Non-Cryst. Solids, 54 (1983) pp. 263-275.

[19] A. Gaber, M.A. Gaffar, M.S. Mostafa, E.F. Abo Zeid: J. Alloy. Compd., 429 (2007) pp. 167-175.

[20] M.J. Starink: Thermochim, Acta., 404 (2003) pp. 163-176.

[21] M. Liu, Y. Yan, Z. Liang, C.S.T. Chang, J. Banhart: Proc. of ICAA13 (2012)

[22] D.W. Pashley, J.W. Rhodes and A. Sendorek: J. Inst. Metals, 92 (1966) pp. 41-49.

[23] M. Murayama, K. Hono: Acta Mater. 47(5) (1999) pp. 1537.

[24] M. Torsæter, H. S. Hasting, W. Lefebvre, C. D. Marioara, J. C. Walmsley, S. J. Andersen, R. Holmestad: J. Appl. Phys. 108 (2010) 073527.

[25] Y. Aruga, M. Kozuka, Y. Takaki, T. Sato: Materials Science & Engineering A 631 (2015) pp. 86-96.

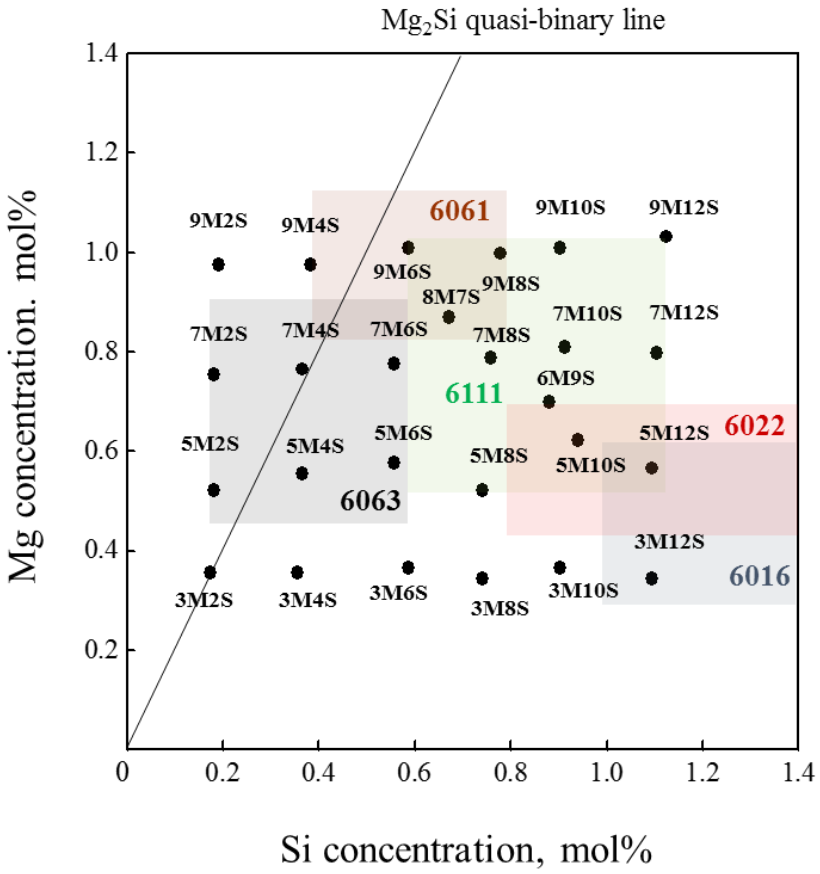


Figure 2.1 Locations of the Mg and Si concentration (mol%) of the used Al-Mg-Si alloys. Each of shaded areas represent compositions of the commercial alloys of 6xxx series.
*The letters of M and S are abbreviation of Mg and Si.
*The number in front of M and S represent mass% of Mg and Si, respectively.

Table 2.1 Chemical composition of the examined Al-Mg-Si alloys, mol%

| Alloy | Elements, mol% | | | | Mg/Si | Mg + Si |
|---|---|---|---|---|---|---|
| | Mg | Si | Fe | Al | | |
| 9M2S | 0.98 | 0.19 | 0.05 | Bal. | 5.08 | 1.17 |
| 9M4S | 0.98 | 0.38 | 0.05 | Bal. | 2.54 | 1.36 |
| 9M6S | 1.01 | 0.59 | 0.05 | Bal. | 1.72 | 1.60 |
| 9M8S | 1.00 | 0.78 | 0.05 | Bal. | 1.28 | 1.78 |
| 9M10S | 1.01 | 0.90 | 0.06 | Bal. | 1.12 | 1.91 |
| 9M12S | 1.03 | 1.12 | 0.06 | Bal. | 0.92 | 2.16 |
| 8M7S | 0.87 | 0.67 | 0.01> | Bal. | 1.29 | 1.54 |
| 7M4S | 0.77 | 0.37 | 0.05 | Bal. | 2.10 | 1.13 |
| 7M6S | 0.78 | 0.56 | 0.05 | Bal. | 1.40 | 1.33 |
| 7M8S | 0.79 | 0.76 | 0.05 | Bal. | 1.04 | 1.55 |
| 7M12S | 0.80 | 1.10 | 0.06 | Bal. | 0.72 | 1.90 |
| 6M9S | 0.70 | 0.88 | 0.04 | Bal. | 0.80 | 1.58 |
| 5M6S | 0.58 | 0.56 | 0.04 | Bal. | 1.04 | 1.13 |
| 5M8S | 0.52 | 0.74 | 0.04 | Bal. | 0.71 | 1.26 |
| 5M10S | 0.62 | 0.94 | 0.07 | Bal. | 0.66 | 1.56 |
| 5M12S | 0.57 | 1.10 | 0.06 | Bal. | 0.52 | 1.66 |
| 3M8S | 0.34 | 0.74 | 0.04 | Bal. | 0.47 | 1.08 |
| 3M10S | 0.37 | 0.90 | 0.07 | Bal. | 0.41 | 1.27 |
| 3M12S | 0.34 | 1.10 | 0.06 | Bal. | 0.31 | 1.44 |

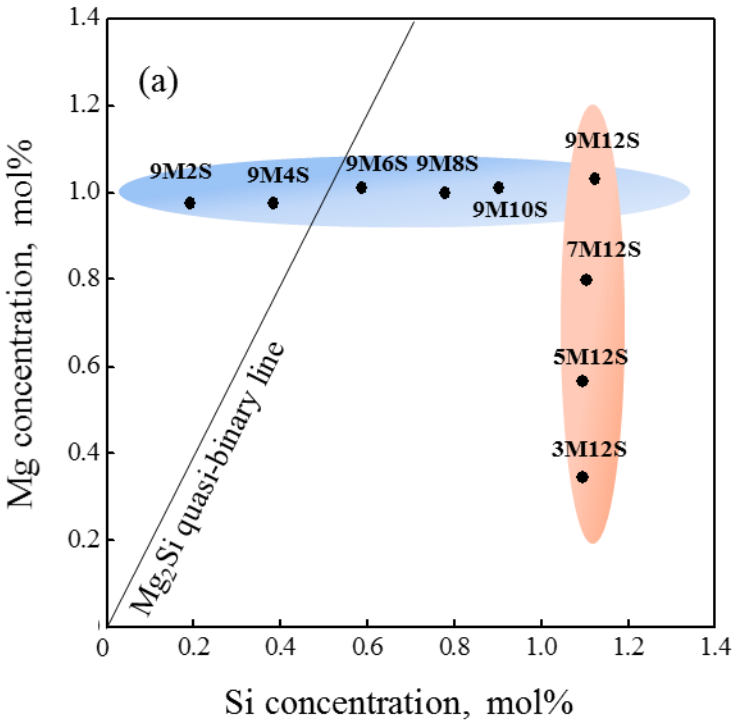


Figure 2.2 Locations of Mg and Si concentration (mol%) of the examined alloys.
(a) The blue shaded area and red shaded area are selected to investigate the effect of Si and Mg concentration, respectively.
(b) The green, purple and orange shaded areas are selected to investigate the effect of the Mg/Si ratio when the (Mg + Si) is constant as 1.5, 1.3 and 1.1 mol%.

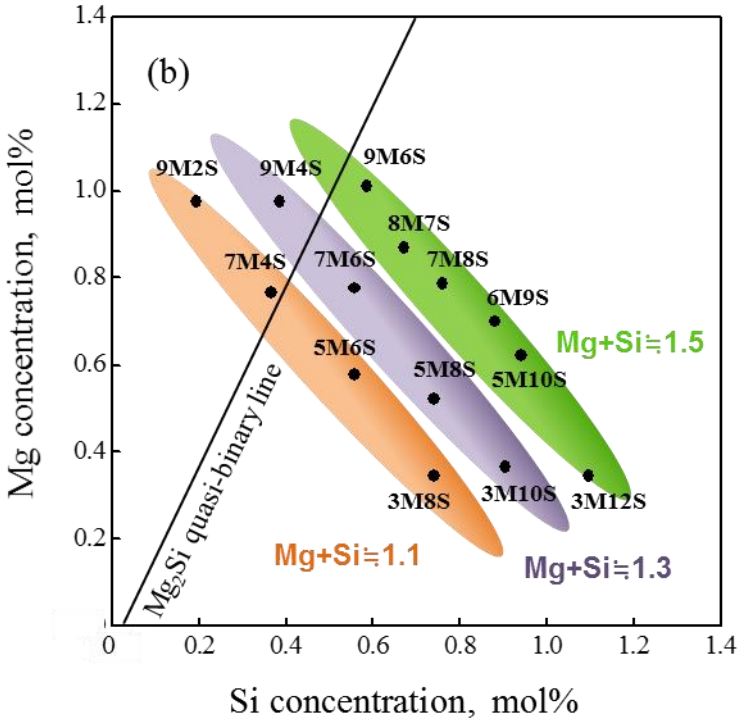


Figure 2.2 Continued.

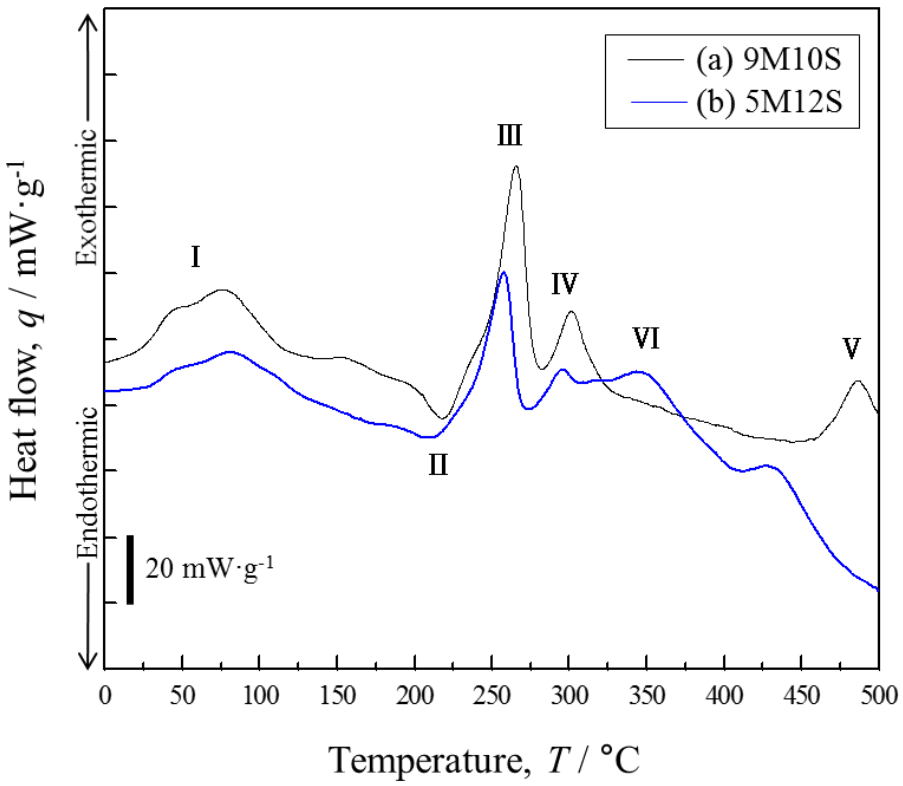


Figure 2.3 DSC curves for the as-quenched alloy (a) 9M10S and (b) 5M12S alloy in a heating rate of 10 °C/min. The respective peaks indicate the following :

Peak Ⅰ : formation of nanoclusters of Mg and Si
Peak Ⅱ : dissolution pre-formed nanoclusters into the matrix
Peak Ⅲ : precipitation of β“
Peak Ⅳ : precipitation of β'
Peak Ⅴ : precipitation of β
Peak Ⅵ : U1, U2 and B' phase (only appearance in excess Si alloys)

(a) Nanocluster peaks and peak separation for 9M10S alloy

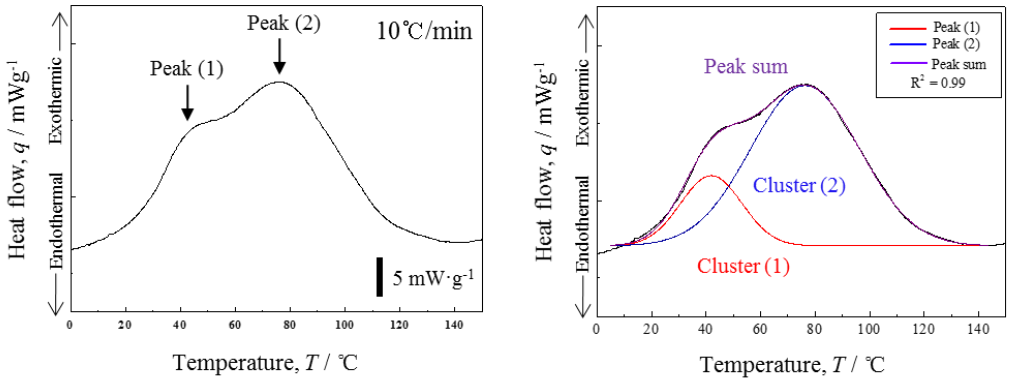


(b) Nanocluster peaks and peak separation for 5M12S alloy

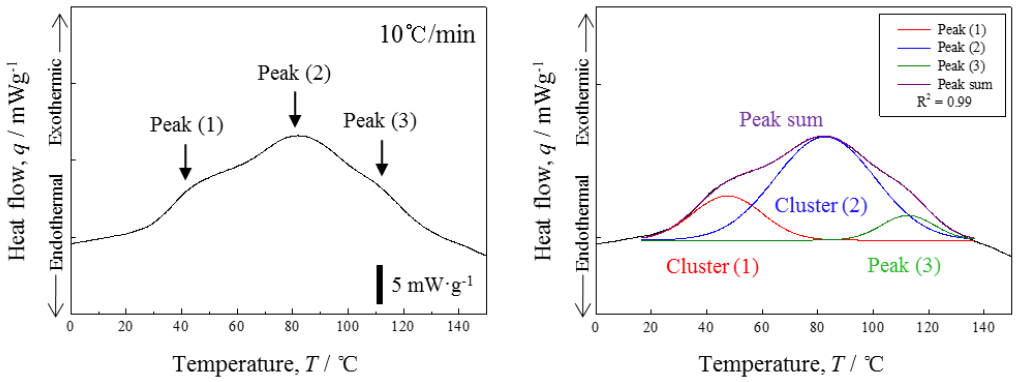


Figure 2.4 DSC results corresponding to the formation of Cluster (1) and Cluster (2) for (a) 9M10S and (b) 5M12S alloys. Peak (3) is observed in 5M12S alloy with excess Si. The multiple overlapped peaks are fitted and separated by using Gaussian function method.

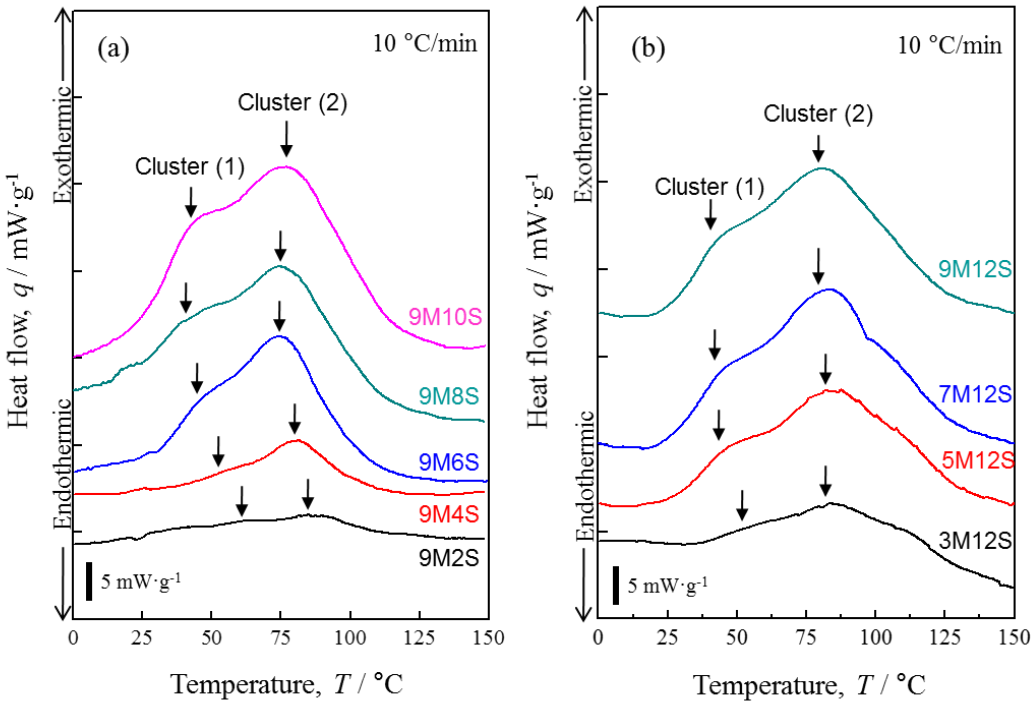


Figure 2.5 DSC results showing the formation of Cluster (1) and Cluster (2) in the as-quenched alloys with the different (a) Si with the fixed Mg concentration and (b) Mg with the fixed Si concentration.

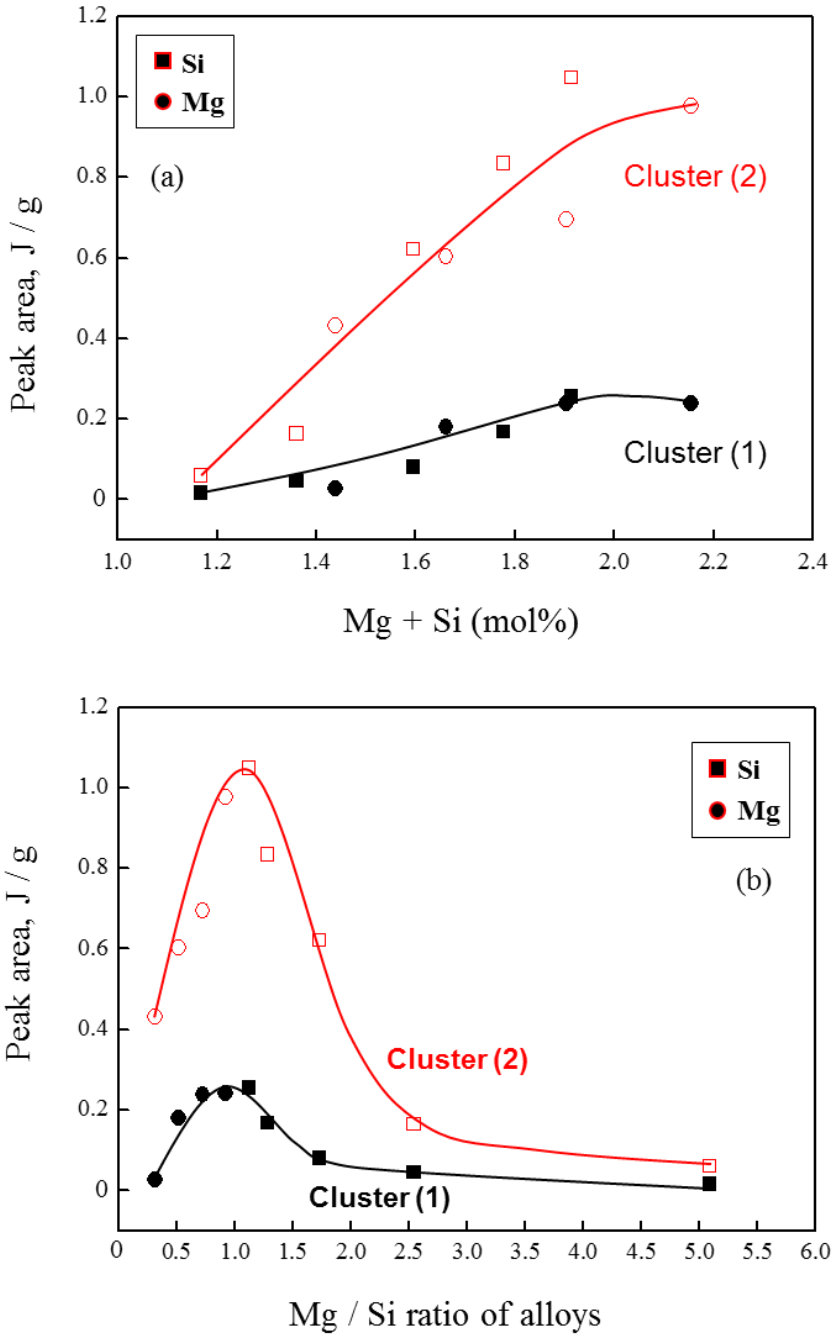


Figure 2.6 Peak areas for Cluster (1) and Cluster (2) obtained by DSC curves as a function of (a) total Mg + Si concentration and (b) Mg/Si ratio of examined alloys.

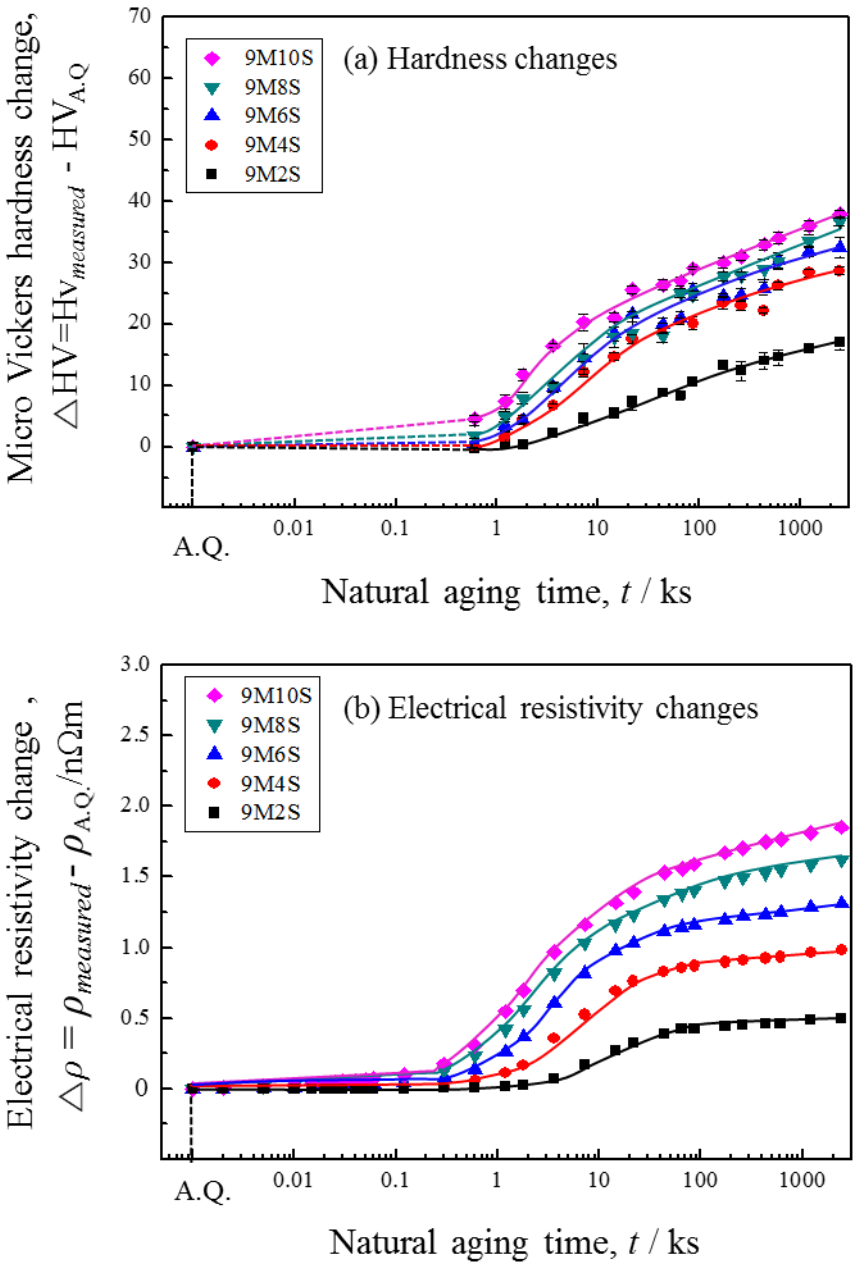


Figure 2.7 (a) Hardness changes and (b) Electrical resistivity changes during natural aging for various alloys with the different Si concentration.
A.Q. : as-quenched.

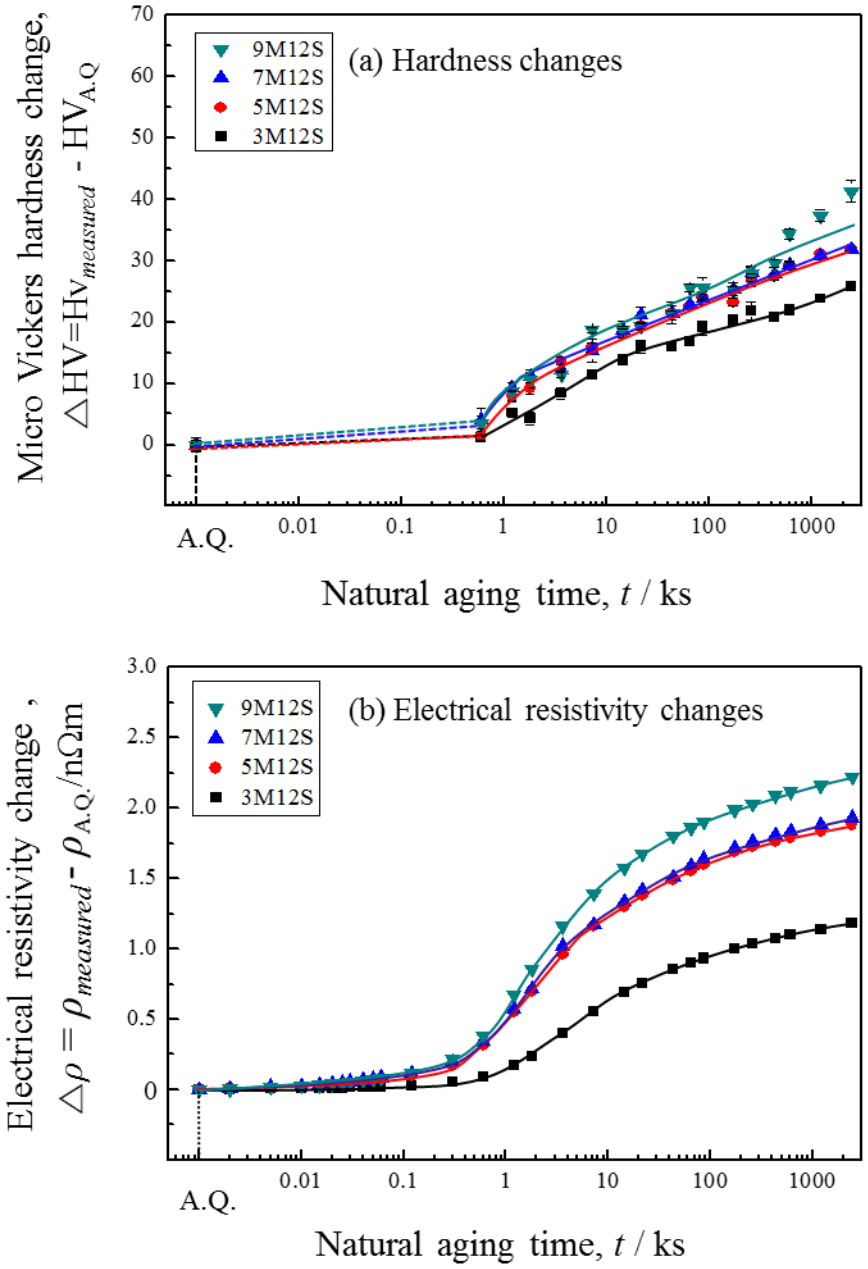


Figure 2.8 (a) Hardness changes and (b) Electrical resistivity changes during natural aging for various alloys with the different Mg concentration.
A.Q. : as-quenched.

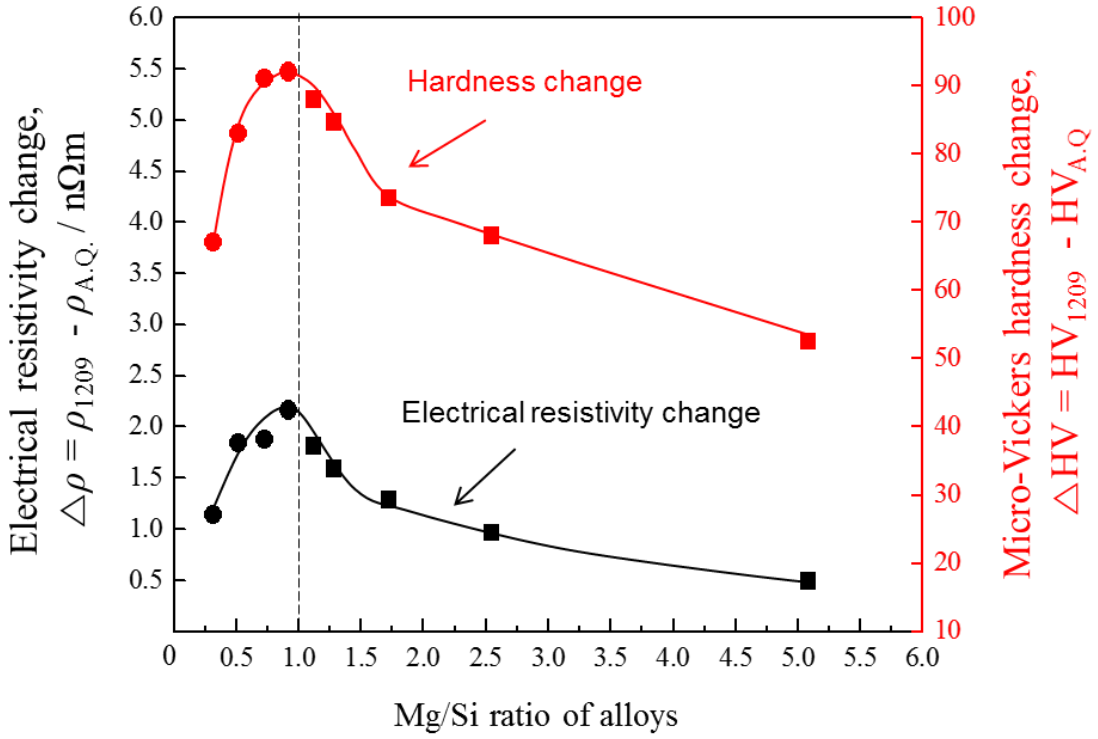


Figure 2.9 Hardness change and electrical resistivity change at 1209 ks as a function of Mg/Si ratio for various alloys aged at room temperature.

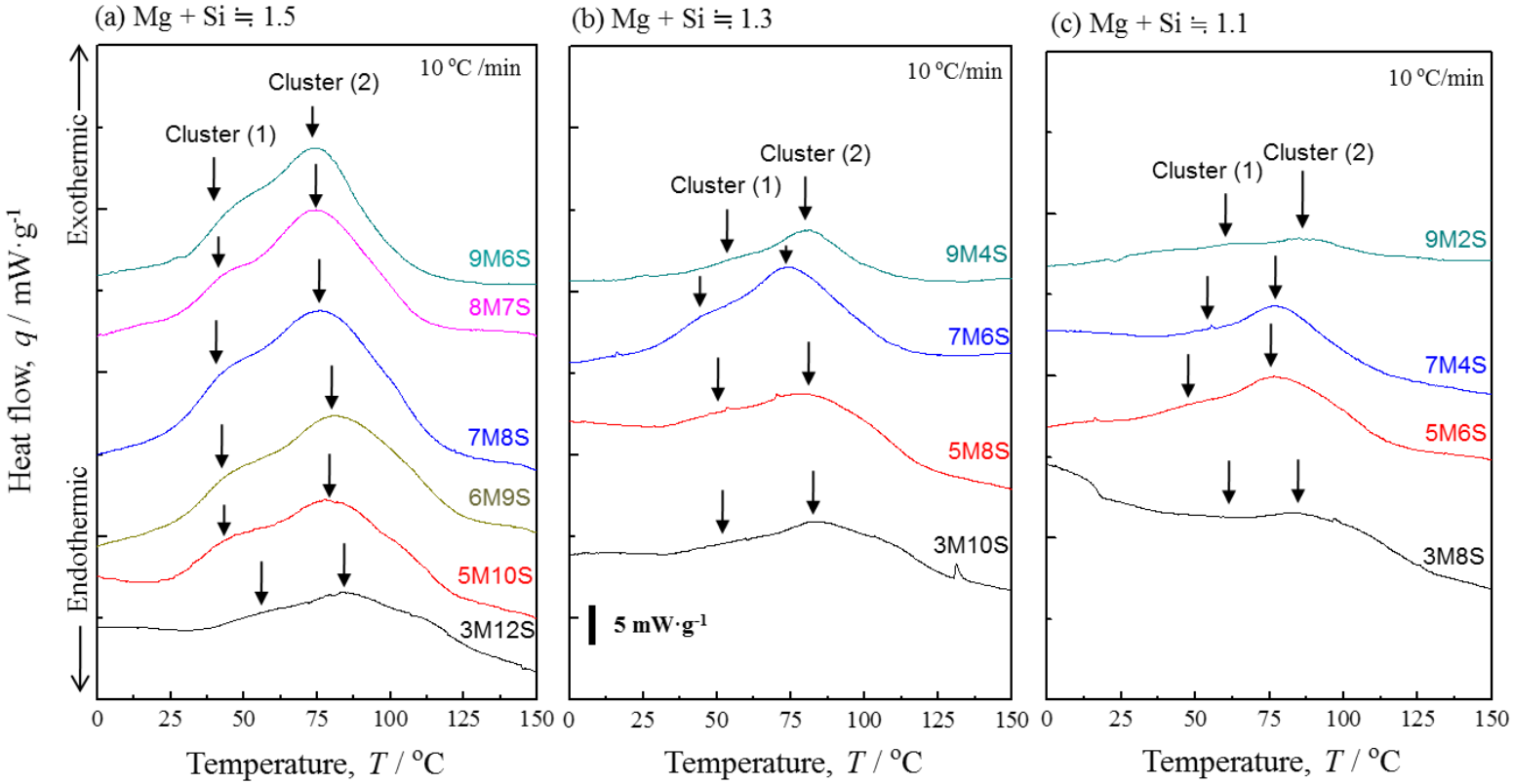


Figure 2.10 DSC results showing the nanoclusters formed at low temperature in the as-quenched alloys of (a) Mg + Si ≒ 1.5, (b) Mg + Si ≒ 1.3 and (c) Mg + Si ≒ 1.1. Exothermic peaks of Peak (1) and Peak (2) are detected in all used alloys.

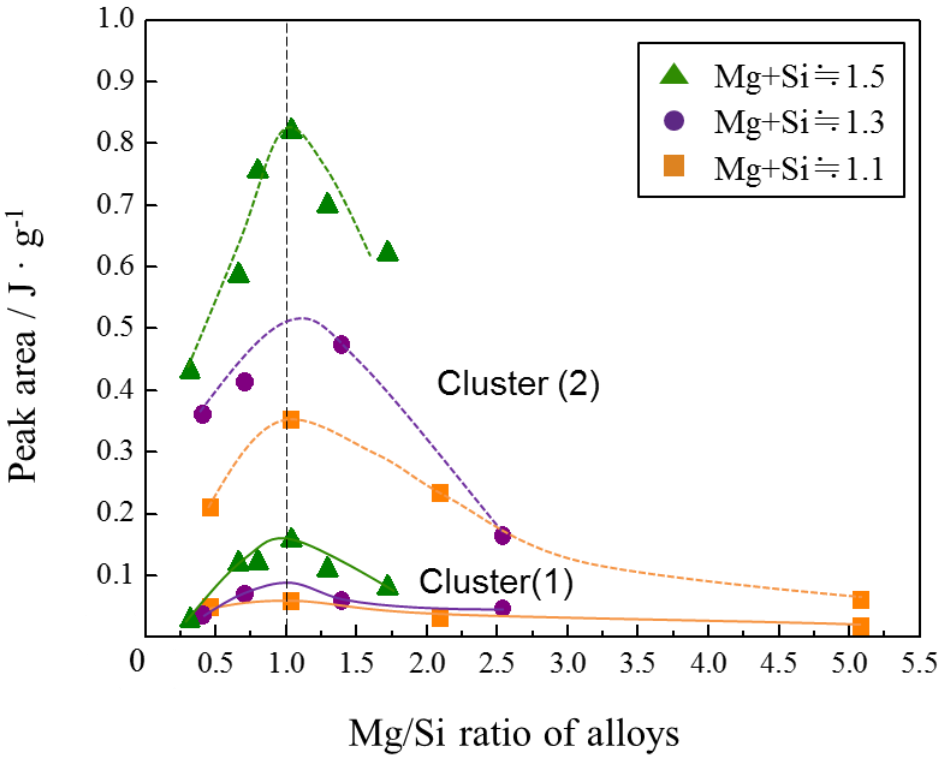


Figure 2.11 Peak areas of Cluster (1) and Cluster (2) obtained by the DSC results as a function of the Mg/Si ratio in the as-quenched alloys with constant Mg + Si concentration

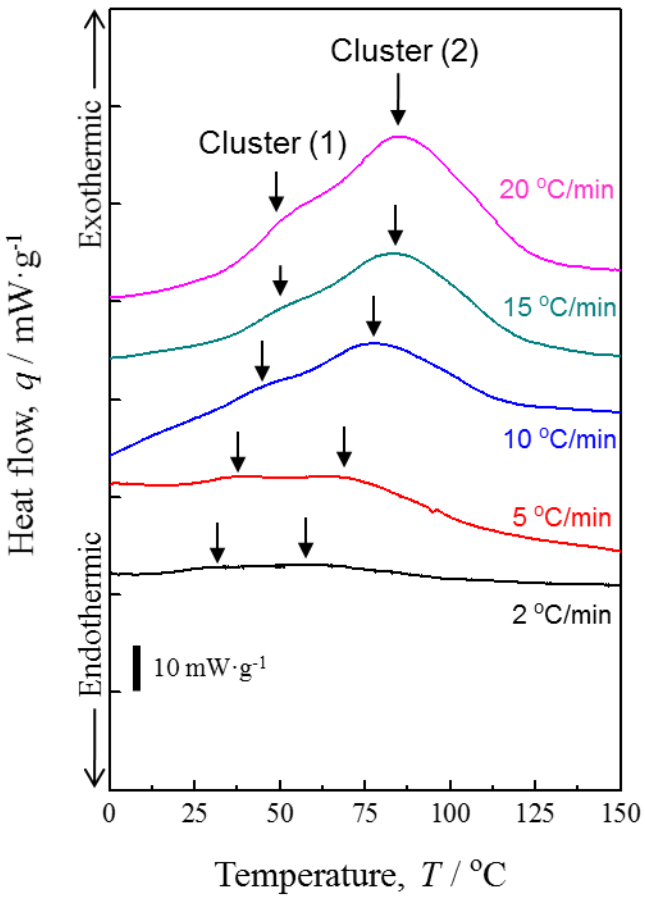


Figure 2.12 DSC curves of the 7M8S alloy with the different heating rate from 2 to 20 °C/min. Two detected peaks corresponding to Cluster (1) and Cluster (2) are shifted to higher temperatures with increasing heating rate as indicated by arrows.

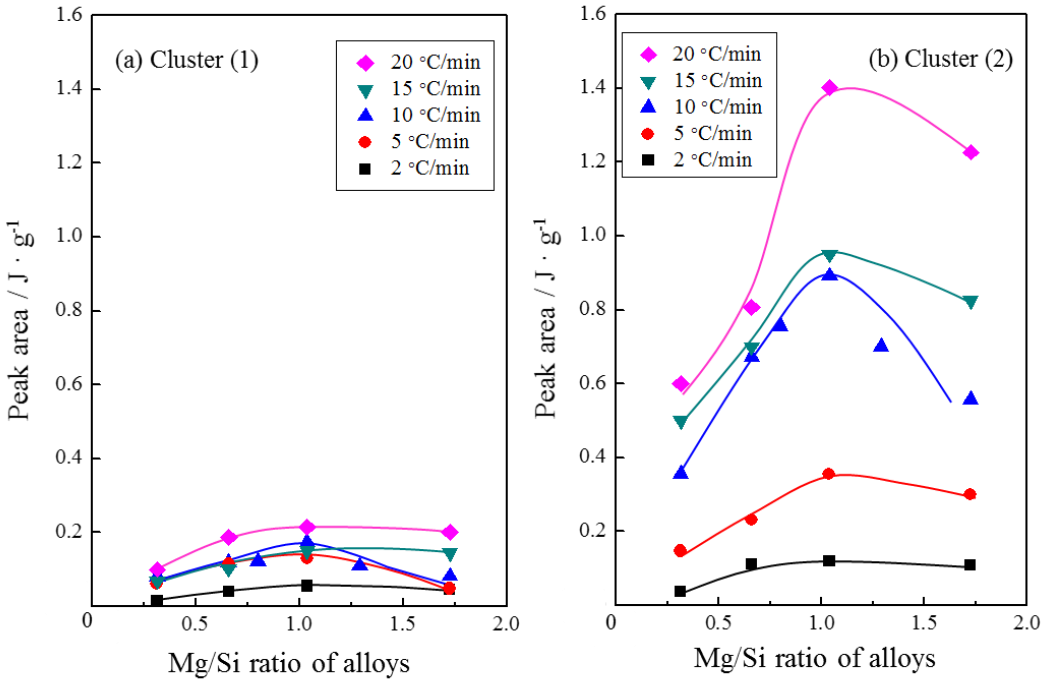


Figure 2.13 Peak area vs. Mg/Si ratio of (a) Cluster (1) and (b) Cluster (2) obtained from DSC curves with various heating rates of 2, 5, 10, 15 and 20 °C/min. (Mg + Si ≒ 1.5 mol%)

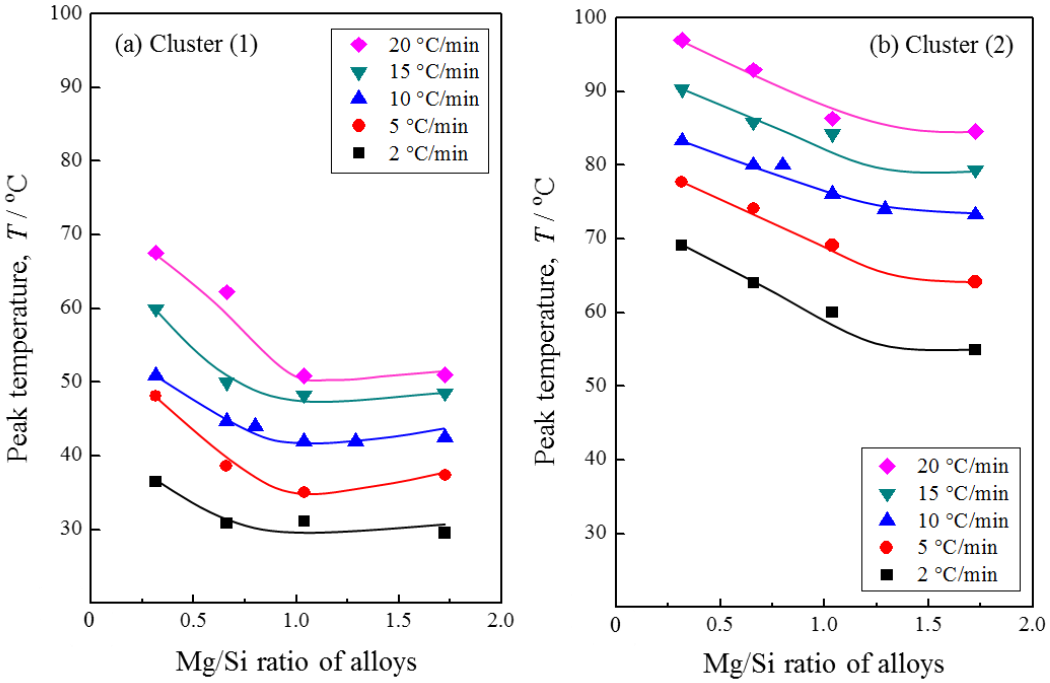


Figure 2.14 Peak temperature vs. Mg/Si ratio of (a) Cluster (1) and (b) Cluster (2) obtained from DSC curves with various heating rates of 2, 5, 10, 15 and 20 °C/min. (Mg + Si ≒ 1.5 mol%)

(a) Cluster (1)

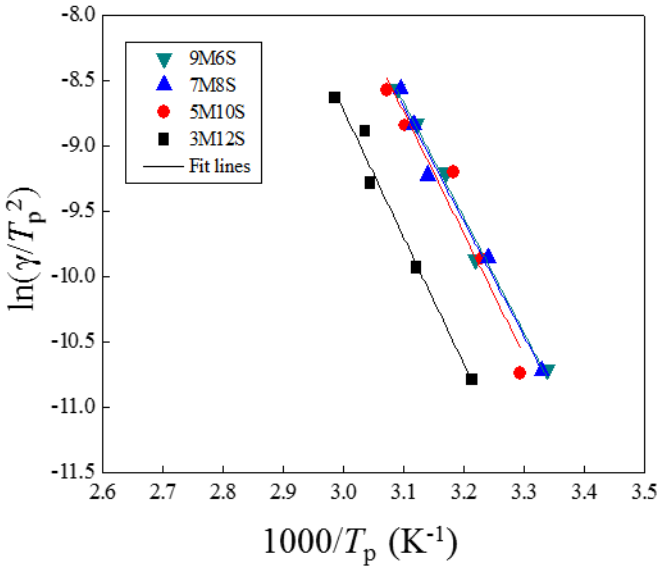


(b) Cluster (2)

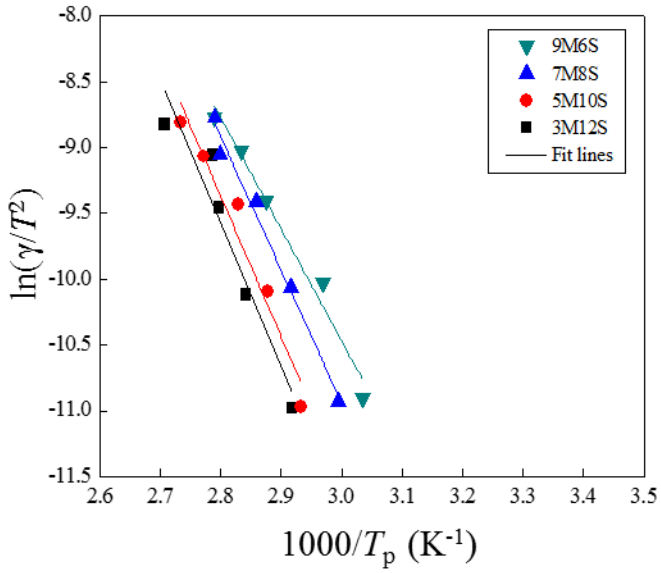


Figure 2. 15 $\ln(\gamma/T_p^2)$ as a function of $1000/T_p$ of (a) Cluster (1) and (b) Cluster (2) showing the activation energy obtained by using the Kissinger's method.
(Mg + Si ≒ 1.5 mol%)

Table 2.2 Activation energy values for the formation of Cluster (1) and Cluster (2) determined by the Kissinger's method.

| Alloys | Mg/Si | Activation energy, kJ/mol | |
|---|---|---|---|
| | | Cluster (1), $E_1$ | Cluster (2), $E_2$ |
| 3M12S | 0.314 | 80.65 | 89.96 |
| 5M10S | 0.660 | 77.49 | 88.63 |
| 7M8S | 1.038 | 72.83 | 83.89 |
| 9M6S | 1.724 | 73.25 | 77.02 |

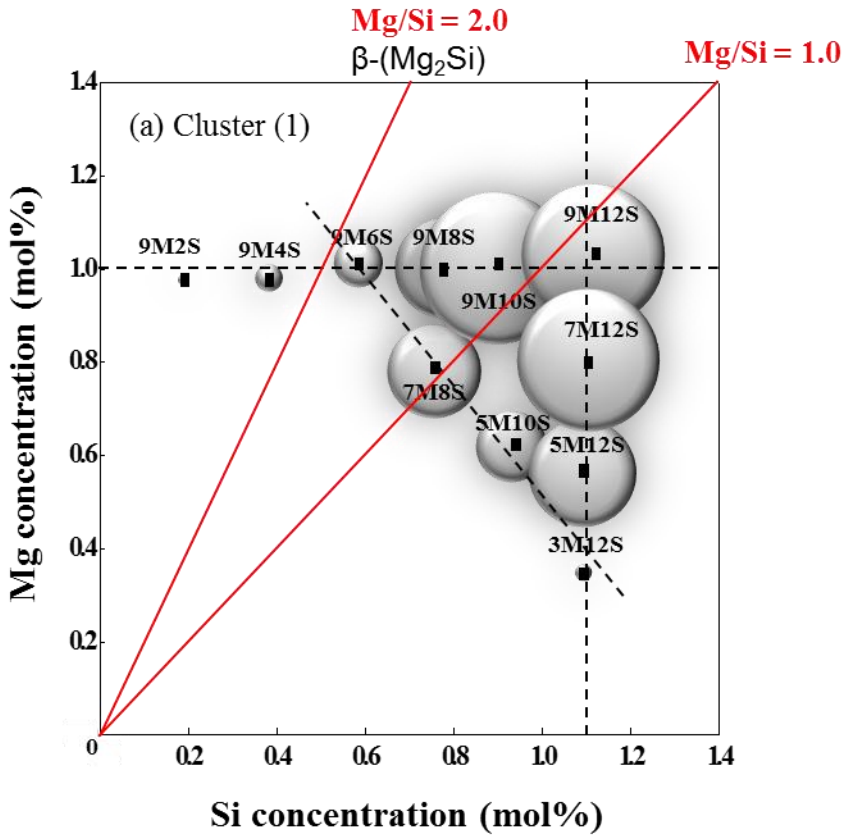


Figure 2.16 Distribution of volume fraction of (a) Cluster (1) and (b) Cluster (2) represented as the function of the Mg and Si concentration. Each of area is represented as a normalized value by the maximum value.

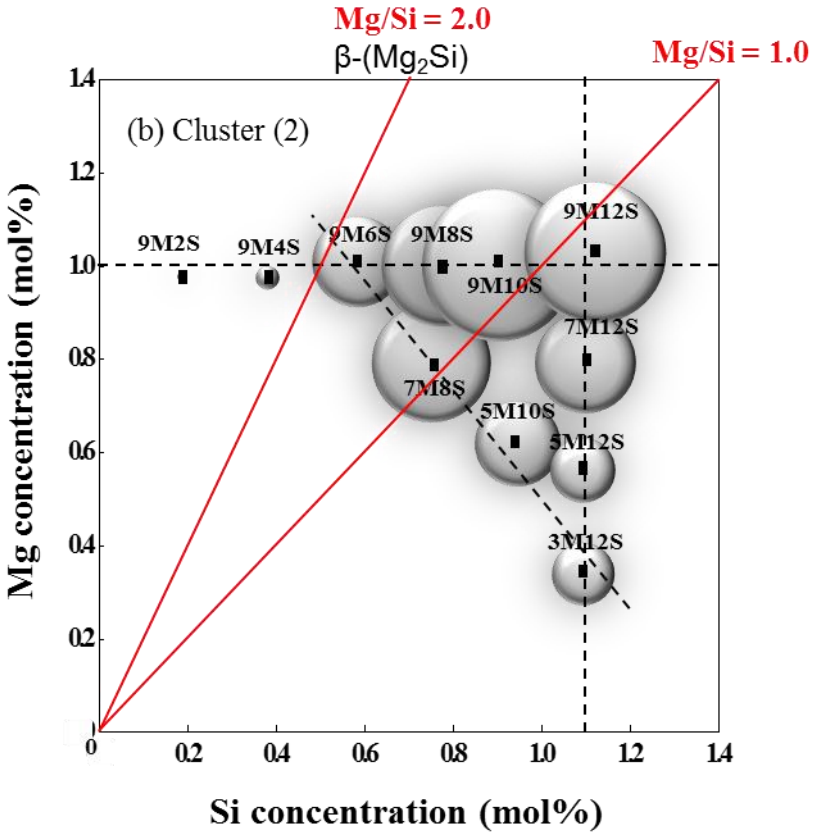


Figure 2.16 Continued.

# Chapter 3.
# Three-dimensional Atom Probe Analysis of Solute Clusters Formed in Natural- and Pre-Aged Alloys with Different Mg/Si Ratio

## 3.1 Introduction

In the previous chapter, two-overlapped peaks correlated with Cluster (1) and Cluster (2) formation were observed using DSC measurements. It was noted that the volume fractions of Cluster (1) and Cluster (2) are most enhanced when the Mg/Si ratio of alloy composition is close to 1.0. The DSC analysis is greatly useful to identify the nanocluster formation as the indirect method. However, the structural and compositional information such as internal composition and size of solute-clusters cannot be obtained by this thermal analysis. In addition, in order to explain the influence of alloy compositions on the age-hardening behavior during artificial aging, the internal composition of nanoclusters must be clarified. As appearance of developed instruments such as the three-dimensional atom probe (3DAP), the formation of nanoclusters in Al-Mg-Si alloys were directly observed [1-5]. They found that the presence of separated Si-clusters, Mg-clusters and Mg-Si co-clusters. However, it is difficult to characterize solute-clusters due to the different measurement conditions, heat-treatment conditions and alloy compositions. Therefore, in the present chapter, the characteristics of solute-cluster formed in natural- and pre-aged alloys is systemically investigated in the alloys with the different Mg/Si ratio by means of the 3DAP analysis. The aim of the present thesis is to investigate the alloy composition, aging temperature-time dependence on the nanocluster formation behavior. Finally, the idea of the new categorization of clusters is proposed in order to explain the two-step aging behavior of the Al-Mg-Si alloys based on 3DAP results.

## 3.2 Experimental Procedure

### 3.2.1 Alloy Compositions

High purity 8M7S, 7M8S and 6M9S alloys were received from Kobe Steel, Ltd. in the form of a 1.3 mm thick cold-rolled sheet. The chemical composition of examined alloys is described in Table 3.1(a) and (b). The weight percent (mass%) is converted to the atomic percent for precise evaluation of the atomic composition ratio as shown in Table 3.1 (b). These alloys have a different Mg/Si ratio range from 0.80 to 1.29, as well as the constant total concentration (Mg+Si) of 1.5 mol% and were selected with consideration for the DSC results obtained in **Chapter 2**. The location of examined alloys in the present chapter is shown in Fig. 3.1.

### 3.2.2 Heat Treatments

The cold-rolled sheets of various alloys were solution treated for 1.8 ks in a salt bath furnace at 570 °C and quenched to the same temperature as that in the following aging treatment. The heat treated alloys were aged at room temperature for 108 ks (30 hours) and 7560 ks (roughly 2000 hours). The rest of alloys were pre-aged at 90 °C for 18 ks (5 hours) in an oil bath furnace. All natural- and pre-aged samples are designated by the NA-S (short-term natural aging), NA-L (long-term natural aging and PA.

### 3.2.3 Three-dimensional Atom Probe (3DAP)

Atom probe tomography (APT) is a powerful technique for visualization of the atomic-scale microstructure with quantitative data analyses. In the advanced instruments, more than 10 million atoms are routinely acquired and structurally and chemically identified. The specimen is required to be needle-shaped for the high efficiency of the field evaporation. Electrochemical polishing is a conventional technique for specimen

preparation. The standard two-stage method [6] is employed in the present study. In the first "rough-polishing" step, "neck" in the center of the specimen is formed using a double layer electropolishing method. The specimen is repeatedly dipped into a layer of electrolyte, 25 % perchloric acid in acetic acid, on top of an insert liquid such as 2% perchloric acid + 98% 2-butoxyethanol at 10 V DC power supply at RT. In a "final polishing" step, the specimen's end diameter is sufficiently achieved by micro-loop polishing. APT analyses were carried out using a LEAP$^{TM}$ 3000HR instrument (CAMECA Instruments Inc.) located in Kobe Steel Ltd. [7]. The analyses were performed at a specimen temperature of 30 K (-243 °C), a voltage pulse fraction (pulse voltage/steady-state voltage) of 20%, and a pressure in the specimen chamber below $10^{-8}$ Pa. Visualization and quantitative evaluation of the 3DAP dataset were performed using the IVAS software 3.6 (CAMECA Instruments Inc.). In the data reconstruction procedure, regions of non-uniform atom distribution such as close proximity to a low index pole were not included. Two separate experimental runs were carried out for each condition, and consistent results were obtained between the runs. The maximum separation algorithm [8], which is the most common method, was employed to identify atomic clusters. The parameter $d_{max}$ represents a distance between two solute atoms. In the present study, two solute atoms are defined to be in the same cluster when the $d_{max}$ is below 0.75 nm. The extremely small clusters are filtered on the basis of removing all atomic clusters that consist of less than 10 atoms in $N_{min}$ (a minimum number of solute clusters). The ideal parameter $d_{max}$ and $N_{min}$ is selected in a randomized system of solid solution of the same composition. This was tested by randomly assigning the atom identities to positions in the data and optimized by applying different parameter $d_{max}$ and $N_{min}$ on this randomized data. The main objective to use 3DAP is to characterize individual clusters in terms of size, chemical composition, morphology and distribution.

## 3.3 Results

### 3.3.1 Quantitative Statistical Analysis of the Solute-atom Clusters

The APT analysis volumes and the quantitative information about solute-atom clusters detected after NA and PA are listed in Table 3.2. The range from 3.7 million atoms to 10.7 million atoms are acquired and provided for the atomic cluster analysis with aging conditions. The number of clusters between 237 and 1075 were detected for each material of the NA and PA. The spatial element distribution of Mg and Si atoms obtained by the maximum separation method is visualized in Fig. 3.2. The number density of clusters is larger in the order of NA-S, NA-L and PA, concurrently 7M8S, 8M7S and 6M9S alloys. The PA samples have higher number density of clusters than that of NA samples even though a short PA time. Table 3.3 shows the average atomic cluster values for each dataset obtained after NA and PA. The average cluster-size showed in two ways that number of solute atoms in each clusters and radius of gyration ($l_g$) and the associated Guinier radius ($r_G$) [6]. The clusters have approximately similar average sizes between 1.21 to 1.33 nm regardless the holding time of NA. The average radii of clusters for PA samples, however, tend to be larger than that those of NA samples. Interestingly, there were outstanding differences in the average Mg/Si ratio of clusters. From these values, it is noted that the 8M7S (relatively High-Mg alloy) produces more Mg-rich clusters and the 6M9S (relatively High-Si alloy) produces more Si-rich clusters. The average Mg/Si ratio of 7M8S (almost equal Mg:Si alloy) is precisely located between both alloys. These results suggest that the alloy composition is closely correlated with cluster composition distribution. Therefore, the size distribution (number density vs. size), composition distribution (number density vs. normalized atomic ratio) and its combined distribution (normalized atomic ratio vs. size) is investigated in detail in the next section.

### 3.3.2 Size and Composition Distribution of the Solute-atom Clusters

To investigate how the cluster size and composition vary in each dataset, the histogram of solute clusters is first described in Fig. 3.3 and Fig. 3.4. Figure 3.3 shows the size distribution for each cluster in the alloys after NA and PA as a function of total number of Mg+Si atoms. The top in the number density can be seen in nearly 12 (Mg+Si) atoms, and 1.1 mm converting into Guinier radius for all alloys. A number of large-sized clusters over 40 atoms were clearly observed in PA samples of both (a) 8M7S and (c) 6M9S alloys, concurrently small-sized clusters still exist. The number density of small-sized clusters become higher in the order of NA-S, NA-L and PA. As shown in Fig. 3.3 (c), the large-sized clusters were observed in comparison with other alloys after long-period NA, resulting in an increased in cluster size. These results indicate that the cluster size distribution is much more related with aging conditions than the alloy composition. Interestingly, the composition distribution of clusters shows a significant difference on the alloy composition as well as aging conditions. Figure 3.4 shows the number density of clusters as a function of the value of Mg/(Mg+Si) inside clusters. There is significant difference in the highest number density with the alloy composition. The most outstanding difference can be seen in the short-period NA samples (see NA-S). In addition, the Mg/Si ratio with highest number density has a tendency to be close to 1.0 in the long-period NA, as well as PA that even though the aging time is short. Figure 3.5 shows the dependence of the alloy composition on size and composition distribution of each cluster in the NA-S condition. As mentioned in Fig. 3.3, there is no significant difference in the size distribution for the different alloy compositions. On the other hand, in Fig. 3.5 (b), it can be seen that the 8M7S (relatively High-Mg alloy) has higher number density of Mg-rich clusters and the 6M9S (relatively High-Si alloy) has higher number density of Si-rich clusters. The 7M8S (almost equal Mg:Si) alloy is precisely located between both alloys. These deflection phenomena with the alloy composition can be improved to be naturally aged for a long time (NA-L) and pre-aged (PA) as shown in Fig. 3.4. The

dependence of alloy composition, aging temperature and time on solute-atom clustering will be discussed in more details in the next section.

Figure 3.6 shows the relationship between the cluster-size and normalized atomic ratio with alloy compositions after NA-S, NA-L and PA. The small-sized clusters have a wide various atomic ratio in all aging conditions and alloys. On the other hand, the large-sized clusters exhibit a narrow distribution and converges in a certain specific ratio. What is interesting in this data is that the atomic ratio to be converged in a certain value is different with alloy compositions. In the 8M7S alloy, the value approaches to 1.3 of the Mg/Si ratio, which is extremely close to the atomic ratio of the alloy composition, while to a higher ratio than that of the alloy composition in the 6M9S alloy. The large-sized clusters, moreover, can be frequently observed in PA compared to NA-S. It is noted that the large-sized clusters with a certain atomic ratio are promoted by PA treatment.

## 3.4 Discussion

### 3.4.1 Compositional, Aging Temperature and Time Dependent of Clusters

In the present chapter, the characteristics of clusters in alloys with the various Mg/Si ratio were investigated in accordance with aging temperature and time using 3DAP. Several studies about solute-clusters using 3DAP have been carried out [1-5], however, it was difficult to characterize solute-clusters due to the different measurement conditions, heat-treatment conditions and alloy compositions. Torsaeter et al. [9] investigated the influence of the alloy composition on clustering in Al-Mg-Si alloys with Mg-rich (Mg:Si ratio 2:1) and Si-rich (Mg:Si ratio 1:2). They reported that natural aging produced Mg-rich clusters in the High-Mg alloy and Si-rich clusters in the High-Si alloy, while pre-aging promoted the formation of clusters with 1.0 of the Mg/Si ratio regardless alloy compositions. So far, however, there has been no investigation about the characteristic of solute-clusters with the extremely small change of the Mg/Si ratio. The present study

examines the three alloy compositions with 0.8, 1.04 and 1.29 in the Mg:Si ratio, which has unusually narrow interval. These three alloy compositions were selected to produce sufficient amount of clusters on the basis of the DSC analysis as mentioned in **Chapter 2**. Figure 3.3 and Figure 3.4 show the alloy composition, aging temperature and time dependent on solute-clusters obtained by the 3DAP analysis. As shown in Fig. 3.3, the size distribution of solute-clusters has no significant difference with alloy compositions, while is different with aging temperature and time. After the prolonged NA time, the number density of the large-sized clusters becomes larger than that of the small-sized clusters. It is noted that the solute-clusters grow hardly during NA. However, the number density of both the small- and large-sized clusters was enhanced by PA at 90 °C. It is indicated that the solute-clusters during PA grow rapidly due to the rapid diffusion rate. These results are in a good agreement with the result by Serizawa et al. [2-3], they examined the growth rate of solute-clusters formed at RT and 100 °C. The most interesting finding was that the compositional distribution of solute-clusters is significantly different with the alloy composition, aging temperature and time as shown in Fig. 3.4. Compared with NA-S in (a) 8M7S and (c) 6M9S alloys, 8M7S (relatively excess Mg added) alloy has higher number density of Mg-rich clusters than Si-rich clusters. It is noted that the clustering in the initial stage of NA is formed by significantly affected by the matrix concentration of alloys. These deflection phenomena with the alloy composition is shifted toward the value approximately 1.0 of the Mg/Si ratio after prolonged NA. On the contrast, in the PA condition, the Mg/Si ratio of each cluster approaches to 1.0 with increasing the size due to long-range diffusion at elevated temperature.

### 3.4.2 Correlation between Alloy Compositions and Cluster Compositions

It is most important to understand the cluster composition and clustering process because the nanocluster is closely related with the β″-phase, the strengthening phase in

Al-Mg-Si alloys. According to Marioara et al. [10], the atomic arrangement and volume fraction of the β″-phase can be changed when the examined alloy composition is far from the ideal Mg/Si ratio = 5/6. Namely, the precipitation mechanism is determined by the characteristics and morphology of solute-clusters as a precursor of the β″-phase. Figure 3.7 shows the correlation between the Mg/Si ratio of the examined alloys and average Mg/Si ratio of clusters with different aging conditions. Comparing to the present results and literature results, the values taken from the literature of Torsaeter et al. [9] and Zandbergen et al. [11] are also included respectively. From these data, the average Mg/Si ratio of clusters formed at a short-term natural aging is significantly dependent on the Mg/Si ratio of alloys. It is also seen that the High-Si alloy leads to the higher number density of Si-rich clusters, while Mg-rich clusters in the High-Mg alloy. On the other hands, the alloy with the balanced Mg/Si ratio of 1.0 presents almost similar average Mg/Si ratio even though different heat treatments. This result may be explained by the suppression of long-range diffusion at RT, resulting in the localized atomic rearrangement and aggregation of neighboring atoms. Moreover, at elevated temperature of 90 °C, these compositional imbalance is drastically improved due to higher probability of long-range diffusion. As prolonged PA, the average Mg/Si ratio of clusters approaches from 1.0 to 1.2, resulting in the favorable condition as nucleation sites for the precipitates of the β″-phase.

### 3.4.3 Proposal of New Solute-cluster Categorization

In **Chapter 2**, the two-overlapped exothermic peaks were detected at the lower temperature by means of DSC, indicating the Cluster (1) and Cluster (2) formed at around R.T. and 373K. Serizawa et al. [3] and Yamada et al. [12] reported that the Cluster (1) and Cluster (2) are considered as Si-rich clusters and Mg-Si clusters, respectively. However, Kim et al. [13] suggested that the Mg-Si co-clusters are likely to form although during natural aging. Therefore, more detailed approaches in the viewpoint of volume fraction

and internal structure of nanoclusters are required to understand the alloy composition-dependence on the two-step aging behavior. Based on the 3DAP results in the present chapter, solute-clusters with wide range of atomic ratio and size, i.e. Si-rich clusters, Mg-Si clusters and Mg-rich clusters, were found as shown in Fig. 3.6. It is noted that the number density of each cluster is different with the alloy composition, aging temperature and time. The detailed compositional and dimensional information provided by 3DAP results is able to categorize and classify solute-clusters as shown in Fig. 3.8. The new categorization is carried out as follows.

$$\begin{aligned} &\text{Si-rich cluster : } Mg/(Mg+Si) \leq 0.4 \\ &\text{Mg-Si cluster : } 0.4 < Mg/(Mg+Si) \leq 0.6 \\ &\text{Mg-rich cluster : } 0.6 < Mg/(Mg+Si) \end{aligned} \tag{3.1}$$

Mg-Si clusters have a narrow composition distribution and act as effective nucleation sites of precipitates due to the similarity of the internal structure as well as the size. The most important point is boundary between Si-rich clusters and Mg-Si clusters. In the present study, small-sized Si-rich clusters are determined with Mg/(Mg+Si) less than 0.4. Aruga et al. [5] reported that the Si-rich clusters with the extremely low Mg/Si ratio cannot be dissolved during 443K aging, namely negative effect on precipitation. Small-sized Mg-rich clusters with Mg/(Mg+Si) higher than 0.6 repeats the cycle of formation and annihilation without any special effect on precipitation. Figure 3.9 shows the fraction of each cluster group, i.e. Si-rich clusters, Mg-Si clusters and Mg-rich clusters, with (a) natural aging at R.T. and (b) pre-aging at 363K in the 6M9S alloy. The fraction of Mg-rich clusters initially increases and remain unchanged regardless of aging temperature. However, Si-rich clusters and Mg-Si clusters gradually increase in the number density with aging time. The most interesting point is that the Mg-Si clusters drastically increase in the number density by pre-aging at 363K. Therefore, these differences of fraction can affect the two-step aging behavior. In conclusion based on thermal analysis in **Chapter 2** and 3DAP results (see Fig. 3.10), Cluster (1) and Cluster (2) were composed of Si-rich

clusters, Mg-Si clusters and Mg-rich clusters regardless of alloy composition. The fraction of three types of solute-clusters is different depending on aging temperature and time. In the next chapter, the correlation between the fraction of solute-clusters and two-step aging is discussed.

## 3.5 Conclusions

The nature of solute-clusters formed in the natural- and pre-aged alloys was discussed with different Mg/Si ratio by means of the 3DAP analysis. In addition, the influence of alloy compositions on internal composition of solute-clusters with aging temperature and time was also investigated. The obtained results are summarized as follows:

1. The number density of clusters is larger in the order of NA-S, NA-L and PA, concurrently 7M8S, 8M7S and 6M9S alloys. The PA samples have higher number density of clusters than those of NA samples even though in a short PA time. The clusters have approximately the same average size between 1.21 to 1.33 nm regardless the holding time of NA. On the other hand, the average radius of clusters for the PA samples tend to be larger than that of the NA samples.

2. It is noted that the 8M7S (relatively High-Mg alloy) produces more Mg-rich clusters and the 6M9S (relatively High-Si alloy) produces more Si-rich clusters. The average Mg/Si ratio of the 7M8S (almost equal Mg:Si alloy) is precisely located between both alloys. These results indicate that the alloy composition is closely correlated with the cluster composition distribution.

3. The small-sized clusters have a wide various atomic ratio of compositions in all aging conditions and alloys. The large-sized clusters exhibit a narrow distribution and converges in a certain specific ratio of compositions. It is interesting in these

data is that the atomic ratio of the cluster composition is converged in a certain value which is different depending the alloy compositions.

4. The solute-atoms formed during NA and PA can be classified into Si-rich clusters, Mg-Si clusters and Mg-clusters based on the results of size and composition distribution. It is noted that the fraction of Si-rich clusters, Mg-Si clusters and Mg-clusters is different depending the alloy compositions, aging temperature and time.

## References


[1] G.A. Edwards, K. Stiller, G.L. Dunlop, M.J. Couper: Acta Mater., 46 (1998) pp. 3893.

[2] A. Serizawa, S. Hirosawa, T. Sato: Mater. Sci. Forum, 519-521 (2006) pp. 245

[3] A. Serizawa, S. Hirosawa, T. Sato: Metall. Mater. Trans., 39A (2008) pp. 279.

[4] M. Murayama, K. Hono: Acta Mater. 47(5) (1999) pp. 1537.

[5] Y. Aruga, M. Kozuka, Y. Takaki, T. Sato: Materials Science & Engineering A 631 (2015) pp. 86-96.

[6] M.K. Miller, Atom Probe Tomography, Kluwer Academic/Plenum Publishers, New York (2000).

[7] Y. Aruga, M. Kozuka, Y. Takaki, T. Sato: Metall. Mater. Trans. A 45 (2014) pp. 5906-5913.

[8] J.M. Hyde, C.A. English, in: G.E. lucas, L. Snead, M.A. Kirk, R.G. Elliman (Eds.), Materials Research Symposia, 650, Materials Research Society, Pittsburgh, PA (2001) p. R6.6.

[9] M. Torsæter, H. S. Hasting, W. Lefebvre, C. D. Marioara, J. C. Walmsley, S. J. Andersen, R. Holmestad: J. Appl. Phys. 108 (2010) 073527.

[10] C.D. Marioara, S.J. Andersen, H.W. Zandbergen, R. Holmestad, Metall. Mater. Trans. A 36 (2005) pp. 691-702.

[11] M.W. Zandbergen, Q. Xu, A. Cerezo, G.D.W. Smith: Acta Materialia, 101 (2015) pp. 136-148.

[12] K. Yamada, T. Sato, A. Kamio: Mater. Sci. Forum, 331-337 (2000) pp. 669.

[13] J. Kim, E. Kobayashi, T. Sato: Materials Transactions, Vol. 56, No. 11 (2015) pp. 1771-1780.

Table 3.1 (a) Chemical composition of examined Al-Mg-Si alloys, mass%

| Alloy | Elements, mass% | | | |
|---|---|---|---|---|
| | Mg | Si | Fe | Al |
| 8M7S | 0.78 | 0.70 | 0.01 | Bal. |
| 7M8S | 0.73 | 0.81 | 0.01 | Bal. |
| 6M9S | 0.62 | 0.93 | 0.09 | Bal. |

Table 3.1 (b) Chemical composition of examined Al-Mg-Si alloys, mol%

| Alloy | Elements, mol% | | | | Mg/Si | Mg + Si |
|---|---|---|---|---|---|---|
| | Mg | Si | Fe | Al | | |
| 8M7S | 0.87 | 0.67 | <0.01 | Bal. | 1.29 | 1.54 |
| 7M8S | 0.81 | 0.78 | <0.01 | Bal. | 1.04 | 1.59 |
| 6M9S | 0.70 | 0.88 | 0.04 | Bal. | 0.80 | 1.58 |

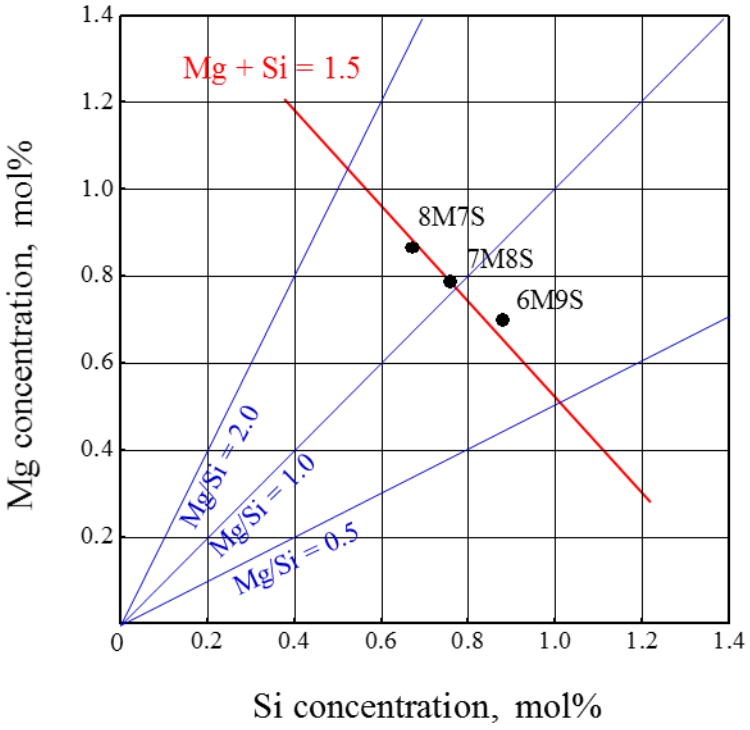


Figure 3.1 Locations of the examined Al-Mg-Si alloys (mol%). The manufactured alloys have a different Mg/Si ratio with constant (Mg+Si) concentration of 1.5 mol%.

Table 3.2 Statistical analysis of APT measurements after different NA time and PA at 90 °C using the maximum separation method with $d_{max}$=0.75 nm, $N_{min}$=10

| Alloy | Sample | Number of atoms analyzed(M) | Number of clusters detected | Number density of cluster ($10^{23}/m^3$) |
|---|---|---|---|---|
| 8M7S | NA-S | 3.7 | 237 | 15.0 |
| | NA-L | 7.7 | 445 | 17.2 |
| | PA | 9.7 | 878 | 22.3 |
| 7M8S | NA-S | 4.2 | 222 | 12.7 |
| | NA-L | 9.2 | 640 | 16.8 |
| 6M9S | NA-S | 9.6 | 591 | 15.1 |
| | NA-L | 6.9 | 662 | 21.3 |
| | PA | 10.7 | 1075 | 24.1 |

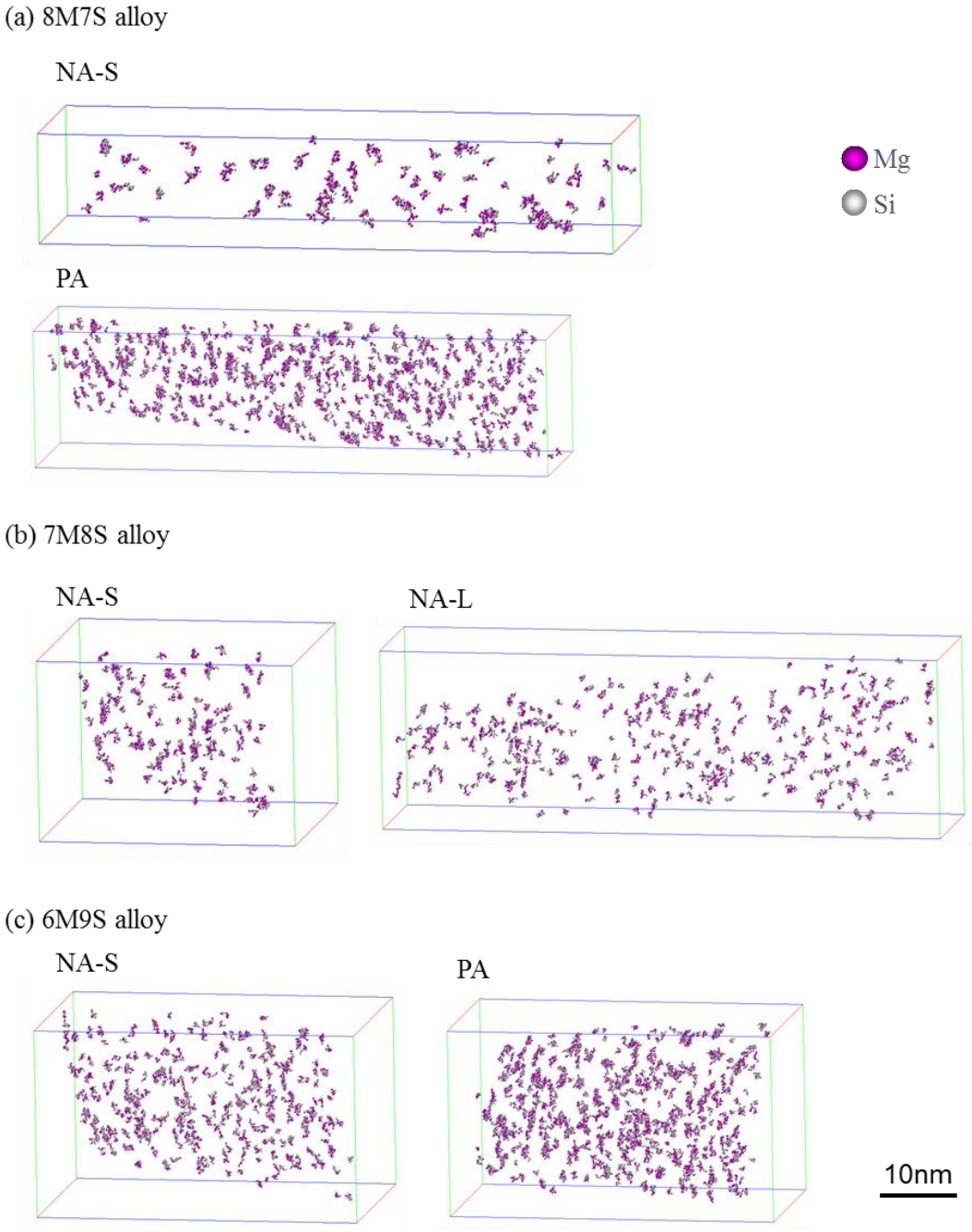


Figure 3.2 Atom maps showing the 3D elemental distribution of Mg and Si atoms obtained by the maximum separation method with $d_{max}$ = 0.75 nm and $N_{min}$ = 10 in the (a) 8M7S, (b) 7M8S and (c) 6M9S alloys after natural aging for 108 ks (NA-S), 7560 ks (NA-L) and pre-aging for 18 ks at 90 °C (PA).

Table 3.3 Average atomic cluster parameters for each dataset after different NA time and PA at 90 °C using the maximum separation method with $d_{max}$=0.75 nm, $N_{min}$=10

| Alloy | Sample | Average cluster size (number of solute atoms) | Average radius of clusters, $r_G$(nm) | Average Mg/Si ratio of clusters |
|---|---|---|---|---|
| 8M7S | NA-S | 16.6 | 1.26 | 1.87 |
| | NA-L | 15.5 | 1.22 | 1.50 |
| | PA | 20.3 | 1.39 | 1.39 |
| 7M8S | NA-S | 15.4 | 1.25 | 1.25 |
| | NA-L | 14.0 | 1.21 | 1.33 |
| 6M9S | NA-S | 15.9 | 1.24 | 1.04 |
| | NA-L | 21.2 | 1.33 | 0.96 |
| | PA | 19.2 | 1.33 | 1.07 |

(a) 8M7S alloy

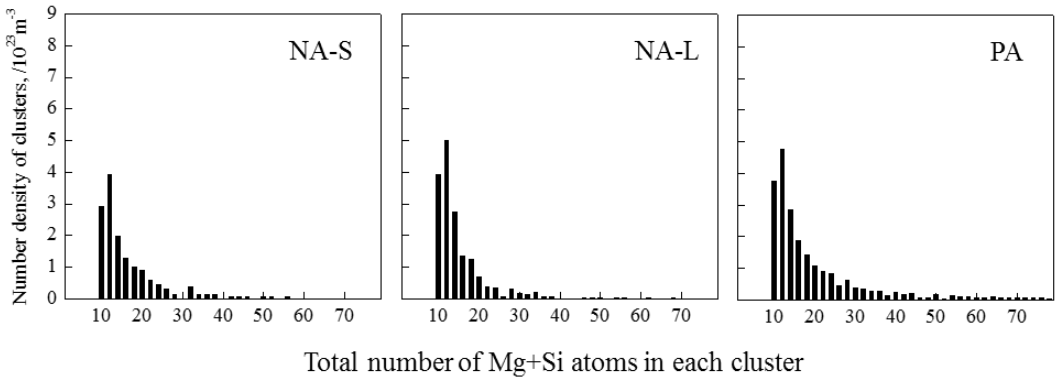


(b) 7M8S alloy

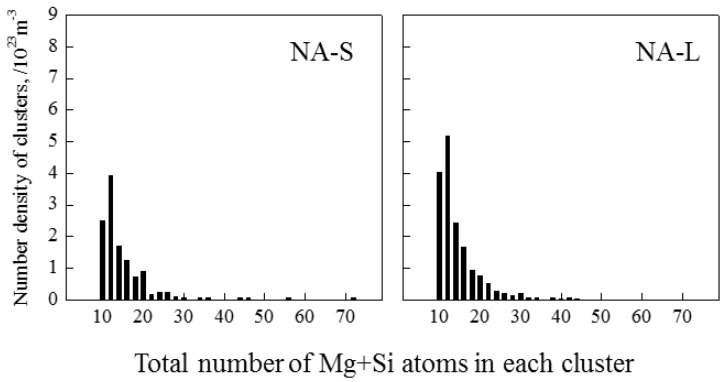


(c) 6M9S alloy

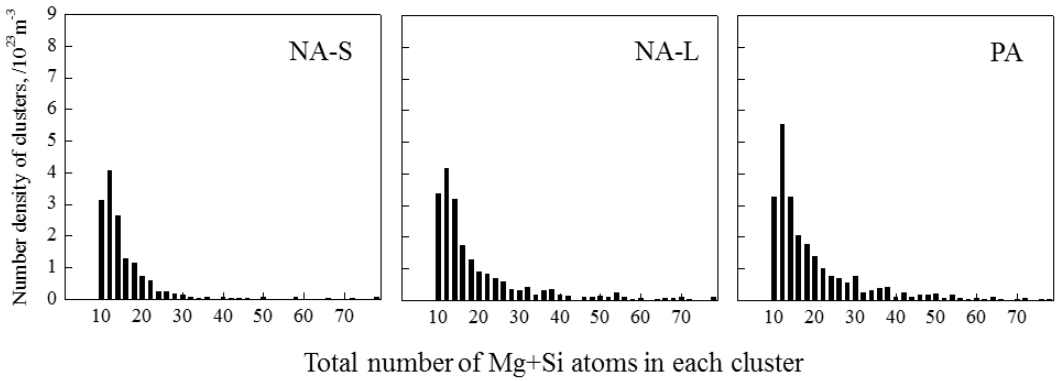


Figure 3.3 Size distribution of clusters in the (a) 8M7S, (b) 7M8S and (c) 6M9S alloys after natural aging for 108 ks (NA-S), 7560 ks (NA-L) and pre-aging for 18 ks at 90 °C (PA).

(a) 8M7S alloy

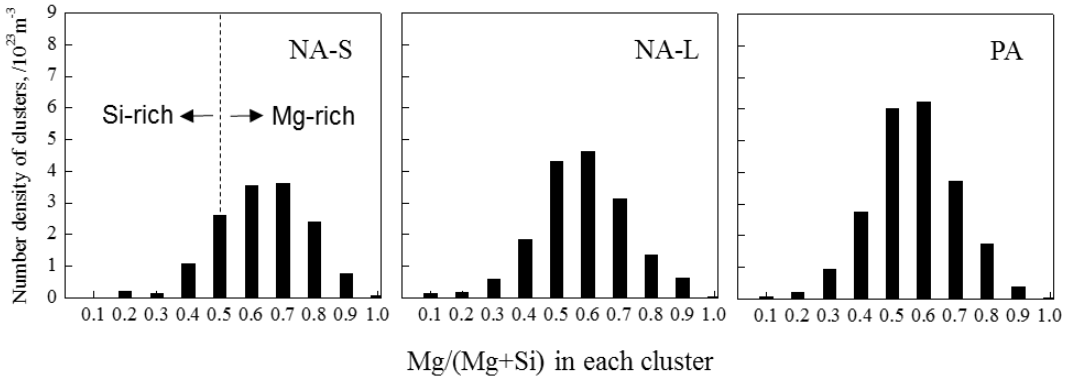


(b) 7M8S alloy

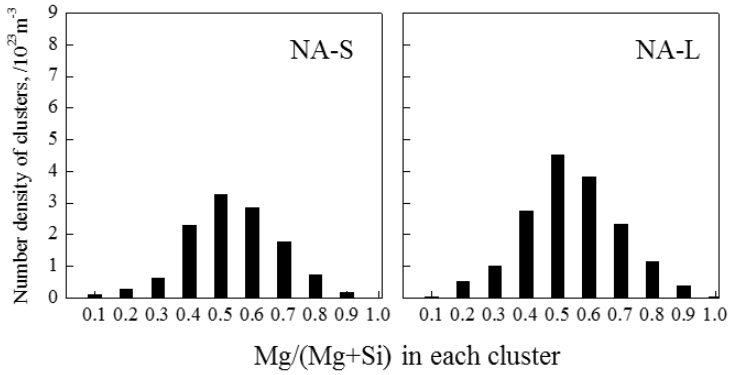


(c) 6M9S alloy

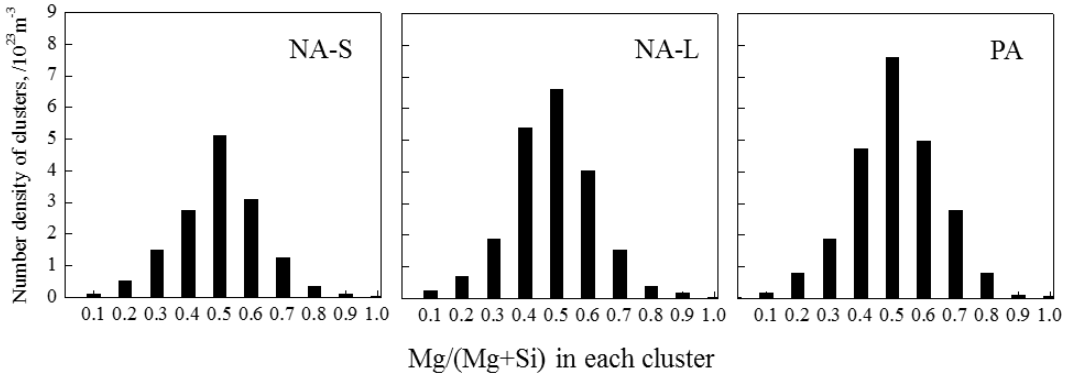


Figure 3.4 Composition distribution of clusters in the (a) 8M7S, (b) 7M8S and (c) 6M9S alloys after natural aging for 108 ks (NA-S), 7560 ks (NA-L) and pre-aging for 18 ks at 90 °C (PA).

(a) Size distribution

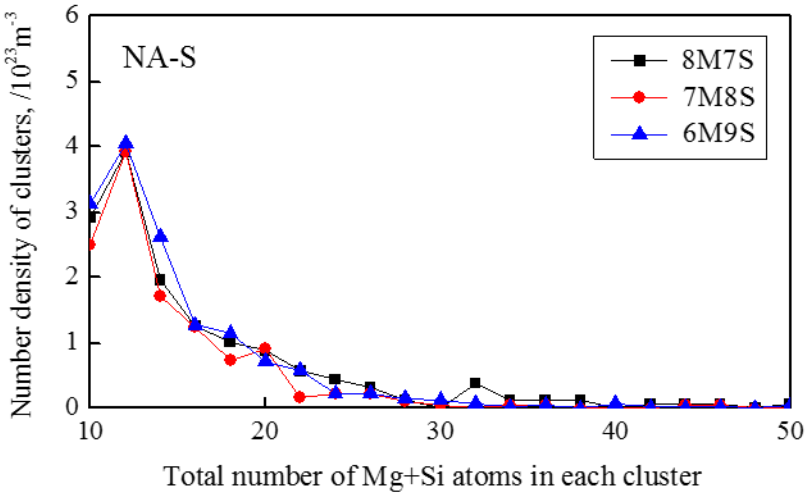


(b) Composition distribution

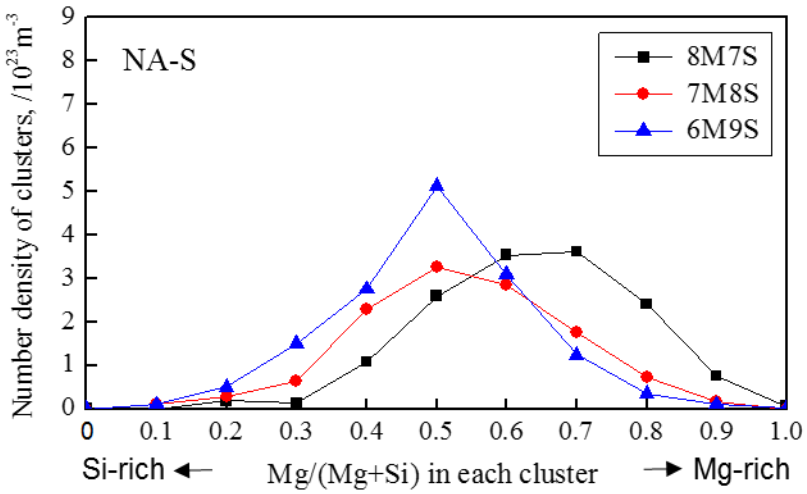


Figure 3.5 Number density of clusters against (a) total number of Mg+Si atoms and (b) normalized atomic ratio in each clusters after natural aging for 108 ks (NA-S) in 8M7S, 7M8S and 6M9S alloys.

(a) 8M7S alloy

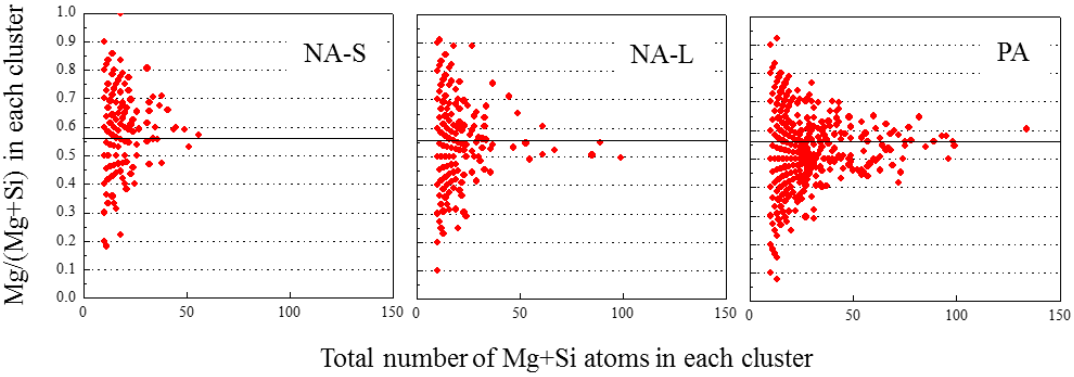


(b) 6M9S alloy

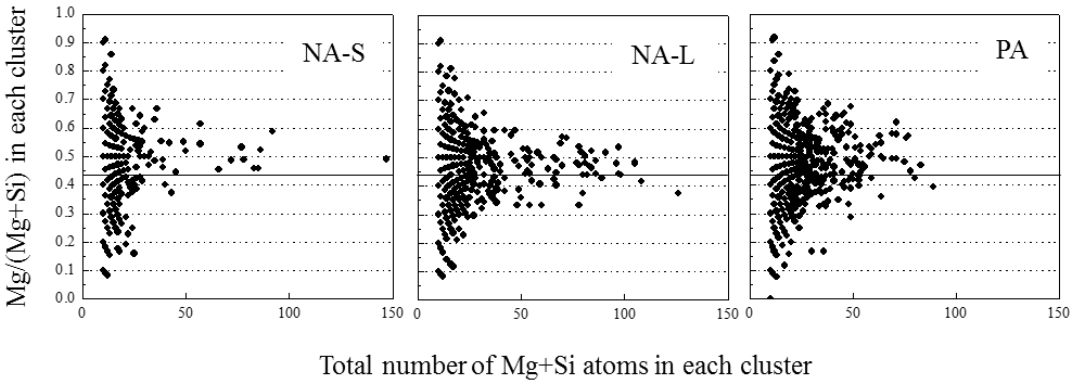


Figure 3.6 Relationship between cluster-size and normalized atomic ratio in the (a) 8M7S and (b) 6M9S alloys after natural aging for 108 ks (NA-S), 7560 ks (NA-L) and pre-aging for 18 ks at 90 °C (PA). The solid line inserted in figures indicates atomic ratio of each alloy.

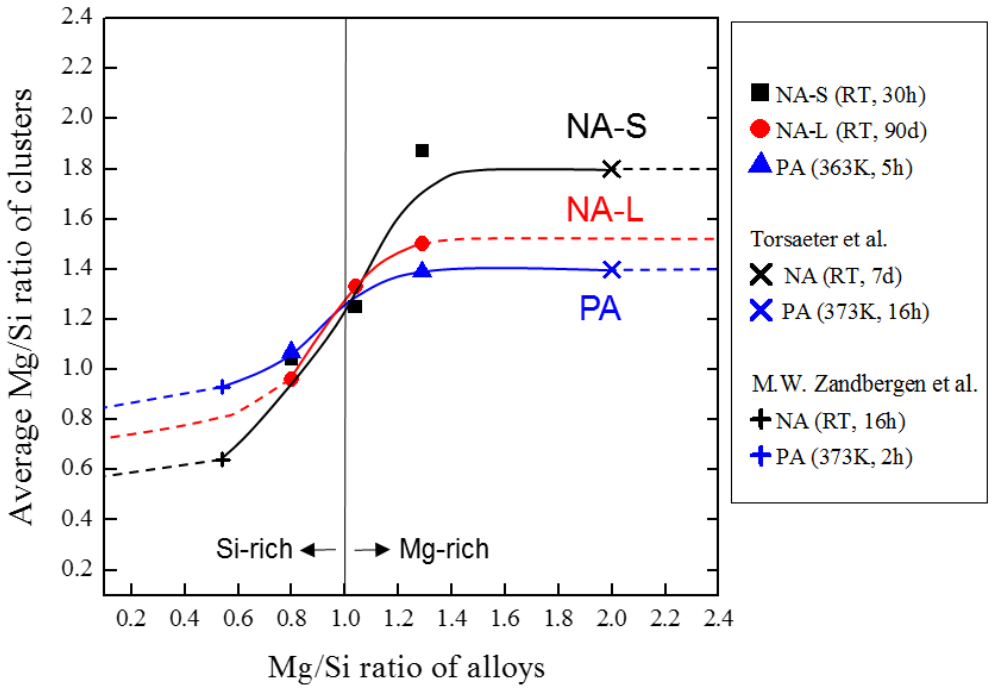


Figure 3.7 Correlation between Mg/Si ratio of examined alloys and average Mg/Si ratio of clusters after natural aging for 108 ks (NA-S), 7560 ks (NA-L) and pre-aging for 18 ks at 90 °C (PA). Values taken from Ref. [9] and Ref. [11] are included respectively.

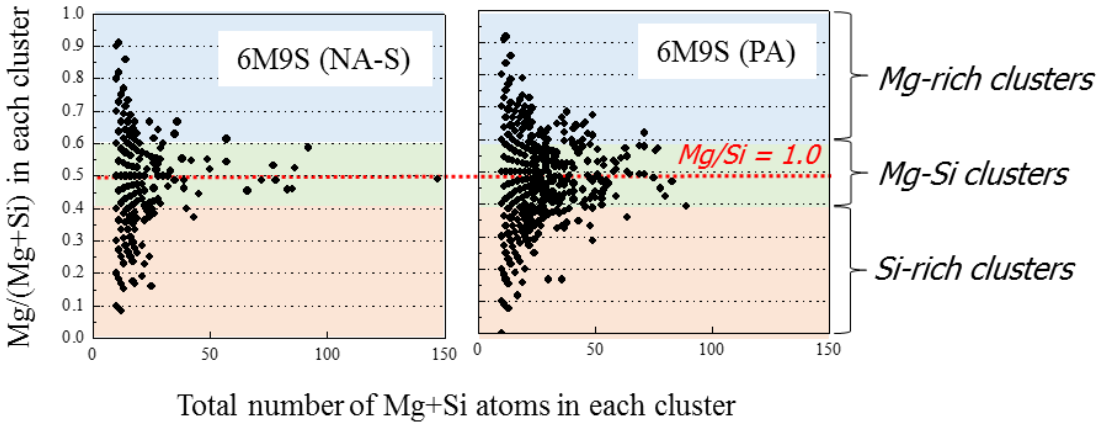


Figure 3.8 Explanation of cluster categorization based on the combined distribution indicating atomic ratio vs. size in each cluster after NA-S and PA in 6M9S alloy.

(a) Natural aging at R.T. (6M9S alloy)

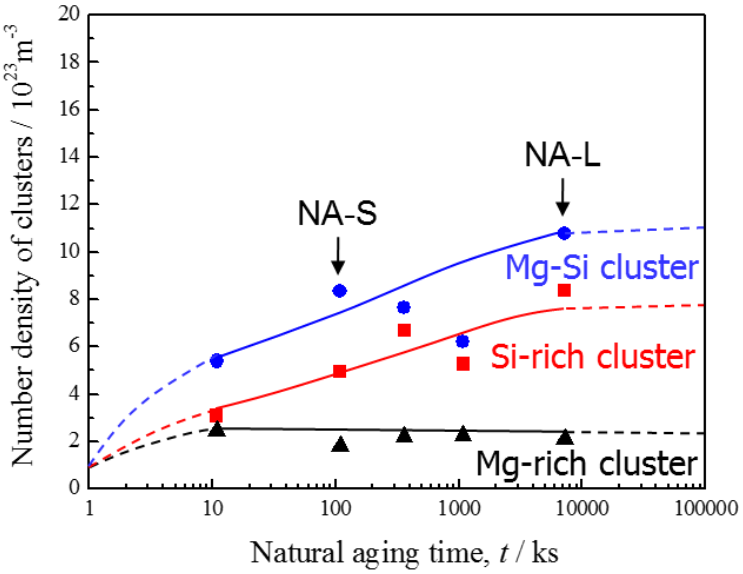


(b) Pre-aging at 363K (6M9S alloy)

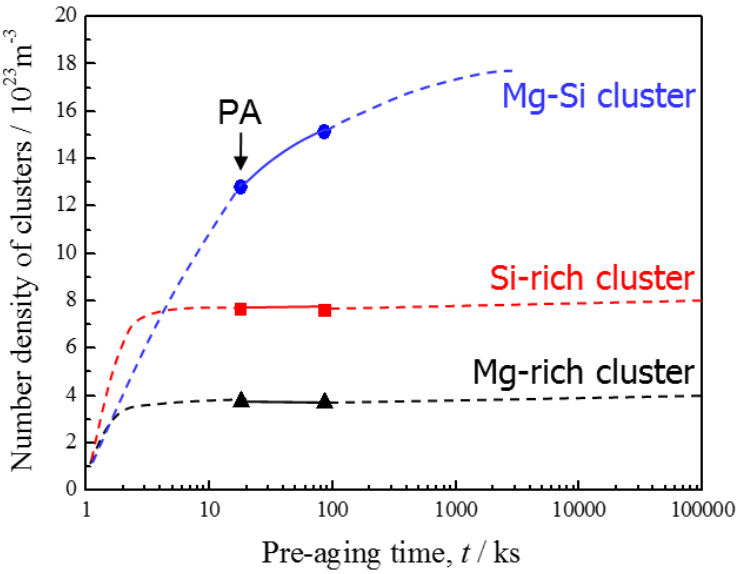


Figure 3.9 Fraction of each cluster, i.e. Si-rich cluster, Mg-Si cluster and Mg-rich cluster, with (a) natural aging at R.T. and (b) pre-aging at 363K in 6M9S alloy.
*Each cluster was classified by combined distribution of size and atomic ratio.
*The values, except for NA-S, NA-L and PA, were calculated by raw data in literature [5,7].

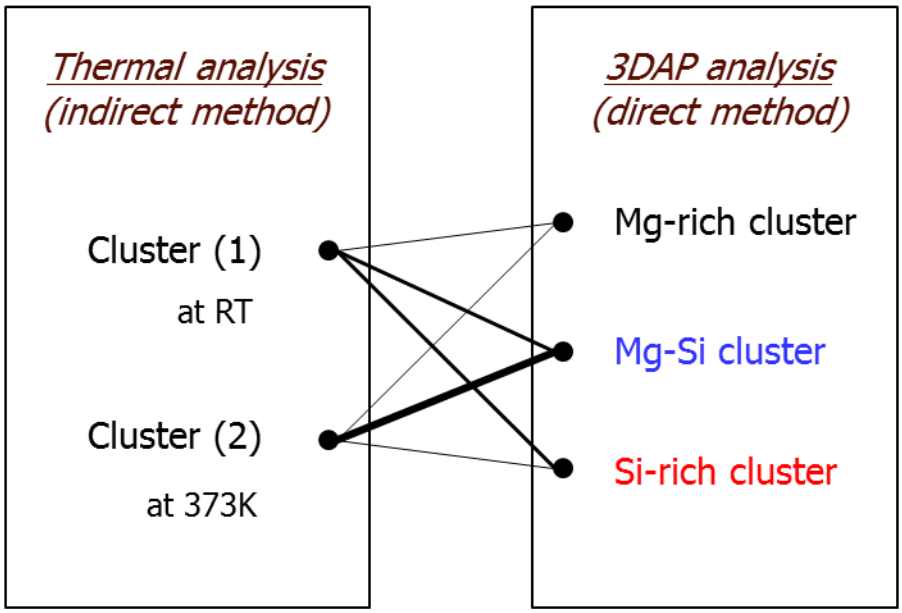


Figure 3.10 Schematic diagram indicating new cluster categorization in comparison with previous approach based on thermal analysis results.
*The thickness of connection lines describe fraction of each cluster.

# Chapter 4.
# Influence of Mg/Si Ratio and Natural- and Pre-aging on Two-step Aging Behavior

## 4.1 Introduction

The two-step aging behavior is greatly important from the viewpoint of industrial, e.g. bake-hardening response, and scientific, e.g. transition behavior from the nanoclusters to *β''*-precipitates. There are several literatures about the two-step aging and they have been tried to reveal these two-step aging behavior [1-6]. Form these previous results, the Al-Mg-Si alloys have a complicated phenomenon with aging treatment, alloying element and alloy composition in comparison with the other heat-treatable alloy series (e.g. 7xxx alloy) [7]. Also, the atomic structure changes during natural aging cause "negative effect of two-step aging" after following artificial aging. It was suggested that "negative effect of two-step aging" can be explained by the structure difference between the cluster and GP-zone during the pre-aging [3]. Yamada et al. reported the two exothermic peaks corresponding clustering reaction at lower temperature by using adiabatic calorimetry [1]. And, the cluster formed at RT and around 373K called as Si-rich cluster and GP zone. These are competitively formed each other, and show a different two-step aging behavior. Serizawa et al. proposed the characteristics of the two types of nanoclusters, i.e. Cluster (1) formed at RT and Cluster (2) formed at 373K [2,8]. From the results of 3DAP, Cluster (1) has a various atomic composition after natural aging, while Cluster (2) approaches a certain Mg/Si ratio with increasing in size, which is very close to that of the *β''*- ($Mg_5Si_6$) phase. It is noted that the "negative effect of two-step aging" is concerned with the atomic composition of the cluster rather than the number density and size of the cluster simply. In **Chapter 3**, it was noted that the 8M7S (relatively High-Mg alloy) produce numerous

Mg-rich clusters and the 6M9S (relatively High-Si alloy) produce more Si-rich clusters. The average Mg/Si ratio of 7M8S (almost equal Mg:Si alloy) is precisely located between both alloys. These results suggest that the alloy composition is deeply correlated with internal composition of clusters. Therefore, the solute-cluster with wide range of Mg/Si ratio was classified into Si-rich clusters, Mg-Si clusters and Mg-rich clusters for more systematic investigation. It was found that each cluster has a different fraction with alloy composition, aging temperature and time. The aims of present chapter are to investigate the influence of Mg/Si ratio on two-step aging behavior and to clarify the correlation between cluster categorization examined by **Chapter 3** and two-step aging behavior. Finally, it will be suggested that the improved two-step aging model considering alloy compositions, aging temperature and time.

## 4.2 Experimental Procedure

High purity Al-Mg-Si alloys were manufactured by Kobe steel, Ltd. in the form of 1.3 mm thick cold-rolled sheet. The chemical composition of examined alloys is described in Table 4.1(a). The weight percent (mass%) is converted to atomic percent for precise evaluation of atomic composition ratio as shown in Table 4.1(b). These alloys have a different Mg/Si ratio, as well as the constant total concentration (Mg+Si) of 1.5 mol%. Figure 4.1 shows that location of examined alloys.

The cold-rolled sheet alloys were solution treated for 1.8 ks in a salt bath furnace at 560 °C and subsequently quenched into ice-water at 0 °C for 60 s. These heat-treated alloys were natural aged at room temperature, pre-aged at 100 °C and artificial aged at 170 °C up to 2419.2 ks (about 1 month) in an oil bath furnace, respectively. These aged samples are called as “single aging”. After each natural aging and pre-aging at 100 °C fitted for purpose, artificial aging was carried out at 170 °C. These aged samples are called as “two-step aging”. Hardness and electrical resistivity measurements are performed in a same way with **Chapter 2**.

## 4.3 Results

### 4.3.1 Single Aging Behavior at RT, 373K and 443K

Figure 4.2 shows the (a) hardness and (b) electrical resistivity changes with aging time during the aging temperature at RT, 373 K and 443 K in 8M7S alloy, which was selected for a proper example in all examined alloys. In naturally aged alloys (see black line), hardness and electrical resistivity changes are almost not changed in the initial stage and subsequently increased, then slow down at prolonged NA time. In pre-aged at 373 K alloys (see red line), hardness and electrical resistivity changes were gradually increased in initial stage, and rapidly increased in hardness, on the contrary, not increased any longer in electrical resistivity. It is noted that the hardness increment is correlated with the strong interaction between nanocluster and dislocation [8]. And, the electrical resistivity is strongly affected by the number of solute atoms in the Al matrix and the formation of precipitates [9]. Figure 4.3 (a) and (b) shows the 3DAP maps obtained after the naturally aging for 108 ks and pre-aging for 18 ks at 363 K in 8M7S alloy. It can be seen that there exist a higher number of nanoclusters. This aggregation of Mg and Si solute atoms with small size prompted the increment of hardness and electrical resistivity.

In Fig. 4.2, the reversal of hardness and electrical resistivity change behavior as prolonged PA time indicates that the PA clusters become larger in size and approach to GP zone. In artificially aged at 443 K alloys (see blue line), hardness was rapidly increased and reached to the top of hardness (near 135HV), then decreased with prolonged aging time. On the other hands, electrical resistivity changes were rapidly decreased after temporary plateau period. The TEM bright-field image and high-resolution TEM image with the FFT pattern obtained by aged 8M7S alloy at 443 K for 36 ks (treated to maximum hardness) are shown in Figure 4.3 (c). The higher density of the needle shaped precipitates in a <001> zone axis of the Al matrix was found, resulting in the maximum value in hardness and decrement in electrical resistivity. Based on the

HRTEM image and FFT pattern in Fig. 4.3 (c), this needle shaped precipitates was expected to a typical $\beta''$-precipitates because it corresponds to characteristics of previous literatures [10-12].

In order to investigate the influence of alloy composition on the nanocluster formation behavior during natural aging and pre-aging at 373 K, hardness measurements were carried out in each examined alloys as shown in Fig. 4.4. The hardness values in as-quenched alloys (AQ) is much lower in 3M12S alloy, the rest of alloys is almost similar. And, it is found that the 7M8S alloy with Mg/Si ratio close to 1.0 exhibits most increased hardness increment in comparison with the other alloys. It is well known that the natural aging causes the "negative effect of two-step aging" due to the retarding formation of precipitates, in direct opposition of pre-aging at 373 K before artificial aging at 443 K. In next section, the influence of Mg/Si ratio, natural aging and pre-aging at 373K on two-step aging will be examined.

### 4.3.2 Two-step Aging Behavior with Mg/Si Ratio

Figure 4.5 shows the hardness changes during direct artificial aging at 443K and after natural aging at RT for 86.4 ks in (a) 9M6S, (b) 8M7S, (c) 7M8S, (d) 6M9S, (e) 5M10S and (f) 3M12S alloys. The hardness changes during direct AA at 443K after pre-aging at 373K are also shown in Fig. 4.5 (b) and (d). In all examined alloys, the hardness is first increased after natural aging for 86.4 ks and pre-aging at 373K for 18 ks, attributed to the nanocluster formation. After that, the entire hardness after NA is generally decreased in comparison with the direct artificial aging. This "negative effect of two-step aging" phenomena can be seen in all examined alloys. On the other hand, in PA conditions, the hardness increases without retarding of age-hardening. Namely, it is noted that the PA can remove and cancel the "negative effect of two-step aging". It also seems to be different behavior with the Mg/Si ratio of alloys as shown in Fig. 4.5 (b) and (d). In most

of literatures [1, 6, 13], the level of "negative effect" was mainly determined by how much the peak hardness is decreased by two-step aging. However, this approach has a risk to only evaluate the transition behavior from nanoclusters to β"-precipitates, because the peak hardness has a low vacancy and matrix concentration as well as additional factor such as growth of precipitate. Therefore, in the present study, the improved evaluation method to evaluate two-step aging behavior was suggested, allowing for end of incubation period and without the influence of precipitation growth. Figure 4.6 shows that detailed description in terms of (a) time delay and (b) hardness change. The time delay ($t_{delay}$) can be determined by time to reach $+10HV$ from the point of $HV_{as\text{-}aged}$ in the case of NA-AA and PA-AA, while $HV_{AQ}$ in the case of direct AA. The value of $t_{delay}$ means the time required to nucleate. The hardness change ($\Delta HV$) can be determined by hardness increment or decrement of initial age-hardening response. The line of $HV_{0.5}$, which means medium hardness value between $HV_{AQ}$ and $HV_{peak}$ based on direct AA, is drawn. And then, the value of $t_{0.5}$ was decided by the intersection point of direct AA and $HV_{0.5}$ lines. Finally, the hardness change ($\Delta HV$) can be calculated as below equation:

$$\Delta HV = HV_{t_{0.5}}^{two-step\ aging} - HV_{t_{0.5}}^{direct\ AA} \quad (4.1)$$

Figure 4.7 shows (a) time delay ($t_{delay}$) and (b) hardness change ($\Delta HV$) results obtained by specific evaluation method to clarify two-step aging behavior. In Fig. 4.7 (a), the value of $t_{delay}$ in NA-AA condition is much longer than other conditions such as direct AA and PA-AA. It means that the natural aging before artificial aging extremely delays the precipitation during aging at 443K in comparison with PA-AA condition. It also can be seen that there was no significant difference with Mg/Si ratio of alloys in all aging conditions. However, the hardness change ($\Delta HV$), as described in Fig. 4.7 (b), shows the obvious difference on alloy compositions. In the case of NA-AA, the all examined alloys indicate the "negative effect on two-step aging". And, it was found that this effect is much higher in High-Si alloy than High-Mg alloy. One of the examined alloys, the 6M9S alloy

(Mg/Si = 0.80) has much stronger "negative effect on two-step aging", whereas the 8M7S alloy (Mg/Si = 1.29) has much weaker. In the case of PA-AA, the 8M7S alloy shows the "positive effect on two-step aging", while 6M9S alloy shows the "negative effect on two-step aging" even though pre-aging before artificial aging. This phenomenon can be explained by correlation between cluster fraction, i.e. Si-rich clusters, Mg-Si clusters and Mg-rich clusters, and two-step aging. It will be discussed in next section by comparison with 3DAP results as mentioned in **Chapter 3**.

## 4.4 Discussion

Much research has been done on the two-step aging behavior, because of its scientific and industrial importance [1-6]. As mentioned in **Chapter 1**, Yamada et al. [1] and Serizawa et al. [2] concluded that "*negative effect of two-step aging"* can be explained by the different characteristics of Cluster (1) and Cluster (2), which formed at around R.T. and 373K. Cluster (1), i.e. Si-rich cluster, is not transformed into the β" phases due to its high thermal stability. Cluster (2), i.e. Mg-Si cluster, can easily developed into β" phases based on its compositional similarity with β" phases. Takaki et al. [14] reported that the Cluster (1) and Cluster (2) are able to coexist in multi-step aging including both natural aging and pre-aging. It was also suggested that the final artificial aging behavior can be determined by the formation amount of Cluster (1) and Cluster (2). In other words, both internal structure and volume fraction of each cluster should be considered in order to clarify two-step aging behavior. In **Chapter 3**, the cluster categorization was systemically done by 3DAP dataset, result in Cluster (1) and Cluster (2) are composed of Si-rich clusters, Mg-Si clusters and Mg-rich clusters. It was also mentioned that each cluster has a different volume fraction with aging temperature and time (see Fig. 3.9). The present author believes that the different fraction of each cluster can affect two-step aging behavior. There are different opinions in the viewpoint of the 3DAP results and two-step aging behavior. M. Torsaeter et al. [15] investigated the clustering behavior formed in

alloy with excess Mg and Si concentration by using the APT analysis. It has been demonstrated that the natural aging produced Mg-rich clusters in excess Mg alloy and Si-rich clusters in excess Si alloy, while pre-aging promoted the formation of clusters with 1.0 of Mg/Si ratio regardless alloy composition. There is possibility that these deflection phenomena of composition distribution affect the "negative effect of two-step aging". However, the findings of the previous research do not support the current study. In Fig. 4.7, the High-Mg alloys have a lower level of "negative effect of two-step aging" even though the Mg/Si ratio of alloy is far from 1.0. Recently, Aruga et al. [16,17] investigated the clustering behavior during natural aging and subsequent artificial aging by using APT with high accuracy and resolution in an Al-Mg-Si alloy. It was noted that the typical Si-rich clusters, which can neither be dissolved nor grow further, lead to the retardation of the hardness increase during AA. Therefore, the correlation between the fraction of Si-rich clusters and Mg-Si clusters and two-step aging behavior are concretely investigated. Figure 4.8 shows the fraction of each cluster obtained by 3DAP results, i.e. Si-rich clusters, Mg-Si clusters and Mg-rich clusters, with natural aging at R.T. and pre-aging at 363K in 6M9S, 7M8S and 8M7S alloys. In Fig. 4.8 (a), (c) and (d), the fraction of Mg-Si clusters is almost constant regardless of alloy compositions, while the fraction of Si-rich clusters is greatly different with alloy compositions. Comparing with Fig. 4.7 (b), the 6M9S alloy with much Si-rich clusters shows the most negative effect on two-step aging. In Fig. 4.8 (a), (b), (d) and (e), the fraction of Si-rich clusters in PA condition is almost same with NA condition, while the fraction of Mg-Si clusters is extremely increased. That is why PA condition shows less negative effect or positive effect on two-step aging as shown in Fig. 4.7 (b). As a results, the two-step aging behavior can be determined by the relative number of Si-rich clusters and Mg-Si clusters. The correlation between hardness change ($\Delta HV$) and fraction of Si-rich clusters and Mg-Si clusters can be formularized as follows:

$$\Delta HV = -\mathrm{A}(N_{Si-rich\ cluster}) + \mathrm{B}(N_{Mg-Si\ cluster}) \tag{4.2}$$

where constant A is greater than constant B, because the influence of Si-rich cluster on negative effect must be greater than Mg-Si cluster on positive effect in the viewpoint of transition behavior. In order to decide the accurate value of constant A and B, the internal structure, i.e. atom arrangement and vacancy behavior, and thermal stability relating with reversion phenomena should be investigated. It will be discussed in next **Chapter 5 and 6** in more detailed.

## 4.5 Conclusions

The two-step aging behavior with the different Mg/Si ratio and natural- and pre-aging was investigated in the present chapter. In addition, the correlation between cluster categorization and two-step aging behavior was discussed. The obtained results are summarized as follows:

1. The “negative effect of two-step aging” phenomena can be seen in all examined alloys. On the other hand, in PA conditions, the hardness increases without retarding of age-hardening. Namely, it is noted that the PA can remove and cancel the “negative effect of two-step aging”. The 6M9S alloy (Mg/Si = 0.80) has much stronger “negative effect on two-step aging”, whereas the 8M7S alloy (Mg/Si = 1.29) has much weaker. In the case of PA-AA, the 8M7S alloy shows the “positive effect on two-step aging”, while 6M9S alloy shows the “negative effect on two-step aging” even though pre-aging before artificial aging.

2. Two-step aging behavior can be determined by the relative number of Si-rich clusters and Mg-Si clusters regardless of aging temperature. In NA condition, the 6M9S alloy with much Si-rich clusters shows the most negative effect on the two-step aging. However, in the PA condition, the fraction of Mg-Si clusters is extremely increased. That is why the PA condition shows less negative effect or positive effect on two-step aging

## References


[1] K. Yamada, T. Sato, A. Kamio: Journal of Japan Institute of Light Metals, 51 (2001) pp. 215-221.

[2] A. Serizawa, S. Hirosawa, T. Sato: Metallurgical and Materials Transactions A, 39 (2008) pp. 243-251.

[3] D.W. Pashley, J.W. Rhodes and A. Sendorek: J. Inst. Metals, 92 (1966) 41-49.

[4] J. langerweger: Proc. Aluminium Technology (1986) Paper No. 49.

[5] C.S.T. Chang, I. Wieler, N. Wanderka and J. Banhart: Ultramicroscopy, 109 (2009) pp. 585.

[6] J. Kim, E. Kobayashi, T. Sato: Materials Transactions, Vol. 56, No. 11 (2015) pp. 1771-1780

[7] G.W. Lorimer, R.B. Nicholson, The Mechanism of Phase Transformations in Crystalline Solids, The Institute of Metals, London, 1969, pp. 36.

[8] A. Serizawa, T. Sato, W.J. Poole: Philosophical Magazine Letters, Vol. 90, No. 4 (2010) pp. 279-287.

[9] K. Osamura, Y. Hiraoka, Y. Murakami: Philos. Mag., 28 (1973) pp. 809.

[10] C.D. Marionara, S.J. Andersen, J. Jansen, H.W. Zandbergen: Acta Materialia, 51 (2003) pp. 789-796.

[11] S.J. Andersen, H.W. Zandbergen, J. Jansen, U. Tundal, O. Reiso: Acta Materialia, 46 (1998) pp. 3283-3298.

[12] J.P. Lynch, L.M. Brown, M.H. Jacobs: Acta Metallurgica, 30 (1982) pp. 1389-1395.

[13] H. Suzuki, M. Kanno and Y. Shiraishi: J. Jpn. Inst. Light Metals, Vol. 28, No. 5 (1978) pp. 233-240.

[14] Y. Takaki, T. Masuda, E. Kobayashi and T. Sato: Materials Transactions, Vol. 55, No. 8 (2014) pp. 1257-1265.

[15] M. Torsæter, H. S. Hasting, W. Lefebvre, C. D. Marioara, J. C. Walmsley, S. J. Andersen, R. Holmestad: J. Appl. Phys. 108 (2010) 073527.

[16] Y. Aruga, M. Kozuka, Y. Takaki, T. Sato: Metall. Mater. Trans. A 45 (2014) pp. 5906-5913.

[17] Y. Aruga, M. Kozuka, Y. Takaki, T. Sato: Materials Science & Engineering A 631 (2015) pp. 86-96.

Table 4.1 (a) Chemical composition of examined Al-Mg-Si alloys, mass%

| Alloy | Elements, mass% | | | |
|---|---|---|---|---|
| | Mg | Si | Fe | Al |
| 9M6S | 0.87 | 0.62 | 0.01 | Bal. |
| 8M7S | 0.78 | 0.70 | 0.01 | Bal. |
| 7M8S | 0.73 | 0.81 | 0.01 | Bal. |
| 6M9S | 0.62 | 0.93 | 0.09 | Bal. |
| 5M10S | 0.48 | 0.97 | 0.01 | Bal. |
| 3M12S | 0.36 | 1.17 | 0.01 | Bal. |

Table 4.1 (b) Chemical composition of examined Al-Mg-Si alloys, mol%

| Alloy | Elements, mol% | | | | Mg/Si | Mg + Si |
|---|---|---|---|---|---|---|
| | Mg | Si | Fe | Al | | |
| 9M6S | 0.97 | 0.60 | <0.01 | Bal. | 1.62 | 1.56 |
| 8M7S | 0.87 | 0.67 | <0.01 | Bal. | 1.29 | 1.54 |
| 7M8S | 0.81 | 0.78 | <0.01 | Bal. | 1.04 | 1.59 |
| 6M9S | 0.70 | 0.88 | 0.04 | Bal. | 0.80 | 1.58 |
| 5M10S | 0.53 | 0.93 | <0.01 | Bal. | 0.57 | 1.46 |
| 3M12S | 0.40 | 1.12 | <0.01 | Bal. | 0.36 | 1.52 |

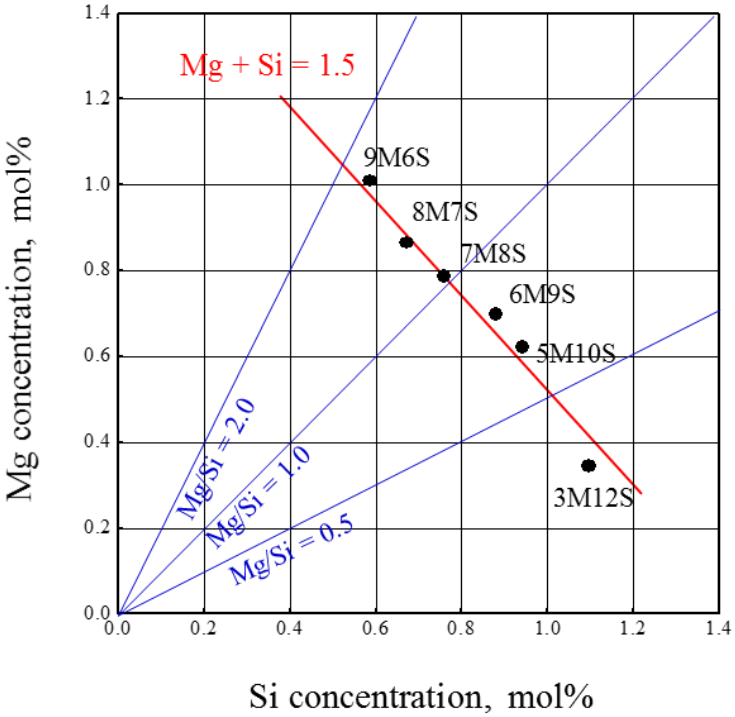


Figure 4.1 Locations of the examined Al-Mg-Si alloys (mol%). The manufactured alloys have a different Mg/Si ratio with constant (Mg+Si) concentration of 1.5 mol%.

(a) Hardness change

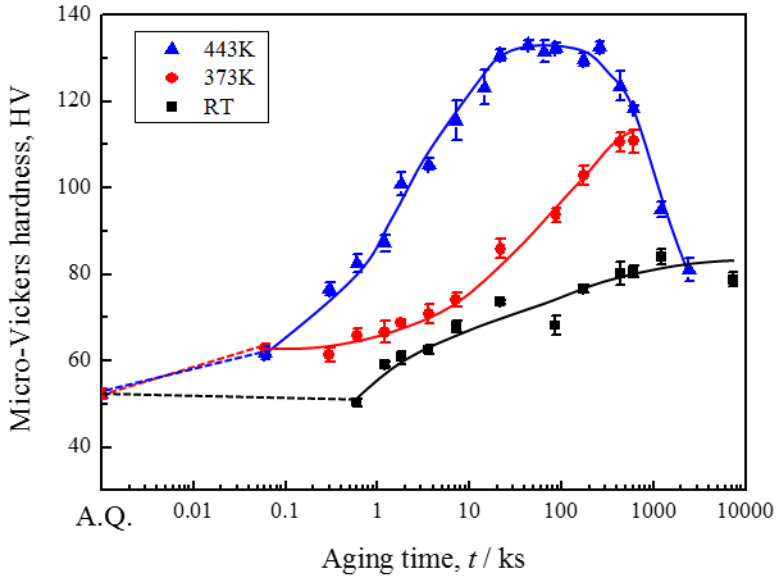


(b) Electrical resistivity change

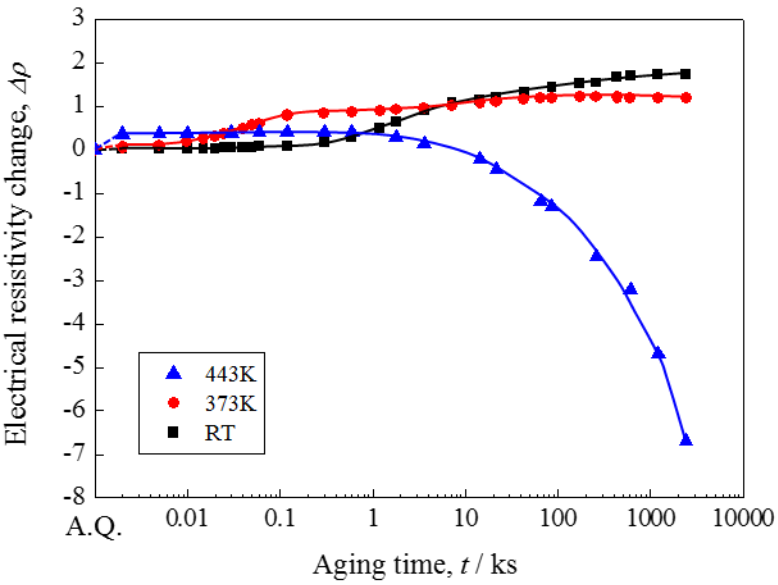


Figure 4.2 (a) Hardness and (b) electrical resistivity changes with various aging temperature at RT, 373K and 443K in 8M7S alloy

(a) Atom map after natural aging 108 ks (NA-S)

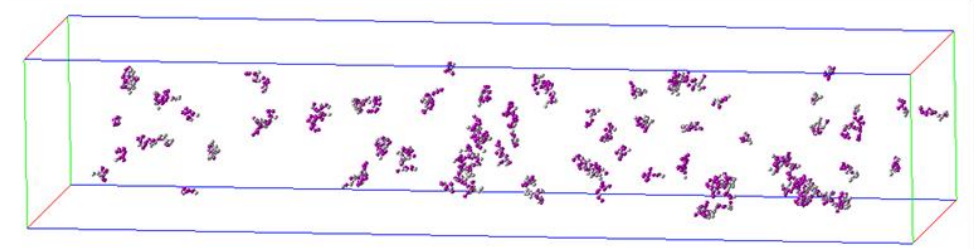

(b) Atom map after pre-aging 18 ks at 363 K (PA)

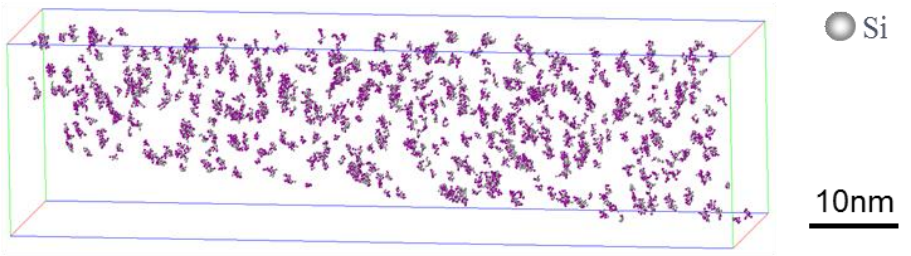


Figure 4.3 Atom map showing the 3D elemental distribution of Mg and Si atoms obtained by the maximum separation method with with $d_{max}$ = 0.75 nm and $N_{min}$ = 10 in the 8M7S alloy after (a) natural aging for 108 ks (NA-S), 7560 ks (NA-L) and (b) pre-aging for 18 ks at 363 K (PA).
(c) TEM bright field images and HRTEM image taken in the (001) zone axis with the FFT pattern after artificial aging 36 ks at 443 K.

(c) TEM image after artificial aging 36 ks at 443 K

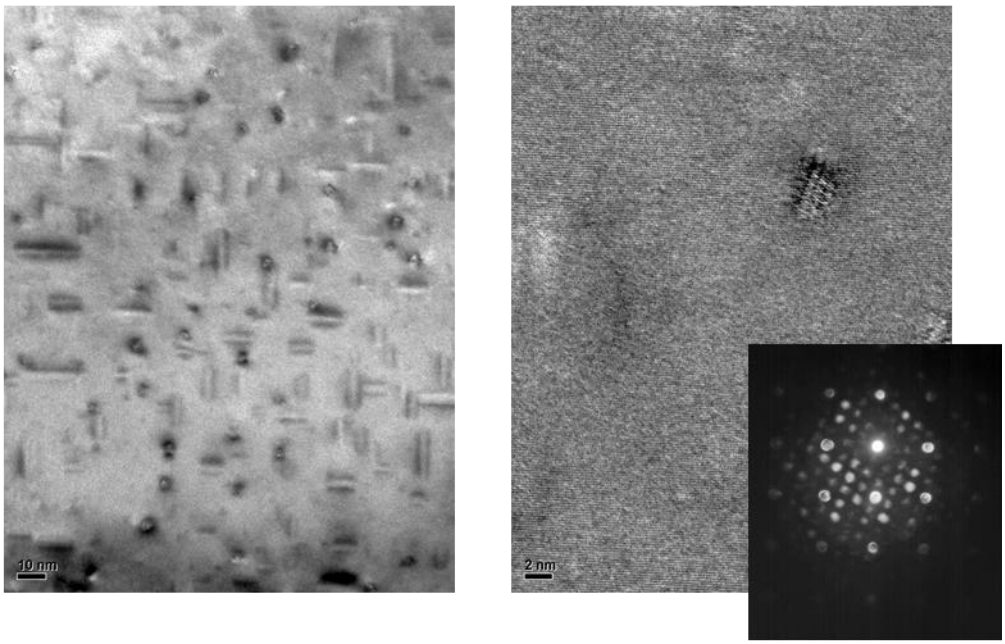


Figure 4.3 Continued.

(a) Natural aging at RT

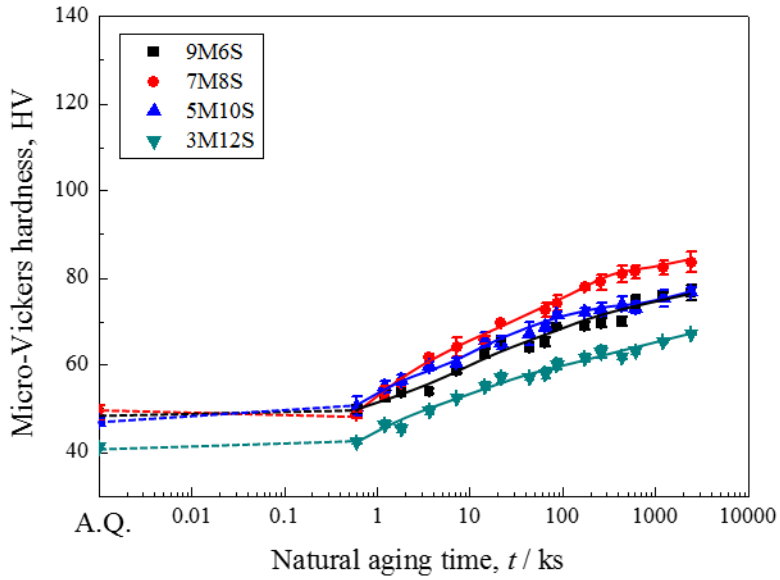


(b) Aging at 373K

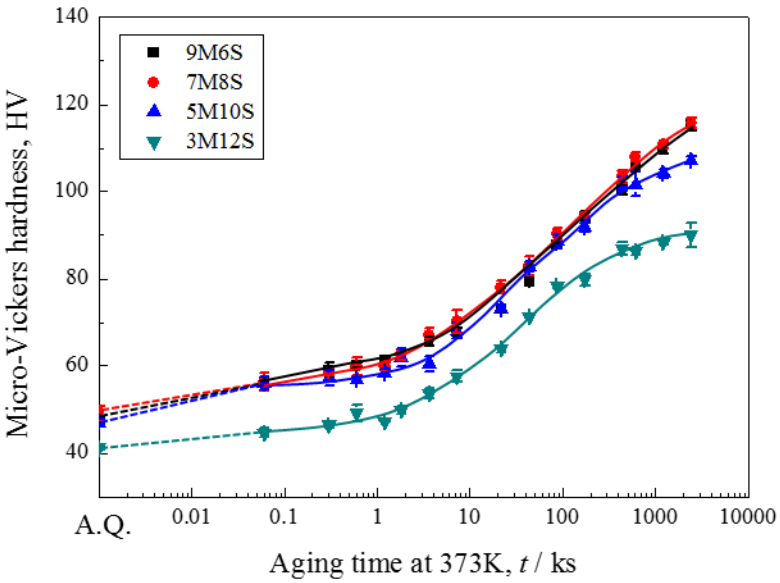


Figure 4.4 Hardness changes during (a) natural aging at RT and (b) aging at 373K in examined Al-Mg-Si alloys.

(a) 9M6S alloy

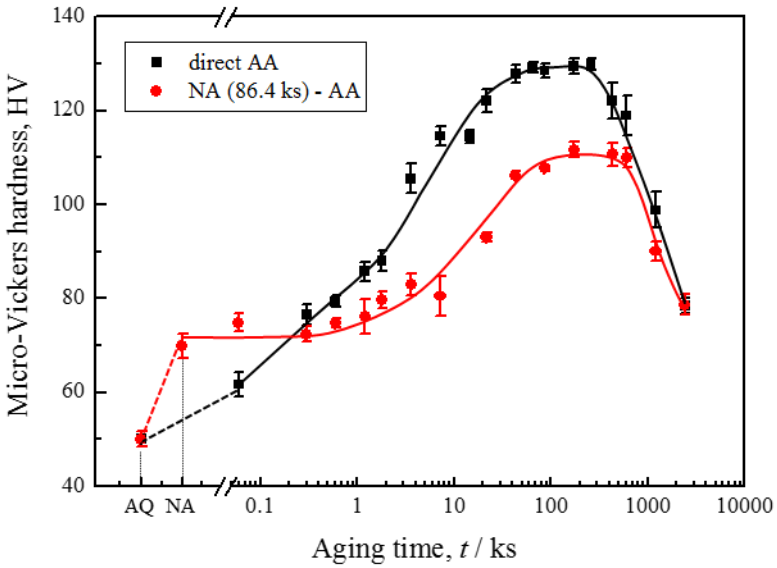


(b) 8M7S alloy

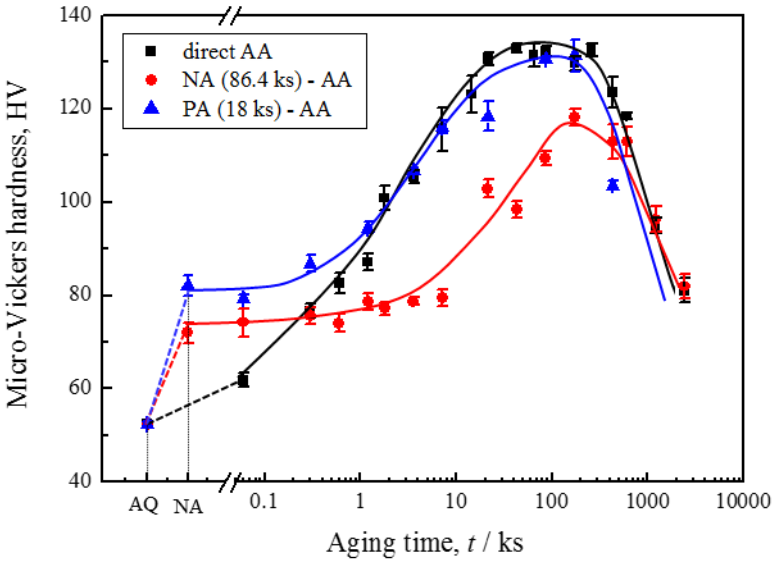


Figure 4.5 Hardness changes during artificial aging at 443K directly and two-step aging after natural aging at RT for 86.4 ks and pre-aging at 373K for 18 ks.
(a) 9M6S, (b) 8M7S, (c) 7M8S, (d) 6M9S, (e) 5M10S and (f) 3M12S alloys.

(c) 7M8S alloy

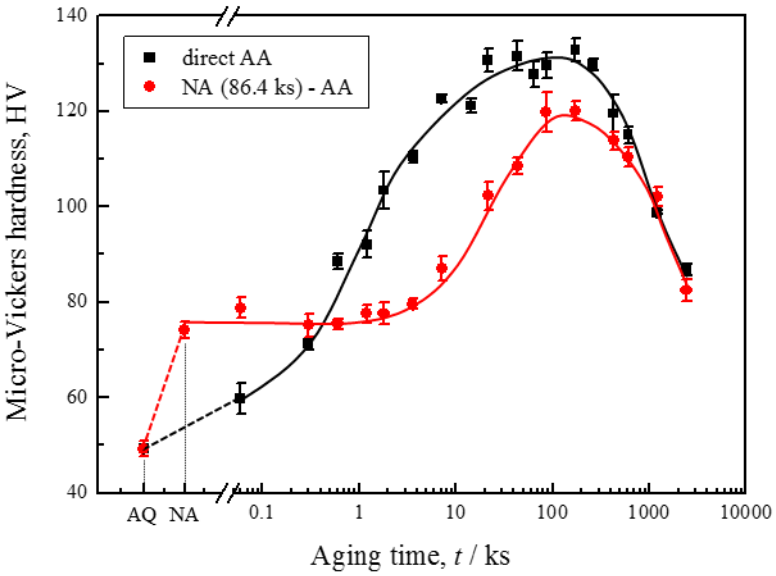


(d) 6M9S alloy

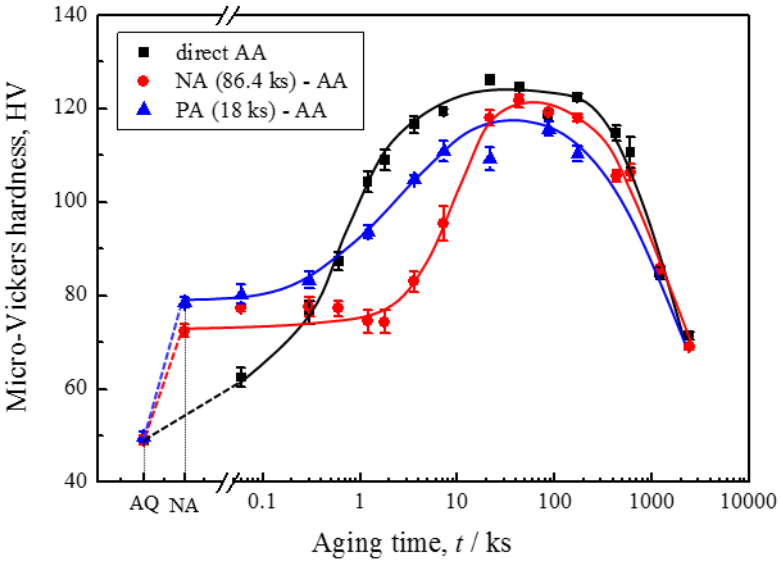


Figure 4.5 Continued.

(e) 5M10S alloy

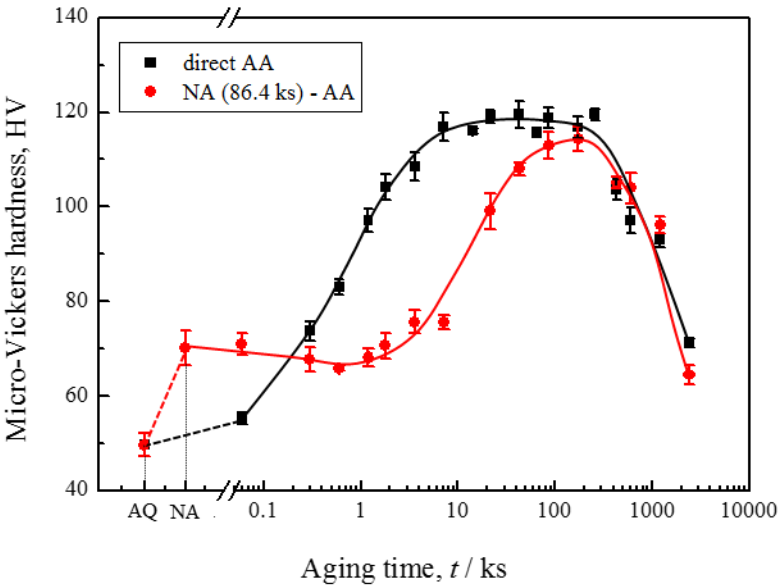


(f) 3M12S alloy

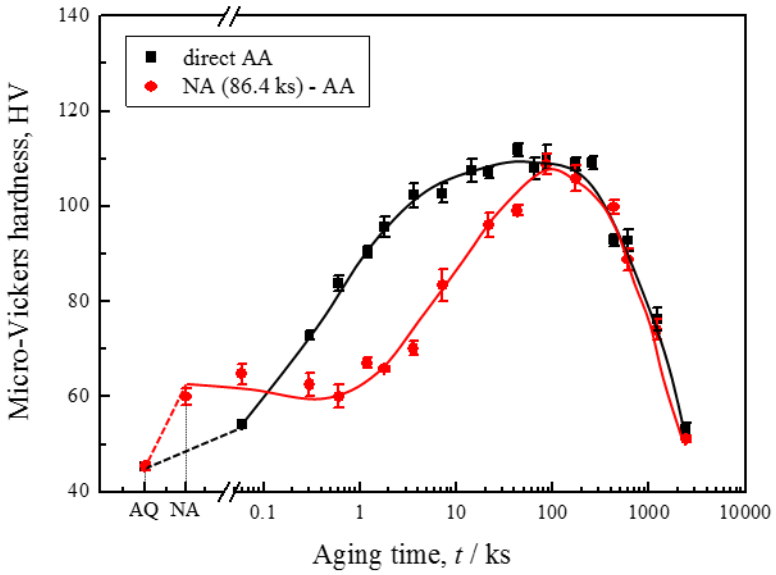


Figure 4.5 Continued.

(a) Time delay

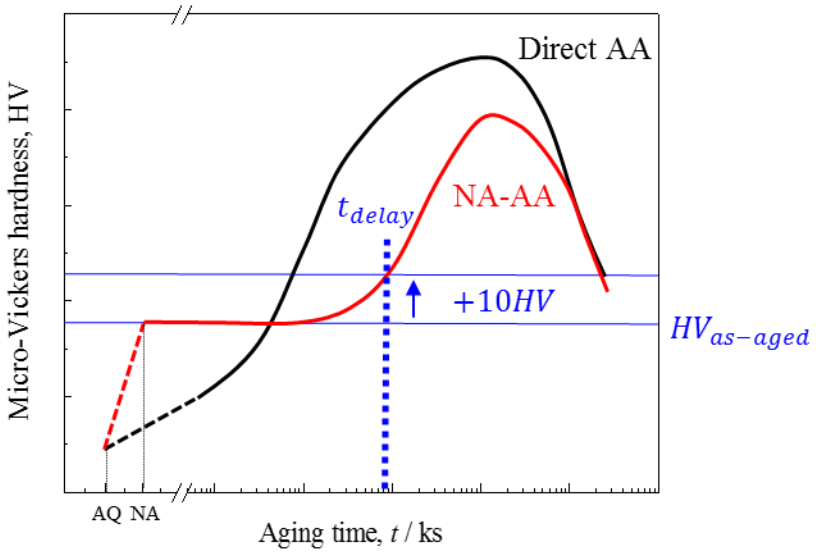


(b) Hardness change

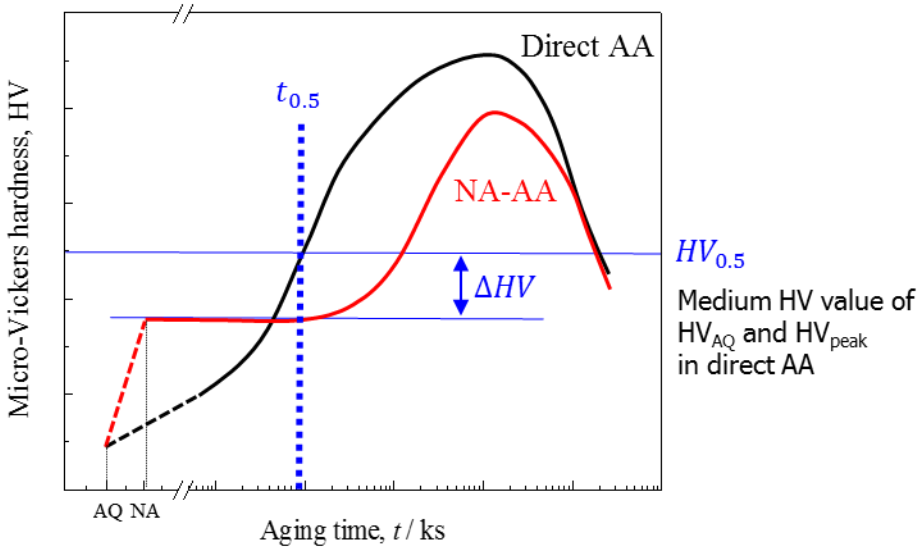


Figure 4.6 Evaluation methods of two-step aging behavior based on direct artificial aging (AA) curve using (a) delay time and (b) hardness change. *$HV_{AQ}$ and $HV_{as\text{-}aged}$ indicate the hardness at the as-quenched alloy and natural aged at RT for 86.4 ks and pre-aged at 373K for 18 ks.

(a) Time delay

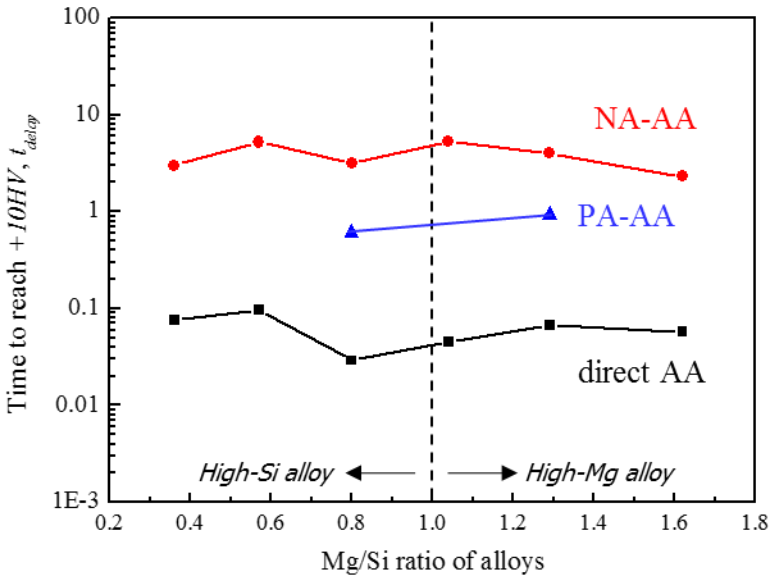


(b) Hardness change

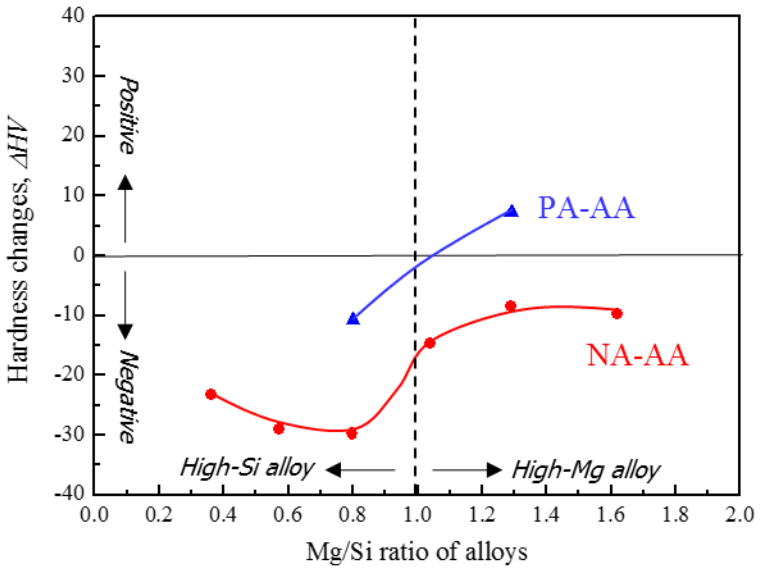


Figure 4.7 (a) Time delay and (b) hardness change obtained by evaluation method of two-step aging behavior in all aging conditions as a function of Mg/Si ratio of alloys.

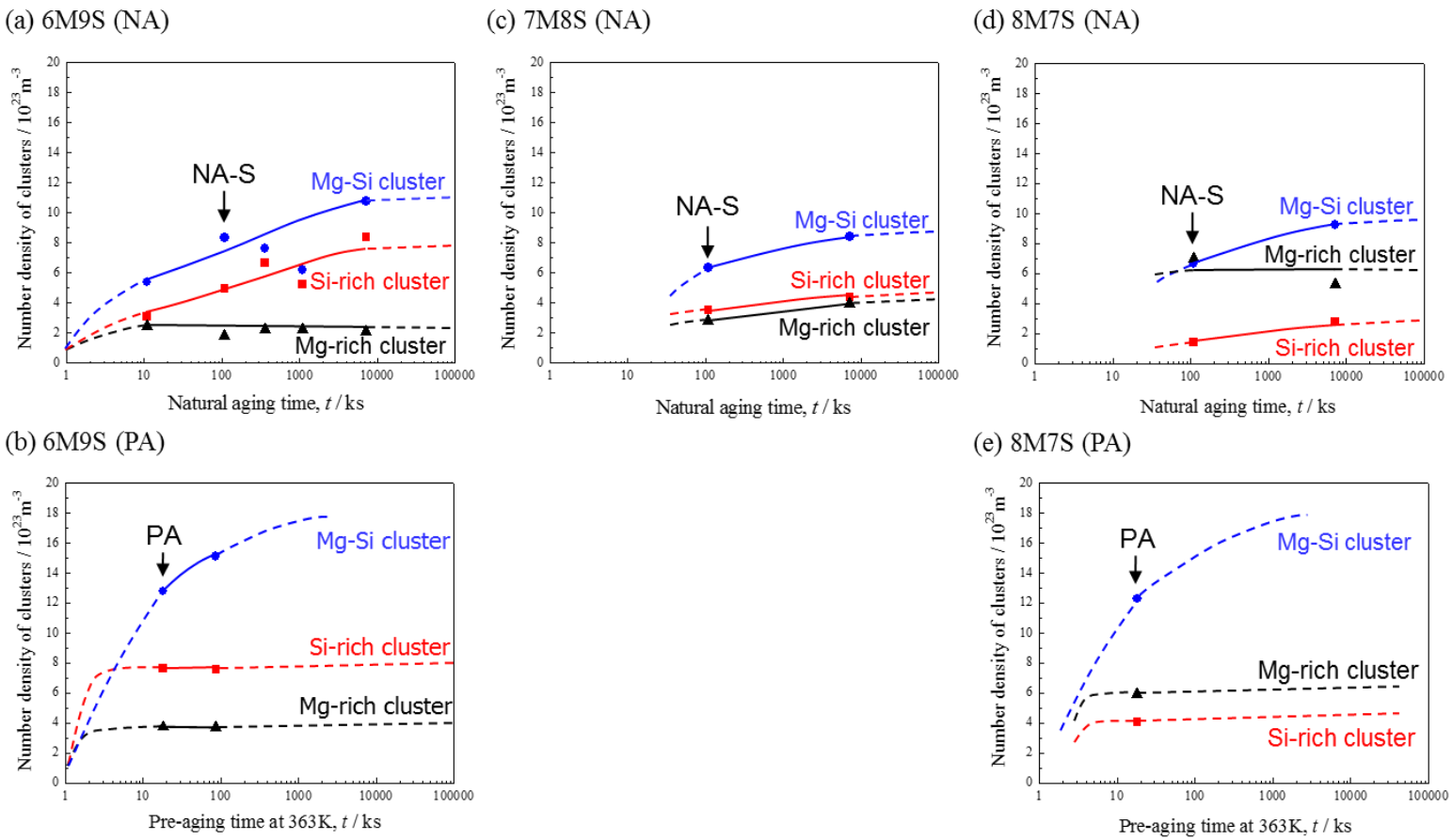


Figure 4.8 Fraction of each cluster obtained by 3DAP results, i.e. Si-rich cluster, Mg-Si cluster and Mg-rich cluster, with natural aging at R.T. and pre-aging at 363K in 6M9S, 7M8S and 8M7S alloys.
*The values, except for NA-S, NA-L and PA, were calculated by raw data in literature [14,15].

# Chapter 5.
# Influence of Quenched-in Excess Vacancies on Nanocl
# uster Formation and Two-step Aging Behavior

## 5.1 Introduction

Age-hardenable phenomenon is one of the most efficient ways for high strength aluminum alloys. The heat-treatable Al-Mg-Si (6xxx) and Al-Zn-Mg (7xxx) alloys have been extensively used as structural materials due to their good mechanical properties and high corrosion resistance. The strength of these alloys is greatly improved by the fine and homogeneously distributed precipitates in the Al matrix. The representative age-hardening sequences of each alloy are as follows [1-4]:

$$6xxx : \alpha(SSSS) \rightarrow \text{nanoclusters} \rightarrow \beta'' \rightarrow \beta' \rightarrow \beta\ (Mg_2Si) \quad (5.1)$$

$$7xxx : \alpha(SSSS) \rightarrow \text{nanoclusters} \rightarrow \text{GP-zone} \rightarrow \eta' \rightarrow \eta\ (MgZn_2) \quad (5.2)$$

where SSSS is the supersaturated solid solution. The main strengthening phase of alloys is β'' and η', respectively [1,4]. The precipitation behavior of these nano-sized precipitates is strongly associated with the initial stage of precipitation such as nanoclusters and GP-zones formed at the lower temperature aging. Therefore, it is most important to understand the initial clustering stage with a driving force caused by the super-saturated solid solution and quenched-in excess vacancies. In Al-Mg-Si alloys, natural aging (NA) is a frequent cause of the negative effect on the following paint-baking process done at around 170℃ [5,6]. The main reason for this is due to the remaining Si-rich clusters with

high thermal stability [7]. On the contrary, the Al-Zn-Mg alloy shows a tendency to be positive effect on the bake-hardening response [8]. These experimental results suggest the difference in the formation behavior of the initial clustering in Al-Mg-Si and Al-Zn-Mg alloys. The research dealing with these points is extremely rare in terms of quenched-in excess vacancies.

In addition, these two alloy systems are well known to have the different quench sensitivity [9-11]. Even though quenching rate is very slow after the extrusion or solution heat treatment, the bake hardenability of Al-Mg-Si alloys does not decrease markedly, while that of Al-Zn-Mg alloys changes drastically. These suggest that the behavior of quenched-in excess vacancies is different in extremely in the initial aging stage such as solute-vacancy pairing between both alloy systems. In this paper, the influence of quenching conditions (WQ: water-quench, SQ: step-quench, DQ: direct-quench) on the nanocluster formation in the initial stage at low aging temperature aging as well as the two-step aging behavior was investigated in Al-Mg-Si and Al-Zn-Mg alloys. Furthermore, the role of quenched-in excess vacancies and interaction between solute atoms and vacancy are discussed.

## 5.2 Experimental Procedure

The high purity Al-0.81 at% Mg-0.78 at %Si (designated to 7M8S) and Al-2.17 at% Zn-2.28 at% Mg (Al-5.12 mass% Zn-2.00 mass% Mg) alloys with 1.3 mm thickness were examined. The heat treatment process with a different temperature-time path is shown in Fig. 5.1. These two cold-rolled sheet alloys were solution treated in a salt bath furnace at $T_s$ for $t_s$. And then, three kinds of quenching process were performed, e.g. WQ (water-quench), SQ (step-quench) and DQ (direct-quench), to investigate the influence of quenching conditions on the following heat treatments. The detailed quenching process is as follows:

(1) WQ: subsequently quenched into ice-water and kept for 60 s

(2) SQ: transferred to a salt bath set at $T_b$ within $t_b$ and then cooled down to room temperature

(3) DQ: directly quenched to oil bath at $T_a$

The temperature and time of the individual heat treatment process for the Al-Mg-Si and Al-Zn-Mg alloys are described. The solution treatment and artificial aging conditions were selected to be generally used temperature and time [1-4]. The influence of quenching conditions on the nanocluster formation and two-step aging behavior were investigated by the differential scanning calorimetry (DSC) and micro-Vickers hardness measurements.

## 5.3 Results

### 5.3.1 Determination of Effective Quenching Condition without Solute Loss

Figure 5.2 shows the (a) hardness and (b) DSC results of step-quenched alloys with the various time ($t_b$) at 533 K compared to water-quenched alloys to determine the proper step-quenching time without solute-loss in Al-Mg-Si alloys. The temperature of step-quenching was selected by considering the temperature range that the nanocluster formation does not occur. There are several possible events during step-quenching as follows:

(1) decrease of vacancy concentration ($C_v$), e.g. $C_v$ after step-quenching at 533 K is close to 1/100 of that after as-quenched alloy (~$10^{-5}$)

(2) solute-loss in the matrix by the precipitation, results in the decreased matrix concentration

In Fig. 5.2 (a), the hardness is almost unchanged until $t_b$ = 30 s against that of the water-quenched alloy. After that, the hardness is gradually increased, resulting from the

precipitation. It is noted that the vacancy concentration can be effectively depleted without solute-loss in the matrix by the precipitation in the condition of $t_b$ = 30 s. The fact that this condition is suitable to achieve the purpose of the present study, can also be seen in Fig. 5.3 (b). Figure 5.3 (b) shows the DSC results of the step-quenching alloys with the various time compared to the water-quenched alloys. Focusing the peak as indicated arrows corresponding to the nanoclusters and precipitation of the β”-phase, the heat evolution seems to be different with SQ time compared to WQ. Two overlapped peaks, indicating the nanocluster formation, were detected in the WQ and SQ alloys until 30 s, and then completely disappear after 600 s. Especially, it can be also seen that the peak intensity of the β”-phase is significantly reduced in the $t_b$ = 600 s. The reason of extinction is the precipitation of the β”-phase before starting of heat-up, results in the increment of hardness. Therefore, the most suitable condition is considered as $t_b$ = 600 s on the basis of hardness and DSC results.

### 5.3.2 Influence of Quenching Conditions on Heating Process

Figure 5.3 shows the (a) DSC curves and (b) hardness results obtained during heating process for the comparison between WQ and SQ in the Al-Mg-Si alloys. Two exothermic peaks indicating the Cluster (1) and Cluster (2) at the low temperature and another exothermic peak of the β”-phase at the higher temperature were detected in the examined WQ and SQ alloys. The formation of Cluster (1) and Cluster (2) and precipitation of β” affect to the hardness increment during heating process as shown in Fig. 5.3 (b). In Fig. 5.3 (a), peaks of heat evolution correlated to the Cluster (1), Cluster (2) and β”-phase are slightly changed by SQ, while there is no notable difference in the hardness results between WQ and SQ. Namely, the influence of step-quenching in Al-Mg-Si alloys on heating process is extremely insignificant, while fine structural changes have taken place such as solute-vacancy bonding unaccompanied by any hardness change.

### 5.3.3 Influence of Quenching Conditions on Isothermal Aging

Figure 5.4 shows the hardness results during natural aging after WQ and SQ in the (a) Al-Mg-Si and (b) Al-Zn-Mg alloys. The hardness during natural aging was gradually increased by the formation of nanoclusters in the Al-Mg-Si alloys and GP-zones in the Al-Zn-Mg alloy, respectively. In Fig. 5.4 (a), there is no significant difference between WQ and SQ, namely the free-vacancy exists sufficiently to accelerate nanocluster formation. On the contrary, in Fig. 5.4 (b) the slight hardness changes between WQ and SQ were found in the extremely initial natural aging, which means retarding the GP-zone formation by SQ. Interestingly, this difference between WQ and SQ is shown clearly at elevated temperatures. In Fig. 5.5 (b), the artificially aged Al-Zn-Mg alloys after SQ were hardly hardened, while after WQ the hardness is rapidly increased due to the precipitation of the $\eta'$-phase. In addition, the similar results represent in DQ and SQ alloys, namely it is hard to form the nanoclusters contributing to nucleation sites by SQ. On the other hands, in Fig. 5.5 (a), the age-hardening curve is drawn by the precipitation of the β”-phase regardless the quenching conditions. It is suggested that the Al-Mg-Si and Al-Mg-Zn alloys have a different vacancy behavior, especially the enough vacancies to form nanoclusters and precipitates remain although SQ in Al-Mg-Si alloys. It is treated in the discussion section that how can vacancies behave in Al-Mg-Si alloys.

### 5.3.4 Influence of Quenching Conditions on Two-Step Aging

As mentioned in Fig. 5.4, there is no significant difference between WQ and SQ in the Al-Mg-Si alloys, while the hardening is slightly delayed after SQ as shown in the initial natural aging time for the Al-Zn-Mg alloys. In order to observe this fine difference between WQ and SQ, the two-step aging was performed with various natural aging time. Figure 5.6 shows the hardness changes with the quenching conditions as a function of various natural aging time before artificial aging for 86.4 ks (near peak hardness) at 443

K in Al-Mg-Si alloys. The peak hardness is rapidly decreased from the hardness without NA (as indicated by arrows), and then maintains the certain steady hardness as prolonged NA time. Interestingly, it was found that the degree of the negative effect in the case of SQ is much greater than WQ. It is suggested that the initial supersaturated state after WQ and SQ is obviously different each other. Figure 5.7 shows the hardness changes with the quenching conditions as a function of various natural aging times before artificial aging for 86.4 ks (near peak hardness) at 423 K in Al-Zn-Mg alloys. As mentioned in Fig. 5.5 (b), the peak hardness is obviously distinctive between WQ and SQ without NA. This distinction was maintained for a while of NA. However, the peak hardness after SQ is rapidly increased in a short time later, and then catch up with WQ. After about 100 ks, the positive effect is shown both WQ and SQ conditions. It is suggested that the precipitation in the Al-Zn-Mg alloys is greatly governed by the kinetic-control resulting from SQ. The difference of the vacancy behavior between the Al-Mg-Si and Al-Zn-Mg alloys is discussed in the viewpoint of the role of Si atoms.

## 5.4 Discussion

The influence of quenching conditions on the nanocluster formation and two-step aging behavior is investigated in the present study. The excess vacancies induced by the solution heat treatment (SHT) help diffusion to form the solute-clusters in the initial natural aging time [12]. Therefore, the quenched-in excess vacancies affect significantly the entire precipitation sequence and behavior. According to the previous researches, it is believed that there are three essential mechanisms for excess vacancies supplied by rapid quenching from high temperature [13-15]. First, under “vacancy pump model”, the excess vacancies are simply annihilated by diffusion (concurrently help to diffuse solute atoms), following arrive at thermal equilibrium state [13]. Second, “vacancy trapping model” means that once a solute atom and vacancy encounter each other, it is hard to detach due to the interaction energy between solutes and vacancies [14]. Third, the secondary defects

such as a dislocation loop and vacancy aggregation can be formed [15]. The present study make progress to a discussion with careful consideration of these two mechanisms for excess vacancy behavior. In recent years, there has been an increasing interest in studies about vacancies and solute clustering inside Al alloys by using the muon spin relaxation and positron annihilation spectroscopy [16,17]. Wenner et al. [16] found that the Mg-Si clusters trap and keep vacancies inside the material during aging. This trapping may be closely associated with solute-clustering during NA. Liu et al. [17] reported that after quenching there are two types of positron traps such as vacancy-related defects and vacancy-free solute clusters. Namely, the vacancies are retained by binding to solute-vacancy complexes and transport solute atoms to emerging clusters. The results reported here appear to support these assumptions. The current study found that suitable step-quenching conditions (e.g. 533K, 30 s), which is considered to only reduce the vacancy concentration without solute-loss. As a comparison of Al-Mg-Si alloys, Al-Zn-Mg alloys without Si contents as well as showing different two-step aging behavior and quenching sensitivity as mentioned in introduction. Interestingly, these two kinds of alloys have a different vacancy behavior without the complete depletion of vacancy after SQ condition. The reason about this difference can be explained by focusing the role of Si atoms. In Al-Mg-Si alloys, it is likely to form the Si-V complex after SQ, because of the higher the diffusion coefficient ($D_0$) of Si in the Al matrix and bonding energies of the Si-V complex than Mg-V complex [18]. The current results as shown in Fig. 5.3 (a) and Fig. 5.6 provide reasonable evidence, e.g. the enhancement of peak intensity indicating Cluster (1) formation and the greater negative effect of two-step aging after SQ. On the other hands, in the Al-Zn-Mg alloys excluding Si content, it is found that the great difference between WQ and SQ is as shown in Fig. 5.7. But soon, this great hardness difference becomes narrow toward prolonged natural aging time. It is likely to form the dislocation loops and/or vacancy aggregation in the Al-Zn-Mg alloy by absence of Si atoms. This dislocation loop plays a role of the annihilation point of a vacancy as well as source of vacancy supply into the matrix. Westmacott et al. [19] reported the results of calculation

for the vacancy concentration making dislocation loops. As a result, the dislocation density is much smaller in the order of pure Al and Al-Zn, Mg, Si alloys, concurrently the bonding energy is much higher in the previous order. Thus, the dislocation loops and helical dislocations can be seen frequently in the Al-Zn-Mg alloys excluding Si contents [20]. For these reasons, the examined Al-Mg-Si and Al-Zn-Mg alloy have a different two-step aging behavior and quenching sensitivity.

## 5.5 Conclusions

The influence of quenching conditions on the nanocluster formation and two-step aging behavior in Al-Mg-Si alloys was investigated in the present chapter. In addition, the roles of the quenched-in excess vacancies and Si atoms were discussed in comparison with the Al-Zn-Mg alloy without Si contents.

1. The Al-Mg-Si and Al-Mg-Zn alloys have a different vacancy behaviors, especially the enough vacancies to form nanoclusters and precipitates remain although the condition of SQ in Al-Mg-Si alloys.

2. As a comparison of Al-Mg-Si alloys and Al-Zn-Mg alloys without Si contents, it is likely to form the Si-V complex after SQ in Al-Mg-Si alloys. Therefore, the negative effect of two-step aging is greater after SQ.

3. It is likely to form the dislocation loops and/or vacancy aggregation in the Al-Zn-Mg alloy by absence of Si atoms. This dislocation loop plays a role of the annihilation point of vacancy as well as source of vacancy supply into the matrix.

## References


[1] G.A. Edwards, K. Stiller, G.L. Dunlop and M.J. Couper: Acta Mater. 46 (1998) 3893.

[2] K. Matsuda, Y. Sakaguchi, Y. Miyata, Y. Uetani, T. Sato, A. Kamio and S. Ikeno: J. Mater. Sci. 35 (2000) 179.

[3] S.J. Andersen, C.D. Marioara, A.G. Frøseth, R. Vissers and H.W. Zandbergen: Mater. Sci. Eng. A 390 (1-2) (2005) 127.

[4] H. Inoue, T. Sato, Y. Kojima, T. Takahashi:Metallurgical Transactions A, Vol. 12A (1981) pp. 1429-1434

[5] K. Yamada, T. Sato, A. Kamio: Journal of Japan Institute of Light Metals, 51 (2001) pp. 215-221.

[6] A. Serizawa, S. Hirosawa, T. Sato: Metallurgical and Materials Transactions A, 39 (2008) pp. 243-251.

[7] J. Kim, E. Kobayashi, T. Sato: Materials Transactions, Vol. 56, No. 11 (2015) pp. 1771-1780

[8] G.W. Lorimer, R.B. Nicholson, The Mechanism of Phase Transformations in Crystalline Solids, The Institute of Metals, London, 1969, pp. 36.

[9] E.D. Sweet, B.R. Harker, X. Zhang, M.J. Couper: Proc. 9th Inter. Aluminum Extrusion Technology Seminar, Vol. 1 (2008) pp. 415-424

[10] LIU Sheng-dan et al: J. Central South University, Science and Technology, Vol. 37(5) (2006), pp. 846-849.

[11] Kavalco, Patricia Mariane; C.F. Canale, Lauralice; Totten, George E.: Industrial Heating, Vol. 78 Issue 2 (2011), pp. 39

[12] J. Banhart, M.D.H. Lay, C.S.T. Chang, A.J. Hill, Physical Review B, 83 (2010), pp. 1-13.

[13] L.A. Girifalco and H. Herman, Acta Met. 13, 583 (1965)

[14] H. Kimura, R.R. Hasigute: Acta Metall. 16 (1975), pp. 361-368.

[15] 鈴木寿，菅野幹宏，伊藤吾朗　日本金属学会会報 24(1985)102.

[16] S. Wenner, K. Nishimura, K. Matsuda et al. Metallurgical and Materials Transactions A, 45A (2014) pp. 5777-5781.

[17] M. Liu et al.:Acta Materialia 91 (2015) pp. 335-364

[18] S. Hirosawa, T. Sato, A. Kamio, H.M. Flower: Acta Mater., 48 (2000) pp. 1797-1806.

[19] K.H. Westmacott, R.S. Barnes, D. Hull, R.E. Smallman: Phil. Mag., 6 (1961) pp. 929.

[20] H. Loffler, I. Kovacs, J. Lendvai: Journal of Materials Science, 18 (1983) pp. 2215-2240.

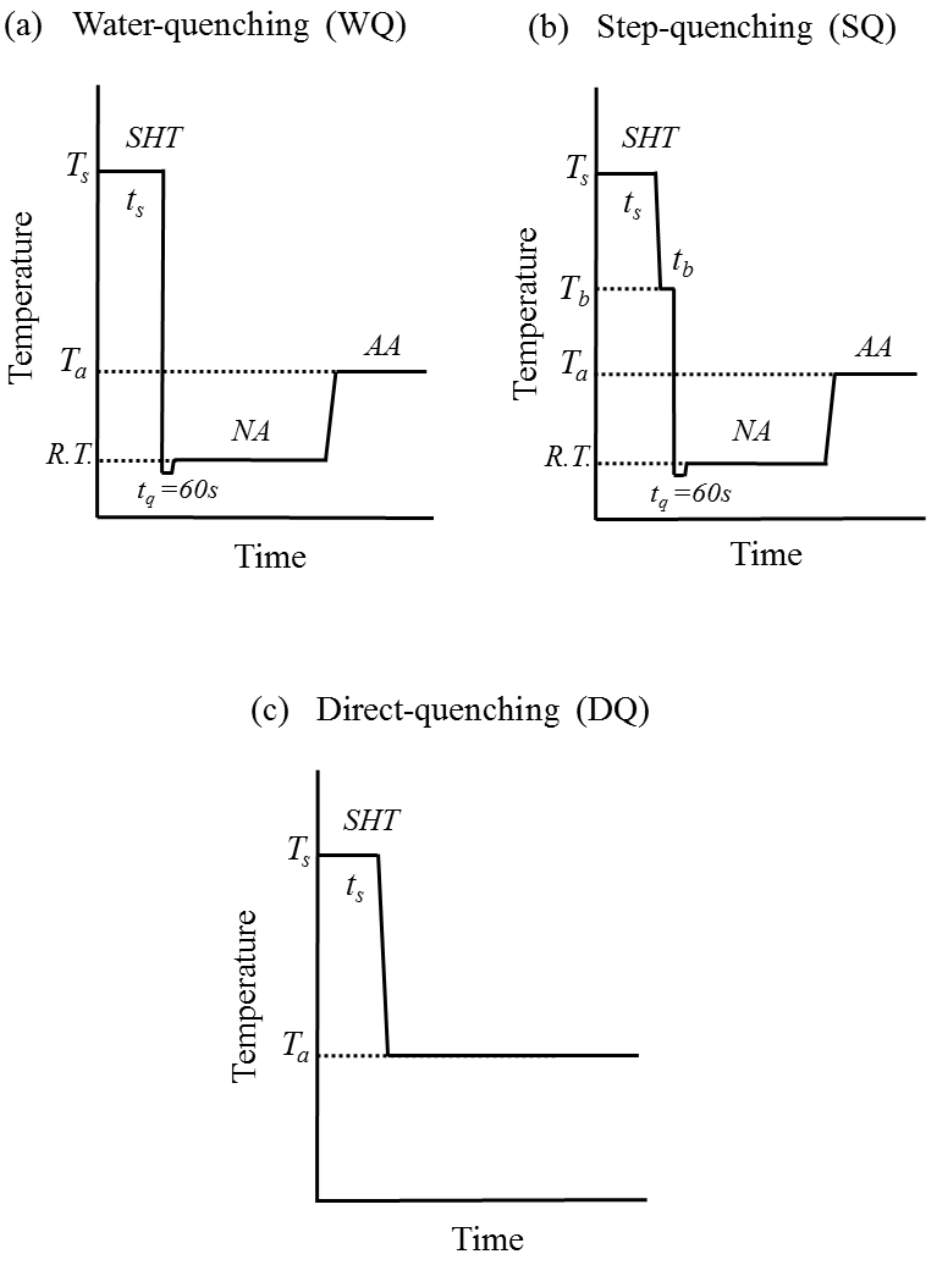


Figure 5.1 Schematic diagram of heat treatment procedures for (a) water-quenching, (b) step-quenching and (c) direct-quenching.
Single-step aging : natural aging (NA) after solution heat treatment (SHT)
Two-step aging : NA for a certain time after SHT, and subsequently artificial aging (AA)

Table 5.1 Temperature and time of individual heat treatment process for the Al-Mg-Si and Al-Zn-Mg alloy.

| Alloys | Solution heat treatment | | Step-quenching | | Artificial aging |
|---|---|---|---|---|---|
| | $T_s$ (Temp.) | $t_s$ (time) | $T_b$ (Temp.) | $t_b$ (time) | $T_a$ (Temp.) |
| Al-Mg-Si alloy | 560 °C | 1.8 ks | 260 °C | 30 s | 170 °C |
| Al-Zn-Mg alloy | 470 °C | 3.6 ks | 260 °C | 30 s | 150 °C |
| | | | 200 °C | 2 min* | |

*This condition of step-quenching were performed only before artificial aging.

(a) Hardness results

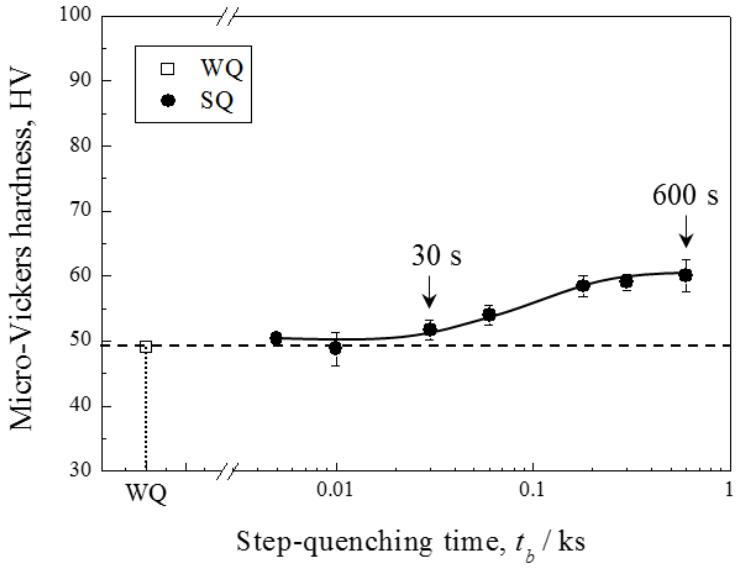


(b) DSC results

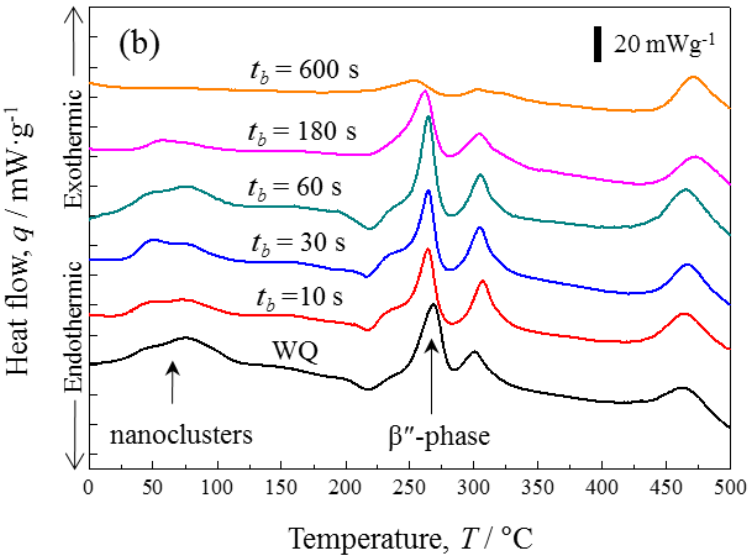


Figure 5.2 Determination of the proper step-quenching time at 533 K without solute-loss in Al-Mg-Si alloys,
(a) Hardness results of water-quenched and step-quenched alloys with the various time
(b) DSC results of step-quenched alloys with the various time compared to water-quenched alloys..

(a) DSC results

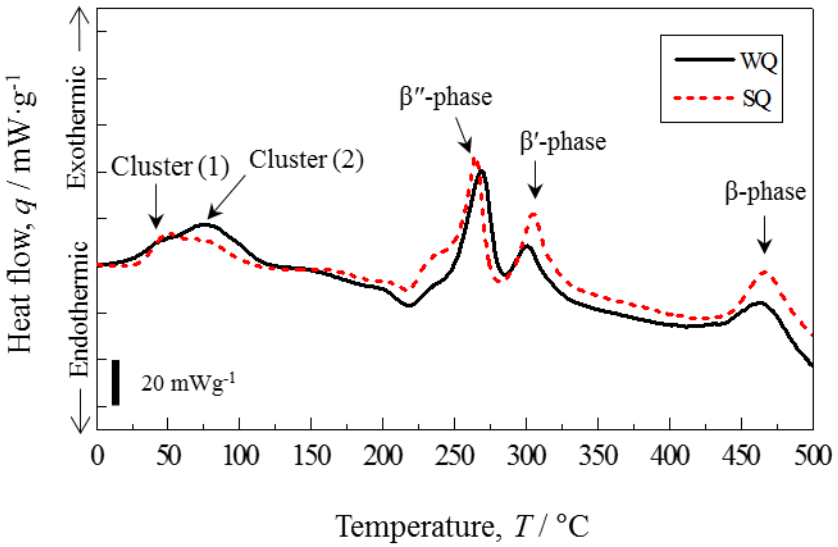


(b) Hardness results during heating process

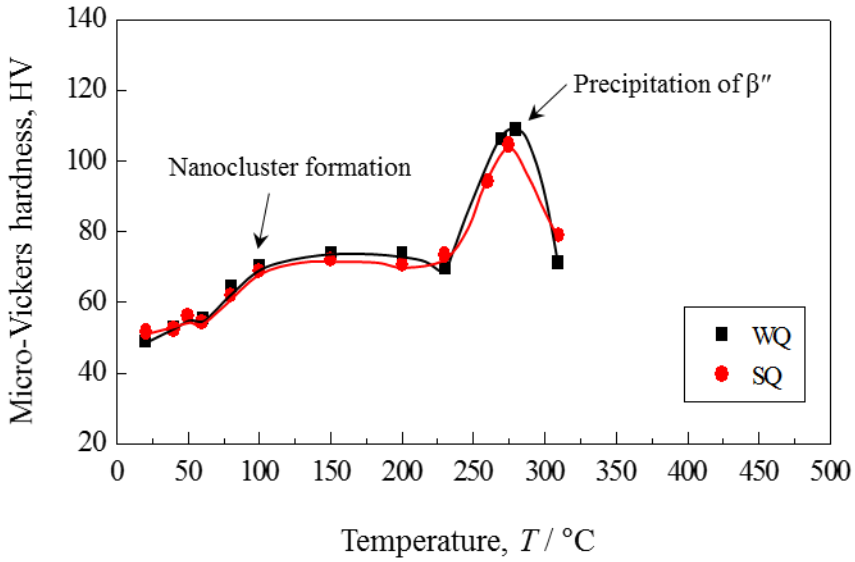


Figure 5.3 (a) DSC curves and (b) hardness results during heating process for the comparison between water-quenched and step-quenched alloys in Al-Mg-Si alloys.

(a) Al-Mg-Si alloy

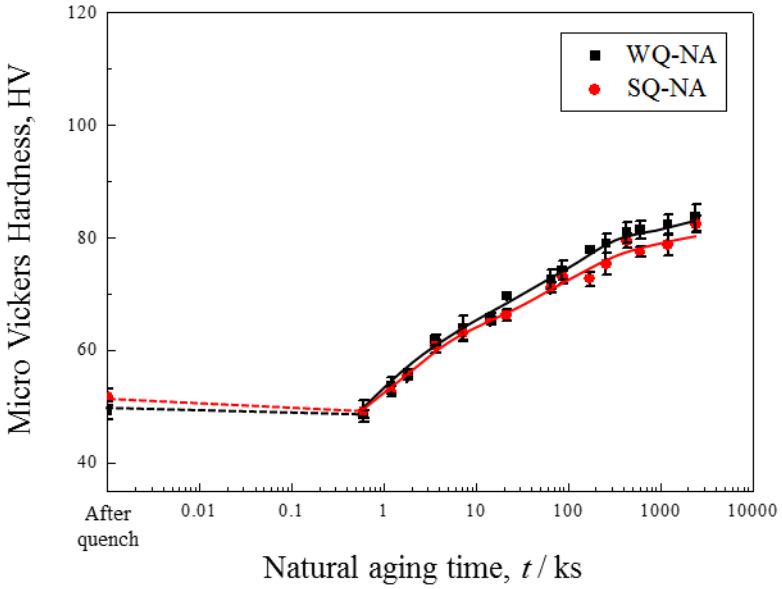


(b) Al-Zn-Mg alloy

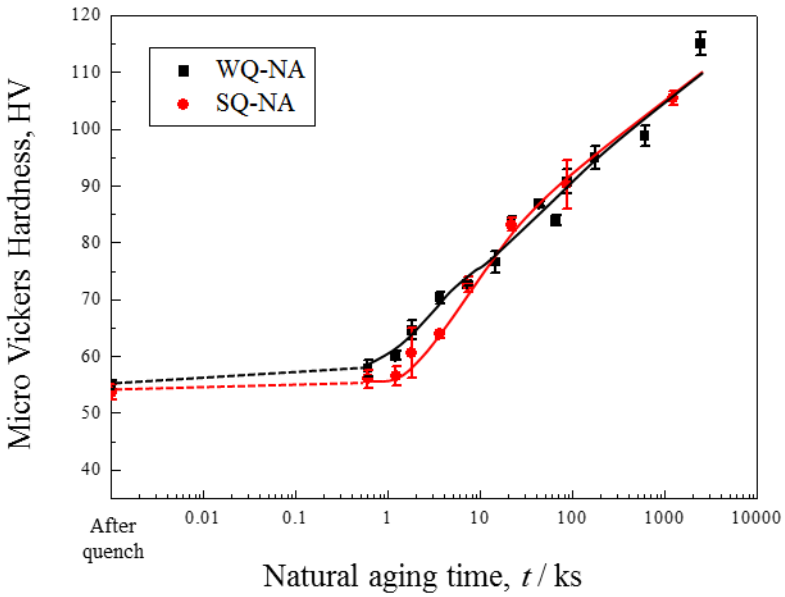


Figure 5.4 Hardness results during natural aging for the comparison between water-quenched and step-quenched (a) Al-Mg-Si and (b) Al-Zn-Mg alloys.

(a) Al-Mg-Si alloy

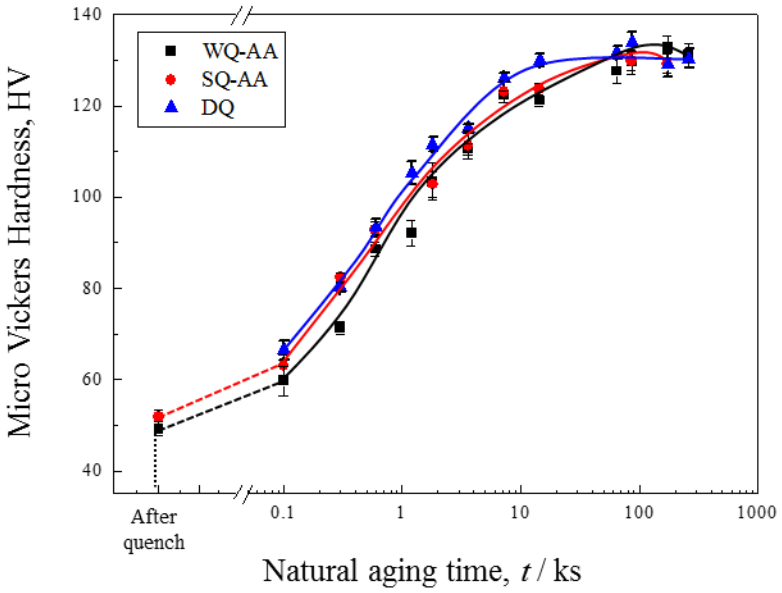


(b) Al-Zn-Mg alloy

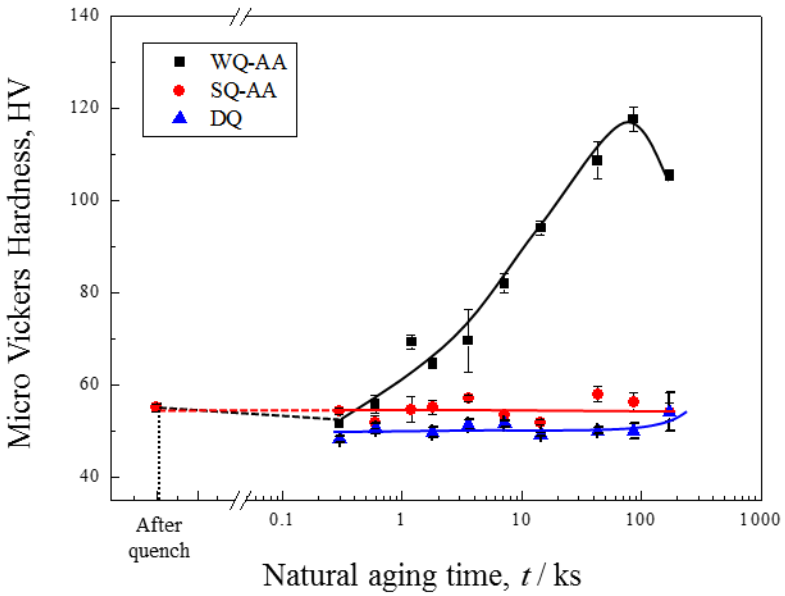


Figure 5.5 Hardness results during artificial aging for comparison between water-quenched, step-quenched and direct-quenched (a) Al-Mg-Si and (b) Al-Zn-Mg alloys

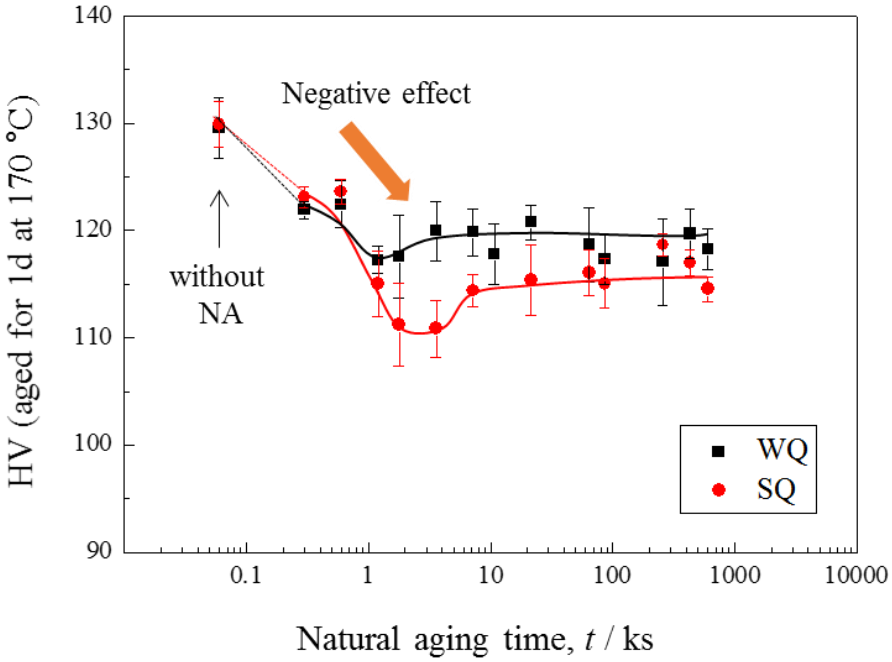


Figure 5.6 Hardness changes with various natural aging time before artificial aging for 86.4 ks at 443 K in water-quenched and step-quenched Al-Mg-Si alloy.

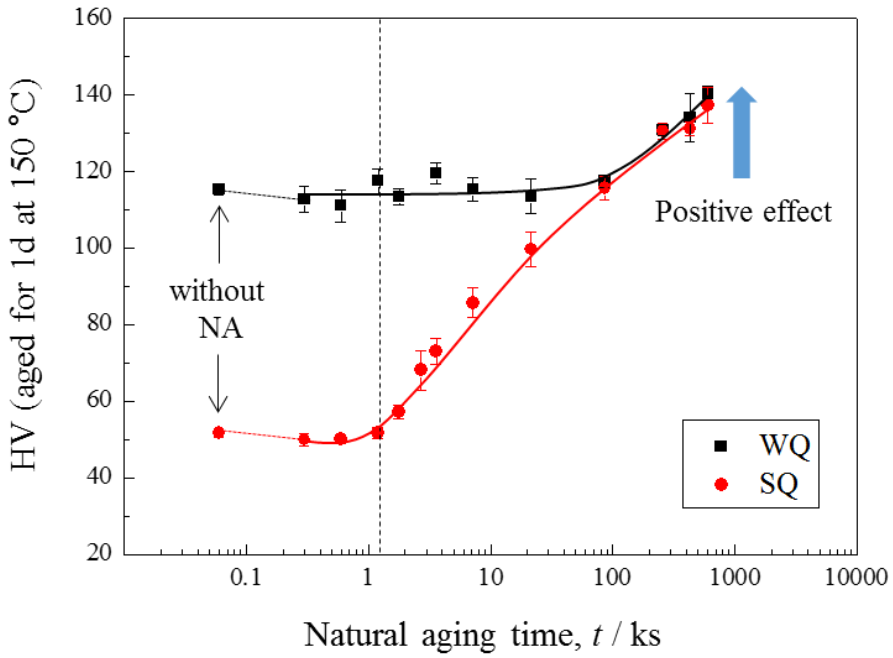


Figure 5.7 Hardness changes with various natural aging time before artificial aging for 86.4 ks at 423 K in water-quenched and step-quenched Al-Zn-Mg alloy.

# Chapter 6.
# Influence of Cluster Characteristics and Its Thermal Stability on Bake-hardening Response

## 6.1 Introduction

In practical field, bake-hardening response is significant factor because the strength of automobile body panels can be determined by paint-baking process. The conventional paint-baking is generally performed at around 443K for 1.2 ks after press-forming in the automobile manufacturing process [1,2], resulting in improving the mechanical strength due to their significant precipitation hardening. The Al-Mg-Si alloy sheets are solution treated at aluminum company and normally transported to automobile company. During this shipping, these Al sheets are essentially exposed at room temperature during prolonged time (≈maximum 1 year) before the paint-baking process. As a results, the natural aging before BH treatment leads to the insufficient BH response [3-7]. Kim et al. [8] reported that the influence of natural aging time on two-step aging behavior of Al-Mg-Si alloys. In addition, they suggested that the thermal stability of nanoclusters and their transition behavior during two-step aging in Al-Mg-Si(-Cu) alloys. Aruga et al. [9] also reported that the BH response is greatly reduced as prolonged natural aging time before BH treatment, due to the partial dissolution of pre-formed clusters [10]. In the present chapter, the influence of Mg/Si ratio of alloy on BH response was firstly investigated in the viewpoint of reversion phenomena. In addition, the correlation between cluster characteristic (i.e. cluster fraction as mentioned in **Chapter 3**) and BH response in terms of thermal stability will be discussed.

## 6.2 Experimental Procedure

High purity 8M7S, 7M8S and 6M9S alloys were provided from Kobe steel, Ltd. in the form of 1.3 mm thick cold-rolled sheet. The chemical composition of examined Al-Mg-Si alloys is described in Table 6.1. The weight percent (mass%) is converted to atomic percent for precise evaluation of atomic composition ratio as shown in Table 6.1 (b). These alloys have a different Mg/Si ratio range from 0.80 to 1.29, as well as the constant total concentration (Mg+Si) of 1.5 mol%. Figure 6.1 shows that location of examined alloys. The cold-rolled sheet alloys were solution treated for 1.8 ks in a salt bath furnace at 560 °C and subsequently quenched into ice-water at 0 °C for 60 s. These heat treated alloys were natural-aged at room temperature for 108 ks (30 hours) and 7560 ks (roughly 2000 hours), which is designated by the NA-S (short-term natural aging), NA-L (long-term natural aging). After each natural aging time, artificial aging was carried out at 170 °C. Hardness measurements are performed in a same way with **Chapter 2**.

## 6.3 Result and Discussion

### 6.3.1 Bake-hardening Response after Short- and Long-term Natural Aging

Figure 6.2 shows the hardness results during artificial aging at 443K after short-term (NA-S) and long-term (NA-L) natural aging in the (a) 8M7S, (b) 7M8S and (c) 6M9S alloys. In all conditions, the hardness increment was retarded by natural aging before artificial aging at 443K. It also seems that the hardness behavior before starting hardness increment is different with alloy compositions. The bake-hardening response was evaluated by the degree of hardness change ($\Delta HV$) after artificial aging at 443 K for 1.2 ks in compared with hardness value without artificial aging. Figure 6.3 shows bake-hardening (BH) response obtained from hardness values (in Fig. 6.2) after artificial aging at 443 K for 1.2 ks with different natural aging conditions, i.e. NA-S and NA-L, as a

function of alloy compositions. It was found that the BH response significantly depends on the natural aging conditions before artificial aging and alloy compositions. In NA-S condition, all examined alloys show the increment of BH response. The most interesting point is that the decrement of BH response can be seen in only 6M9S and 7M8S alloy even though the same long-term natural aging condition. As mentioned in introduction, the decrement of BH response are deeply correlated with reversion of pre-formed nanoclusters. In other words, there was no observation of reversion phenomena in NA-S condition regardless alloy compositions. However, the reversion can be observed in only 7M8S and 6M9S alloys after long-term natural aging (NA-L). It was found that the amount of reversion observed in 6M9S alloy is larger than that of 7M8S alloy. In the next section, what kind of cluster can be mainly dissolved will be discussed in terms of its thermal stability.

### 6.3.2 Correlation between Cluster Characteristic and Bake-hardening Response

As mentioned in **Chapter 3**, the fraction of each cluster, i.e. Si-rich clusters, Mg-Si clusters and Mg-rich clusters are extremely different with alloy compositions and natural aging time. This difference contributes to whether the reversion occur or not as shown in Fig. 6.3. As previous approach, the critical size of clusters was significant factor to determine whether the reversion occur of not [11,12]. Namely, the small-sized clusters than critical size can be dissolved, whereas the large-sized clusters than critical size can be transformed into β"-precipitate. However, the results of a recent research show that the internal structure, i.e. composition and atom arrangement, of clusters is significant factor to determine reversion phenomena. Aruga et al. [9] reported that the formation and reversion of clusters during natural aging and subsequent artificial aging in an Al-Mg-Si alloy (same alloy with 6M9S). They suggested that the typical Si-rich clusters can lead to

the retardation of the hardness increase during artificial aging due to its higher thermal stability. In addition, the decrement of bake-hardening response is deeply correlated with reversion of Mg-Si clusters close to 1.0. Figure 6.4 shows the fraction of each cluster, i.e. Si-rich clusters, Mg-Si clusters and Mg-rich clusters, in 6M9S alloy with different aging time at 443K after NA for 2.8 ks$\times 10^4$ ks (7800 h). Each cluster was classified by same method as mentioned in **Chapter 3** using the 3DAP results provided by literature [9]. The BH response in NA7800 condition shows similar behavior with NA-L condition of the present study. It was found that the fraction of Si-rich clusters and Mg-rich clusters is not changed until 3.6 ks of artificial aging. The most interesting point is that the fraction of Mg-Si cluster is clearly changed during artificial aging. It is noted that the Mg-Si clusters is partially dissolved and again increased during artificial aging. Namely, the decrement of BH response, regarding with reversion phenomena, is deeply correlated with the fraction change of Mg-Si clusters. This can be also explained by different thermal stability between Si-rich cluster and Mg-Si cluster. Kim et al. [8] reported that the thermal stability of clusters formed during natural aging. It is noted that the Si-rich cluster, which formed in initial natural aging, has high thermal stability at 443K due to strong interaction Si-Si bond and Si-Vacancy bond. However, the Mg-Si cluster, which formed in middle natural aging, has low thermal stability at 443K. Based on the present results as shown in Fig. 3.6 (see **Chapter 3**), the 6M9S alloy after long-term natural aging (NA-L) has a larger amount of Mg-Si clusters in comparison with other alloys. These results lead to the great decrement of BH response due to the reversion of unstable Mg-Si clusters in Fig. 6.3. Figure 6.5 shows the correlation between BH response ($\Delta HV$) and fraction of Mg-Si clusters obtained by 3DAP results in short-term natural aged and long-term natural aged 6M9S, 7M8S and 8M7S alloys. It is noted that these two factors show extremely good correlation each other. Therefore, the fraction of unstable Mg-Si clusters is deeply related with reversion phenomena.

## 6.6 Conclusions

The bake-hardening response with different Mg/Si ratio of alloy composition was investigated in the present chapter. In addition, the influence of cluster characteristic and its thermal stability on bake-hardening response was investigated. The obtained results are summarized as follows:

1. In the NA-S and NA-L conditions, the hardness increment was retarded by natural aging before artificial aging at 443K. It also seems that the hardness behavior before starting hardness increment is different with alloy compositions.
2. The BH response significantly depends on the natural aging conditions before artificial aging and alloy compositions. In NA-S condition, all examined alloys show the increment of BH response. The most interesting point is that the decrement of BH response can be seen in only 6M9S and 7M8S alloy even though the same long-term natural aging condition. These phenomena are closely correlated with reversion of pre-formed nanoclusters.
3. The 6M9S alloy after long-term natural aging has a larger amount of Mg-Si clusters in comparison with other alloys. These results lead to the great decrement of BH response due to the reversion of unstable Mg-Si clusters
4. It is noted that the BH response ($\Delta HV$) and fraction of Mg-Si clusters obtained by 3DAP results in short-term natural aged and long-term natural aged 6M9S, 7M8S and 8M7S alloys show extremely good correlation each other. Therefore, the fraction of unstable Mg-Si clusters is closely related with reversion phenomena.

## References

[1] W.S. Millera, L. Zhuanga, J. Bottemaa, A.J. Wittebrooda, P.D. Smetb, A. Haszlerc and A. Viereggec: Mater. Sci. Eng. A 280 (2000) pp. 37-49.

[2] T. Saito, C.D. Marioara, S.J. Andersen, W. Lefebvre and R. Holmestad: Philos. Mag. Vol. 94 (2013) pp. 520-531.

[3] J. Kim, E. Kobayashi and T. Sato: Mateials Transactions, Vol. 52, No. 5 (2011) pp. 906-913.

[4] Y. Aruga, M. Kozuka, Y. Takaki and T. Sato: Metall. Mater. Trans. A45 (2014) pp. 5906-5913.

[5] L. Ding, Y. Weng, S. Wu, R.E. Sanders, Z. Jia and Q. Liu: Materials Science & Engineering A651 (2016) pp. 991-998.

[6] M. Torsaeter, H.S. Hasting, C.D. Marioara, J.C. Walmsley, S.J. Andersen and R. Holmestad: J. Appl. Phys., 108 (2010) 073527

[7] Y. Takaki, T. Masuda, E. Kobayashi and T. Sato: Mater. Trans. 55 (2014) pp. 1257-1265.

[8] J. Kim, E. Kobayashi, T. Sato: Mateials Transactions, Vol. 56, No. 11 (2015) pp. 1771-1780.

[9] Y. Aruga, M. Kozuka, Y. Takaki, T. Sato: Materials Science & Engineering A 631 (2015) pp. 86-96.

[10] L. Ding, Y. Weng, S. Wu, R. E. Sanders, Z. Jia, Q. Liu: Materials Science & Engineering A 651 (2016) pp. 291-998.

[11] G.W. Lorimer and R.B. Nicholson: The Mechanism of Phase Transformation in Crystalline Solids, Institute of Metals Monograph, No. 33 (1969), pp. 36.

[12] M. Murayama and K. Hono: Acta. Mater., Vol. 47, No. 5 (1999) pp. 1537-1548.

Table 6.1 (a) Chemical composition of examined Al-Mg-Si alloys, mass%

| Alloy | Elements, mass% | | | |
|---|---|---|---|---|
| | Mg | Si | Fe | Al |
| 8M7S | 0.78 | 0.70 | 0.01 | Bal. |
| 7M8S | 0.73 | 0.81 | 0.01 | Bal. |
| 6M9S | 0.62 | 0.93 | 0.09 | Bal. |

Table 6.1 (b) Chemical composition of examined Al-Mg-Si alloys, mol%

| Alloy | Elements, mol% | | | | Mg/Si | Mg + Si |
|---|---|---|---|---|---|---|
| | Mg | Si | Fe | Al | | |
| 8M7S | 0.87 | 0.67 | <0.01 | Bal. | 1.29 | 1.54 |
| 7M8S | 0.81 | 0.78 | <0.01 | Bal. | 1.04 | 1.59 |
| 6M9S | 0.70 | 0.88 | 0.04 | Bal. | 0.80 | 1.58 |

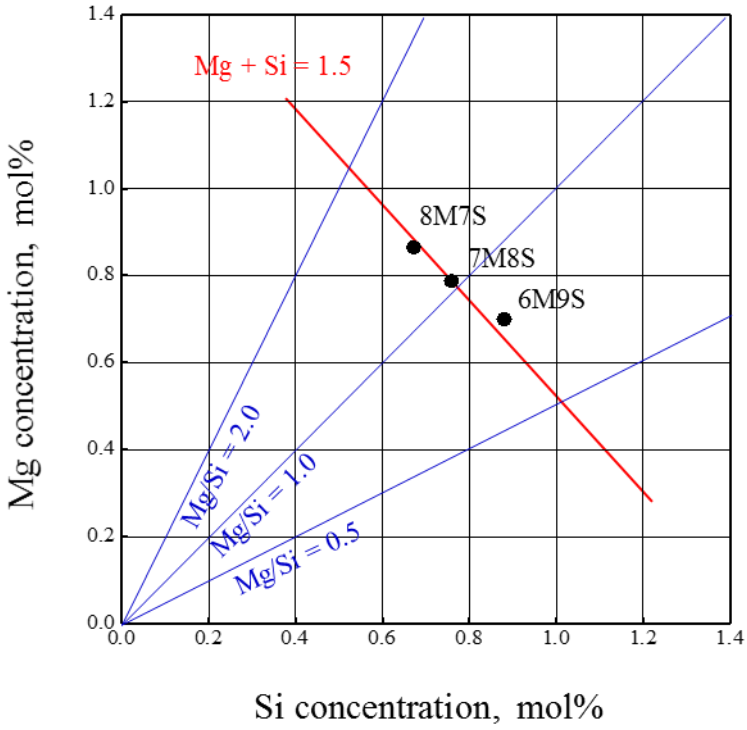


Figure 6.1 Locations of the examined alloys (mol%). The manufactured alloys have a different Mg/Si ratio with constant total concentration (Mg+Si) of 1.5 mol%.

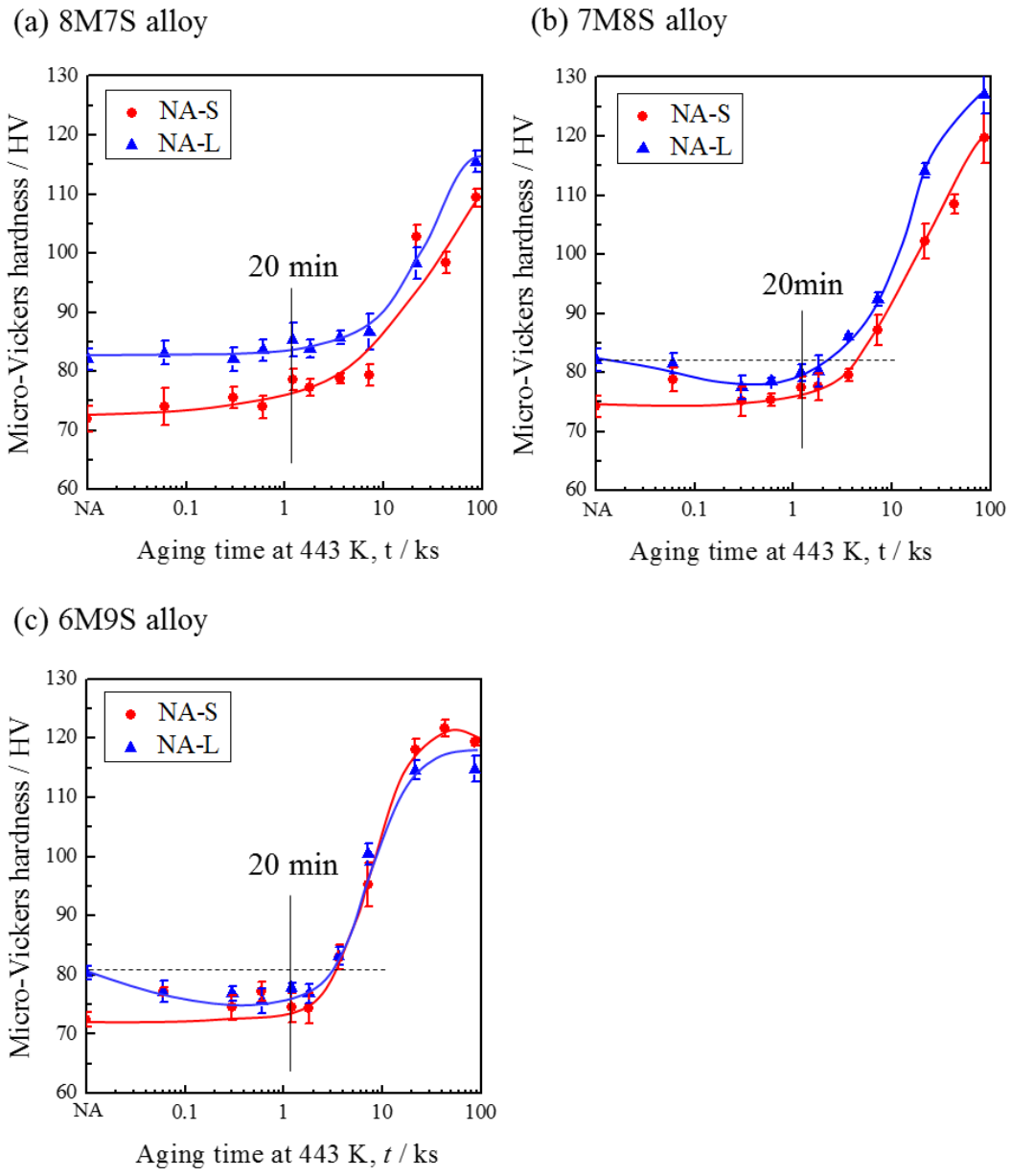


Figure 6.2 Hardness results during artificial aging at 443K after short-term (NA-S, 108 ks) and long-term (NA-L, 7560 ks) natural aging in the (a) 8M7S, (b) 7M8S and (c) 6M9S alloys.

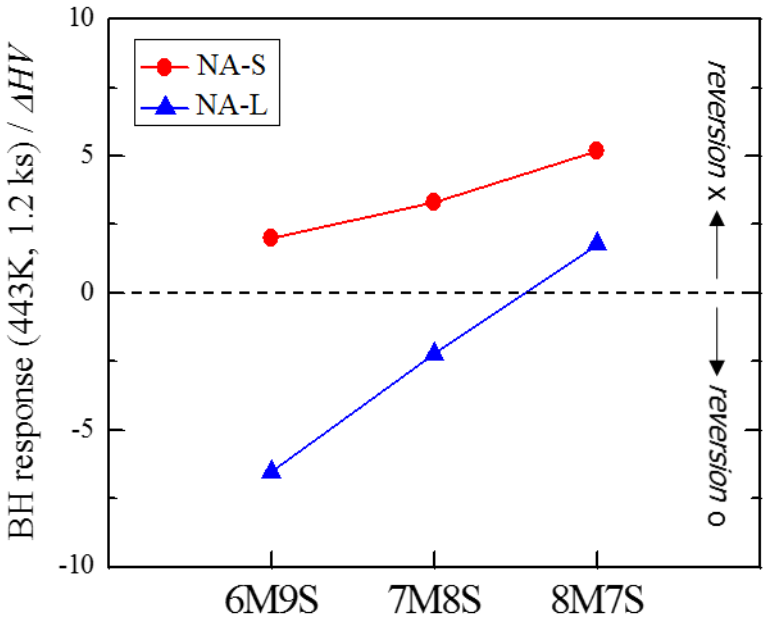


Figure 6.3 Bake-hardening (BH) response obtained from hardness values after artificial aging at 443K for 1.2 ks with different natural aging conditions, i.e. NA-S and NA-L, as a function of alloy compositions.
*BH response was calculated by $HV_{(443K,\ 1.2\,ks)} - HV_{(as\text{-}NA)}$.

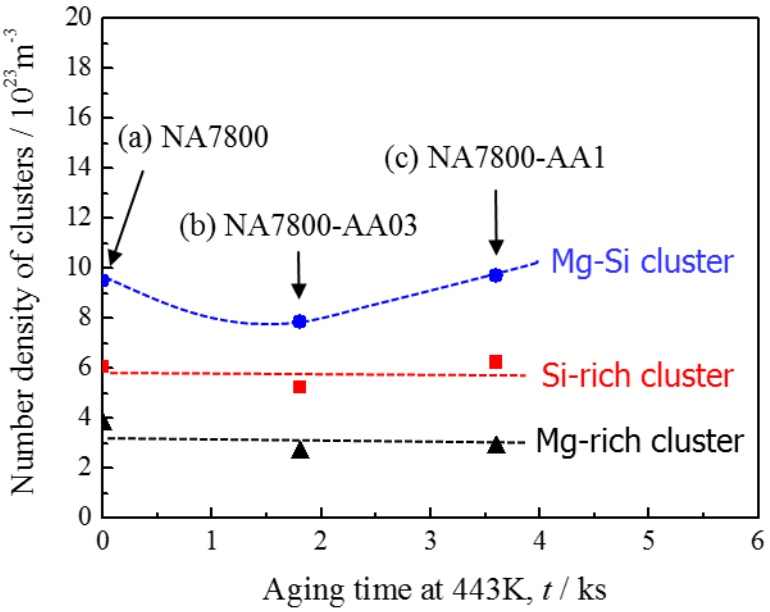


Figure 6.4 The fraction of each cluster, i.e. Si-rich cluster, Mg-Si cluster and Mg-rich cluster, in 6M9S alloy with different aging time at 443K after NA for 2.8 x $10^4$ ks (7800 h).
(a) NA7800, NA for 2.8 x $10^4$ ks
(b) NA7800-AA03, NA for 2.8 x $10^4$ ks and AA for 1.2 ks
(c) NA7800-AA1, NA for 2.8 x $10^4$ ks and AA for 3.6 ks
*The 3DAP data is provided by literature [ ].
*Each cluster was classified by same method as used in chapter 3.

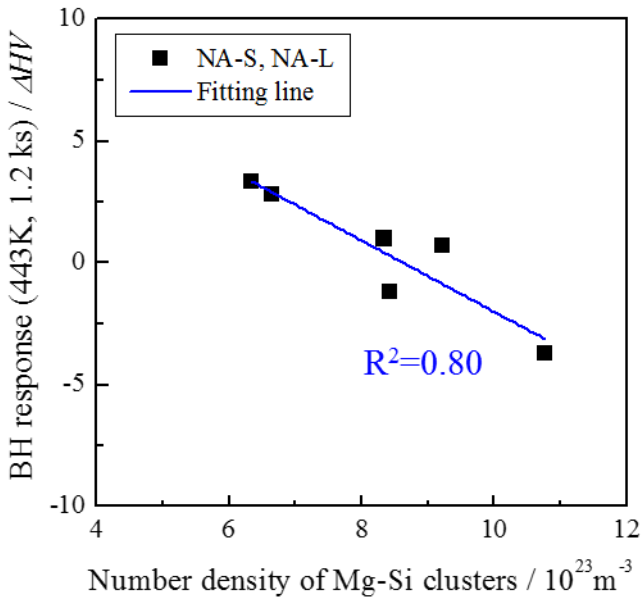


Figure 6.5 Correlation between BH response ($\Delta HV$) and fraction of Mg-Si clusters obtained by 3DAP results in short-term natural aged and long-term natural aged 6M9S, 7M8S and 8M7S alloys

# Chapter 7.
# General Conclusion

The principle objective of the present thesis is described in **Chapter 1**. ***"Composition Dependence of Nanocluster Characteristics in Natural- and Pre-aged Al-Mg-Si alloys Responsible for Two-step Aging Behavior"*** is successfully achieved throughout the previous chapters. Conclusions of the present thesis are summarized in this chapter based on both the obtained experimental results as well as discussion described in each chapter.

The background and motivation of the present thesis as well as literature review are introduced. Based on the current problem, the objectives of the present thesis are described in **Chapter 1** ***"General Introduction"***. The importance and necessity of the study about nanocluster characteristics is described. In addition, the objectives based on the current problems and situations in materials science and industry are explained.

The formation behavior of nanoclusters using mainly DSC analysis with different Mg and Si compositions is investigated in **Chapter 2** ***"Formation Behavior of Nanoclusters with Various Mg and Si Compositions"***. Two exothermic peaks were detected using DSC analysis in the all examined alloys with the different Mg and Si contents. It is clarified that the peak area and peak temperature of two overlapped exothermic peaks depend on the alloy compositions. The overlapped peaks are successfully separated using the Gaussian function method. The formation behavior of nanoclusters strongly depends on the Mg/Si ratio of the alloys more than the total concentration (Mg+Si). The most favorable Mg/Si ratio of the alloys is close to 1.0 for the formation of Cluster (1) and Cluster (2), which is lower Mg/Si ratio than that of equilibrium β-($Mg_2Si$).

The nature of cluster based on its composition and size distribution with alloy composition, aging temperature and time was investigated in **Chapter 3** ***"Three-dimensional Atom Probe Analysis of Solute Clusters Formed in Natural- and Pre-Aged Alloys with Different Mg/Si Ratio"***. It is noted that the 8M7S alloy (relatively Mg-rich alloy) produces more Mg-rich clusters and the 6M9S alloy (relatively Si-rich alloy) produce more Si-rich clusters. The average Mg/Si ratio of 7M8S alloy (almost equal Mg:Si alloy) is precisely located between both alloys. These results suggest that the alloy composition is closely correlated with the cluster composition distribution. As a new finding, Cluster (1) and Cluster (2) were composed of Mg-rich clusters, Mg-Si clusters and Si-rich clusters regardless of the alloy composition. In addition, the fraction of three types of nanoclusters was different with aging temperature and time.

The two-step aging behavior with the different Mg/Si ratio of the alloys and correlation between cluster categorization and two-step aging behavior is investigated in **Chapter 4** ***"Influence of Mg/Si Ratio and Natural- and Pre-Aging on Two-step Aging Behavior"***. The "negative effect on two-step aging" is strongest in the 6M9S alloy and weaker in the 8M7S alloy. It is also noted that the two-step aging behavior can be determined by the relative number of Si-rich clusters and Mg-Si clusters regardless of aging temperature. In the NA condition, the 6M9S alloy with much Si-rich clusters shows the most negative effect on the two-step aging. However, in the PA condition, the fraction of the Mg-Si clusters is extremely increased. That is why the PA condition shows less negative effect or positive effect on the two-step aging

The influence of quenching conditions on nanocluster formation and two-step aging behavior in Al-Mg-Si alloys is investigated in **Chapter 5** ***"Influence of Quenched-in Excess Vacancies on Nanocluster Formation and Two-step Aging"***. The Al-Zn-Mg alloy is considered as a comparison target of Al-Mg-Si alloy because they have a different quench sensitivity and two-step aging behavior. As a result, the Al-Mg-Si and Al-Zn-Mg alloys exhibit a different vacancy behavior. In the Al-Mg-Si alloy, it is likely to form the

Si-vacancy complex after step-quenching (SQ). However, in the Al-Zn-Mg alloy, it is likely to form the dislocation loops and/or vacancy aggregation by absence of Si atoms. This dislocation loop acts as the annihilation point of vacancies as well as the source of vacancy supply into matrix.

The influence of the Mg/Si ratio of the alloys on the BH response and the correlation between cluster fraction and BH response was investigated in **Chapter 6** ***"Influence of Cluster Characteristics and Its Thermal Stability on Bake-hardening Response"***. The BH response significantly depends on the natural aging conditions before artificial aging and alloy compositions. In the NA-S condition, all examined alloys show the increment of the BH response. The most interesting point is that the decrement of the BH response can be seen in only the 6M9S and 7M8S alloys even though the same long-term natural aging condition. These phenomena are closely correlated with reversion of pre-formed nanoclusters. The 6M9S alloy after long-term natural aging has a larger amount of Mg-Si clusters in comparison with other alloys. These results lead to the great decrement of the BH response due to the reversion of unstable Mg-Si clusters

In **Chapter 7**, ***"General Conclusions"***, the overall results and research achievements obtained from **Chapter 2** to **Chapter 6** are summarized. This is the first challenge in the field of Al-Mg-Si alloys that the cluster categorization based on the 3DAP results. It allows us for better understanding a correlation between the cluster fraction and two-step aging behavior. In addition, the dependence of alloy compositions and aging conditions on the nanocluster formation was clarified. Based on these results, the modified two-step aging behavior and optimum nanocluster control conditions were proposed. These research achievements contribute to the practical fields by the precise nanocluster and two-step aging control.